In vitro and *in vivo* studies on the binding and permeation of ketotifen and norketotifen atropisomers in the central nervous system

Feifei Feng

July 2019

Abstract

Ketotifen (K) is a first-generation antihistamine with antiinflammatory potency. It penetrates the blood-brain barrier (BBB) and causes a sedative side effect. Norketotifen (N) is an active metabolite of K. The S-atropisomer of N (SN), however, has antihistaminic and antiinflammatory properties but less sedating side effect than RN and K. This may be due to: (1) higher concentrations of K and RN than SN in the central nervous system (CNS) and/or (2) higher affinity of K and RN than SN for rat brain H_1-receptors. The aim of this thesis was to investigate the mechanism of why SN lacks a sedative side effect.

To determine concentrations of racemic K and N and atropisomers of K and N in buffer solutions and bio-matrices, nonchiral and chiral high-performance liquid chromatography (HPLC) assays were developed and validated. Log P and log D of K and N (both octanol/buffer and liposomes/buffer) were determined to aid in interpretation of *in vitro* cell studies. Rat brain endothelial (RBE4) and colorectal adenocarcinoma (Caco-2) cell monolayers were used as *in vitro* models of the BBB to study the stereoselective uptake and permeability of K and N atropisomers. To investigate the distribution of K and N atropisomers between brain tissue and plasma, the total and free brain-to-plasma (B/P) ratios of K and N atropisomers were measured 5 min post-administration of racemic K and N through the rat tail vein. The affinity of K and N atropisomers to brain H_1 receptors was investigated by determining the extent of inhibition of [^{3}H] mepyramine binding to H_1 receptors in rat brain cell membranes.

The *in vitro* studies indicated active mechanisms for transporting K and N in both RBE4 and Caco-2 cell lines; however, none of these mechanisms were stereoselective. Interestingly, for both cell lines, more N was found binding non-specifically to cell membranes than that of K, though in a non-stereoselective manner. Liposomes/buffer distribution studies aided in interpretation of these results.

Similarly, the total and free B/P ratios of K and N atropisomers suggested a predominant influx mechanism involved in transporting of K and N through the rat BBB. However, this mechanism was not stereoselective for either K or N atropisomers. In addition, K and N non-specifically bound to rat plasma protein and brain tissues in different degree but the non-specific binding was not stereoselective either.

In contrast, H_1 receptor affinity results suggested a stereoselective binding of SN for the H_1 receptors in rat brain, in that SN had a lowest affinity compared with RN, SK and RK. Significant differences in the affinity for the H_1 receptors were found between SN and SK, SN and RK, moreover, between SN and RN. Although the difference was significant but not substantial compared to some published stereoselective affinity for the H_1 receptors, a similar degree of difference was observed and published by other research groups. Thus the lowest affinity of SN for the H_1 receptors could participate in the observed less sedative effect caused by SN.

In conclusion, there was no stereoselective transport of SN through the BBB either *in vitro* or in *vivo*, and there was no stereoselective non-specific binding of SN to rat plasma proteins or brain tissues. The lower sedative effect of SN is due to a lower uptake of N than K into the brain and reduced binding of SN to CNS H_1-receptors.

Acknowledgements

I gratefully acknowledge School of Pharmacy, which give me the chance to be a PhD candidate and support me financially.

I gratefully acknowledge my supervisors for their support. My primary supervisor, Professor Ian G. Tucker, and my secondary supervisor Associate Professor Paul Fawcett. They guided me through my research work, encouraging me to “think like a scientist” and helped me when I was struggling with my writing. Dr Hu Zhang, he was my third supervisor early in my research, though he has never stopped helping and supporting me in my study and life. I want to acknowledge Professor Pauline Norris and Dr Dorothy Saville, who have been kindly checking on me and taking care of me through my study.

I wish to acknowledge my parents for loving me, and supporting me both financially and mentally. My mother and father, Lili Yin and Gaimin Feng, have been supporting me in all the ways they can in my study and my life.

I wish to acknowledge all my friends for being there whenever I needed help.

Dunedin, New Zealand, 2019
Feifei Feng

Publication to date arising from this thesis

Feng, F., Fawcett, J. P., Zhang, H. & Tucker, I. G. (2019) Cell based and H_1-receptor binding studies relative to the sedative effects of ketotifen and norketotifen atropisomers. *J. Pharm. Pharmacol.* (Accepted)

Conference presentations arising from this thesis

Feng, F., Zhang. H, Fawcett, J. P., Yang, L., Tucker, I. G. Stereoselectivity of ketotifen transport in rat brain endothelial cells. *Annual meeting and exposition of American Association of Pharmaceutical Scientists (AAPS)*, Washington DC, USA (23-27 October 2011).

Feng, F., Yang, L., Fawcett, J. P., Tucker, I. G. Ketotifen uptake by rat brain endothelial (RBE4) cells is stereoselective. *Proceedings of the ASCEPT Christchurch, NZ Meeting* (28-30 August 2011).

Feng, F., Fawcett, J. P., Tucker, I. G., Uptake of atropisomers of ketotifen and norketotifen into REB4 cells. *15th Annual Formulation and Delivery of Bioactives Conference*, Dunedin, NZ (13-14 February 2013).

Feng, F., Fawcett, J.P., Tucker, I. G. Unexpected *in vitro* cell uptake of norketotifen compared with ketotifen. *Abstracts of the Annual Australasian Pharmaceutical Science Association (APSA) Conference,* Dunedin, NZ (8-11 December 2013).

Table of Contents

List of Tables

List of Figures

List of Abbreviations

A	Apical side
ABC	Adenosine triphosphate binding cassette
ACN	Acetonitrile
AKR	Aldo-keto reductase
ATP	Adenosine triphosphate
AUC	Area under the curve
B	Basolateral side
BAB	Blood-arachnoid barrier
BBB	Blood-brain barrier
BCRP	Breast cancer resistance protein
BCSFB	Blood-cerebrospinal fluid barrier
B/P ratio	Brain-to-plasma ratio
BUI	Brain uptake index
Caco-2	Colorectal adenocarcinoma (immortalized heterogeneous human epithelial) cells
CAR	Coxsackie and adenovirus receptor
CE	Capillary electrophoresis
Clog P and clog D	Calculated partition coefficient
C_{max}	Maximum plasma concentration
CNS	Central nervous system
CNT	Concentrative nucleoside transporter
COMT	Catechol-O-methyltransferase
CP	Choroid plexus
CPM	Count per minute
CSF	Cerebrospinal fluid
CSP	Chiral stationary phase
CV	Coefficient of variation
CYP	Cytochrome P450
DDI	Drug-drug interaction
EC_{50}	Concentration of an inhibitor where the response (or binding) is reduced by half

ENT	Equilibrative nucleoside transporter
ESAM	Endothelial cell-selective adhesion molecule
FBS	Fetal bovine serum
FDA	U.S. Food and Drug Administration
FGF	Fibroblast growth factor
GC	Gas chromatography
GI	Gastrointestinal tract
GLUT	Glucose transporter
GPCR	G-protein-coupled receptor
GST	Glutathione S-transferase
HBSS	Hank's Balanced Salt Solution
HPLC	High performance liquid chromatography
IS	Internal standard
ISF	Interstitial fluid
K	Ketotifen
K_I	Inhibition constant of a inhibitor
K_d	Equilibrium dissociation constant
LAT	L-amino acid transporter
LC–MS	Liquid chromatography – mass spectrometry
LLE	Liquid-liquid extraction
LLOQ	Lower limit of quantitation
Log $D_{l/b}$	Partition coefficient between liposomes and buffer
Log $D_{o/b}$	Partition coefficient between octanol and buffer
M	Minus
MATE	Multidrug and toxin extrusion transporter
MCT	Monocarboxylic acid transporter
MDR	Multiple drug resistance
MRP	Multidrug-resistance protein
MW	Molecular weight
N	Norketotifen
NB	Non-specific binding
NF-κB	Nuclear transcription factor kappa B
OAT	Organic anion transporter

OATP	Organic anion transporting polypeptide
OCT	Organic cation transporter
OCTN	Organic cation/zwitterion transporter
P	Plus
PA	Permeability surface area product
PAF	Platelet-activating factor
P_{app}	Apparent permeability coefficient
PBCEC	Primary cultured porcine brain capillary endothelial cell
PBS	Phosphate-buffered saline
PET	Positron emission tomography
P-gp	P-glycoprotein
PIR	Proportional impairment ratio
QC	Quality control
R	Axially rectus
RBE4	Immortalized rat brain endothelial cell line
RE	Relative error
RED	Rapid equilibrium dialysis
RI	Refractive index
Rt	Retention time
S	Axially sinister
SB	Specific binding
SD	Standard deviation
SLC	Solute carrier
SP	Stationary phase
TB	Total binding
TEER	Transendothelial electrical resistance
TMN	Tuberomammillary nucleus
$t_{1/2}$	Half-life
UGT	Uridine 5'-diphospho-glucuronosyltransferase
UHPLC	Ultra-high performance liquid chromatography
VAS	Visual analogue scale
V_d	Volume of distribution
ZO	Zonula occludens

Chapter 1 Introduction

1.1 Histamine, histamine receptors

Histamine, a peripheral mediator in allergic reactions and a central nervous system (CNS) neurotransmitter, plays important roles in physiological and pathophysiological functions in human health. It is synthesized in tissues from the amino acid histidine by L-histidine decarboxylation (Ling et al, 2004), particularly abundant in skin, lung and gastrointestinal (GI) tract. It is stored in granules or vesicles of several types of cells including mast cells (main source of histamine), basophils, lymphocytes, platelets, enterochromaffin cells and histaminergic neurons (Carson et al, 2010; Simons and Simons, 2011). Histamine exerts its physiological and pathophysiological functions through histamine receptors.

There are four subtypes of histamine receptors, H_1 to H_4, which all belong to the G-protein-coupled receptor (GPCR) family. They all are heptahelical transmembrane molecule, which transduce extracellular signals via G protein and an intracellular second messenger system. However, H_1 to H_4 receptors are expressed on different tissues at different densities where they mediate different biological effects (Table 1.1).

Table 1.1 Summary of the four subtypes of histamine receptor.

	H_1 receptor	H_2 receptor	H_3 receptor	H_4 receptor
Expression	Eosinophils, dendritic cells, monocytes, cardiovascular system			
	Nerve cells, airway and vascular smooth muscle, endothelial cells, epithelial cells, neutrophils, T and B cells, hepatocytes, chondrocytes, nerve cells and macrophages		Lungs	
	___	Gastric parietal cells	High expression in histaminergic neurons; expression in peripheral neurons, endothelial cells, very low density in glial cells	High expression in bone marrow and peripheral hematopoietic cells, neutrophils, T cells, basophils, mast cells. Moderate expression in spleen, thymus, small intestine, colon
Agonist (examples)	Histaprodifen	Amthamine, dimaprit, impromidine	α-methylhistamine, imetit, immepip, and methimepip	Clobenopropit, imetit, immepip, 4-methylhistamine
Antagonist (examples)	Ketotifen, pomethazine, loratidine, fexofenadine, chlorpheniramine, diphenhydramine, hydroxyzine, cetirizine	Cimetidine, ranitidine, famotidine and nizatidine	Thioperamide, clobenopropit, iodophenpropit, pitolisant (ABT-288), MK-0249, JNJ-17216498** and PF-03654746**	JNJ7777120, UR 65380, UR 63825, VUF-6002, doxepine*, cinnarizine* and promethazine*
Function in the CNS	Sleep/wakefulness, food intake, thermal regulation, emotions/ aggressive behaviour, locomotion, memory, learning	Neuroendocrine	Presynaptic autoreceptor or heteroreceptor, reducing histamine, dopamine, serotonin, noradrenaline, 5-hydroxytryptamine, glutamate, GABA, neuropeptides and acetylcholine release. Postsynaptic effects, activated MAPK, Akt pathways and GIRK activation	___
Function in allergic inflammation and immune modulation	Periphery takes part in acute immune response	Negatively regulate histamine release from basophils and mast cells; inhibit synthesis of antibody, T-cell proliferation, cell mediated cytolysis and cytokine production	Negative feedback mechanism reduces central histaminergic inflammatory; controls neurogenic inflammation	Mediate eosinophil, chemotaxis, cell-shape change, modulate cell migration, regulate allergy and inflammatory responses

* H_1 antagonists were reported to show high affinity for H_4 receptors

** Drugs in clinical trials

Antagonists here refers to inverse agonists because the antagonist prefers binding to an inactive stage of the receptor thereby shifting the equilibrium towards the inactive stage

(Adkinson et al, 2013; Ferreira et al, 2012; Gustavo et al, 2016; Haas et al, 2008; Leurs et al, 2011, Ling et al, 2004; Mahdy and Webster, 2014; Simons and Simons, 2008, 2011; Wang et al, 2016)

The peripheral effects of activating histamine receptors, mainly H_1, H_2 and H_4 receptors, include smooth muscle contraction, increased vascular permeability, vasodilation and stimulation of gastric acid secretion (Simons and Simons, 2011). Therefore, histamine takes part in allergic responses and inflammation in asthma, allergic rhinitis, and food allergy (Wang et al, 2016).

The H_1 receptor mediates allergic reactions including smooth muscle contraction, vasodilation and sensory nerve activation, while the H_2 receptor increases gastric acid secretion in stomach and promotes vasodilation (Faustino-Rocha et al, 2017). The H_4 receptor regulates cell migration, the differentiation of myeloblasts and promyelocytes, and induces chemotaxis. In addition, the H_4 receptor plays an important role in chronic inflammatory skin diseases. Previously, it was thought that the chronic inflammation was due to the activation of H_1 receptors and was, therefore treated with H_1 receptor antagonists. However, this did not work well until the H_4 receptor was found and identified (Faustino-Rocha et al, 2017; Hill et al, 1997; Haas et al, 2008; Leurs et al, 2011). The H_3 receptor peripherally inhibits excess bronchoconstriction and regulates pruritus (Bongers et al, 2007; Leurs et al, 2005). More pertinently, it acts as an auto- and/or heteroreceptor in the CNS to regulate neurotransmission by histamine and other biogenic amines including dopamine, serotonin and noradrenaline (Leurs et al, 2011).

In the CNS, histamine is involved in many important central functions including regulation of sleep and wakefulness, memory and cognition (Table 1.1) (Haas et al, 2008; Mahdy and Webster, 2014; Simons and Simons, 2008). These functions are normally unaffected unless histamine agonists and/or antagonists penetrate the brain. In theory, histamine antagonists are commonly used peripherally to treat allergic conditions. However, some histamine antagonists (e.g., the first-generation H_1 receptor antagonists) do enter the brain and consequently result in side effects.

This thesis is focused on the H_1 receptor antagonist (inverse agonist) ketotifen (K) (Figure 1.1a) and its molecularly-similar active metabolite norketotifen (N) (Figure 1.1c). Both K and N are chiral compounds of a particular class called atropisomers (Figures 1.1b and d). As configurational descriptor, the torsion angel $\tau 1$ (Figure 1.2) and the heterocyclic system together make K atropisomers stable under room temperature as well as physiological conditions (Testa et al,

2016). Due to the structure similarity, this configurational descriptor mechanism also applies to N atropisomers.

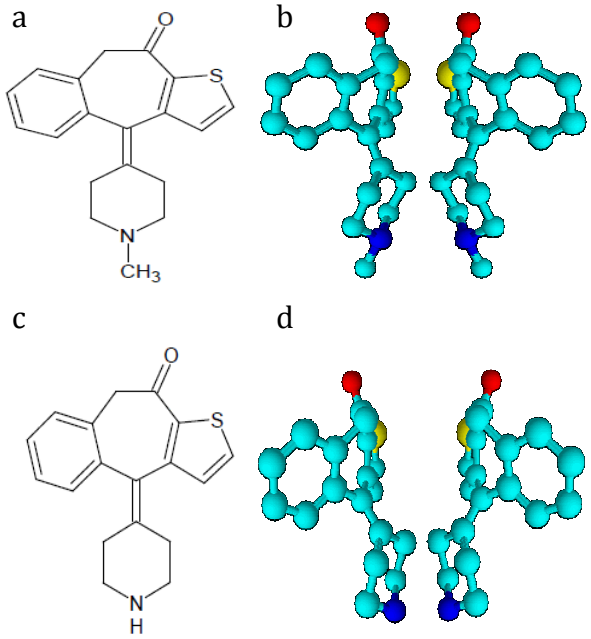

Figure 1.1 Structure of ketotifen (a), norketotifen (c) and mirror images of ketotifen atropisomers (b) and norketotifen atropisomers (d).

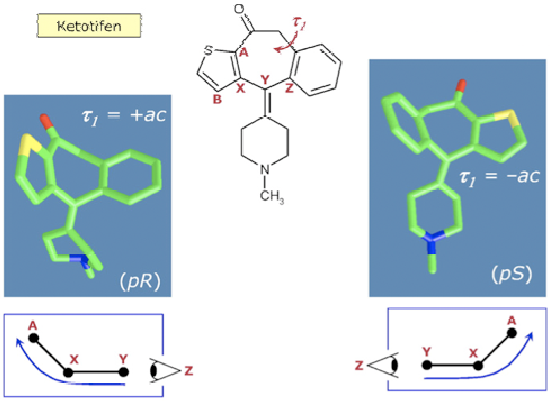

Figure 1.2 An example of the configurational descriptor of ketotifen.

(Testa et al, 2016) (Reproduced with permission)

K shows both antihistaminic and antiinflammatory potency but has a serious sedative side effect because it enters the CNS where it binds to the H_1 receptor. Interestingly, the S-atropisomer of N (SN) is reported to have higher potency without the sedative side effect (Aberg A. K. G, Patent US9439895 B2). To explore the reason why SN has high potency without the sedative side effect, the following sections describe H_1 antagonists, characteristics of K and N, chirality, and the effects of chirality on biological systems.

1.2 H_1 receptor antagonists

Histamine is one of the most important mediators involved in type I hypersensitivity allergy. A large amount of histamine is released from mast cells and basophils in the early phase of allergy to activate histamine receptors. In the late phase of allergy, inflammatory cytokines are secreted and endothelial cells are activated. Consequently, inflammation and tissue injury occur (Stojkovic et al, 2015). In chronic allergic inflammation, histamine activates inflammatory cells including basophils and eosinophils, and releases proinflammatory mediators including leukotrienes and cytokines (Faustino-Rocha et al, 2017). Therefore, to control allergic reactions, antihistamines were designed to inhibit the function of histamine by blocking histamine receptors (e.g., K) or inhibiting the activity of the enzyme L-histidine decarboxylase (Faustino-Rocha et al, 2017). Some antihistamines (including K) show antiinflammatory activity by inhibiting the accumulation and activation of inflammatory cells by suppression of nuclear transcription factor kappa B (NF-κB) (Faustino-Rocha et al, 2017; Simons and Simons, 2011). In this thesis, the word antihistamine will be used to refer to H_1 antagonists.

Antihistamines are widely used in allergic conditions including rhinitis, atopic dermatitis, contact dermatitis, urticarial, allergic conjunctivitis, hypersensitivity reactions to drugs and mild transfusion reactions (Carson et al, 2010; Simons and Simons, 2011). Antihistamines are mainly used to improve symptoms in the early phase of allergic reactions such as sneezing, nasal and conjunctival itching, conjunctival erythema, rhinorrhea and tearing (Simons and Simons, 2008). In addition, some antihistamines, such as K, inhibit histamine release from mast cells and decrease mast cell activity. K inhibits mast cell degranulation by stabilizing their membranes. Therefore, K has both antiallergic and antiinflammatory potency that improve symptoms in both early and late phases of allergic reactions (Grant et al, 1990; Weller and Maurer, 2009).

There are two ways to classify antihistamines. The first is based on their chemical structures where they are divided in to seven groups: alkylamines (chlorpheniramine, acrivastine), piperazines (cyclizine, cetirizine), piperidines (ketotifen, fexofenadine), ethanolamines (diphenhydramine, doxylamine), ethylenediamines (pyrilamine, tripelennamine), phenothiazines (promethazine)

and others (doxepin, emedastine) (Simons and Simons, 2008). The second classification is based on their selectivity for H_1 receptors and their ability to enter the CNS. In this case they are termed either first-generation antihistamines (e.g., K and diphenhydramine) or second-generation antihistamines (e.g., fexofenadine and cetirizine). First-generation antihistamines have (1) low selectivity for H_1 receptors, due to the direct interaction with tryptophan, a highly conserved key residue in GPCR activation (Shimamura et al, 2011) and (2) a marked ability to enter the brain. In contrast, second-generation antihistamines show high selectivity for H_1 receptors and do not or only enter the brain to a limited extent (0–30% of CNS H_1 receptor occupancy) (Mahdy and Webster, 2014). This leads to the difference of side effects (Table 1.2).

Table 1.2 Side effects of first- and second-generation antihistamines.

Mechanism	First-generation antihistamine	Second-generation antihistamine
H_1 receptor inverse agonist	CNS depression (somnolence, impaired cognitive and psychomotor performance) and other CNS effects (seizures, dyskinesia, dystonia, hallucinations)	Minimal or no CNS depression with standard clinical dose
Blockade of muscarinic receptors	Dilation of pupils, blurred vision, dry eyes, dry mouth, urinary retention, hesitancy, constipation, erectile dysfunction, and memory deficits	None or minimal
Blockade of serotonin receptors	Appetite stimulation and weight gain (especially with cyproheptadine and K)	None or minimal
Blockade of α-adrenergic receptors	Peripheral vasodilation, orthostatic hypotension and dizziness	None or minimal
Blockade of cardiac ion channels	Sinus tachycardia (does dependent), reflex tachycardia, prolonged atrial refractive period, and supraventricular arrhythmias	Minimal

Mahdy and Webster, 2014, Simons and Simons, 2011

Through CNS H_1 receptors, histamine regulates vigilance (alertness and attention), cognition, learning, memory, and the circadian sleep-wake cycle (Haas et al, 2008; Leurs et al, 2011; Thakkar, 2011). Therefore, blocking H_1 receptors in the CNS results in various side effects including sedation (Table 1.2).

Although the H_1 receptor is linked to sedation, it remains unclear whether other histamine receptors are involved in the sedative effect.

Three subtypes of histamine receptors are expressed in the CNS, the H_1, H_2 and H_3 receptors. The H_1 and H_2 receptors are both found in some regions of the brain where are involved in regulation of the sleep-wakefulness cycle (Palacios et al, 1981; Vizuete et al, 1997). The expression level of H_1 receptors in these regions is high to moderate whereas the expression level of H_2 receptors is moderate to low. Despite the expression of the H_2 receptor in sleep-wakefulness regulation regions, evidence indicates that the H_2 receptor does not take part in regulation of sleep-wakefulness (Luo and Leung, 2009; Monti et al, 1986, 1990; Onodera et al, 1994; Sastry and Phillis, 1976). However, it has been reported that H_3 antagonists cause dose-dependent prolonged wakefulness suggesting that the H_3 receptor is involved in the regulation of the sleep-wakefulness cycle (Thakkar, 2011). Therefore, H_1 and H_3 receptors are key mediators of histaminergic action on wakefulness, although the H_3 receptor works in the opposite direction to the H_1 receptor (Thakkar, 2011). The human H_3 receptor only shares 22% homology with the H_1 receptor (Gustavo et al, 2016) so that it is unlikely that H_1 and H_3 receptors share common agonists or antagonists. Furthermore, there is no evidence to indicate whether K or N is an H_3 receptor agonist or antagonist. Therefore, the hypothesis of this thesis is that the sedative effects of K and N are due to binding to the H_1 receptor in the brain. The literature also supports this (Gupta et al, 2007; Tashiro et al, 2002, 2008; Yanai et al, 2011; Yanai and Tashiro, 2007).

To evaluate the extent of blockade of CNS H_1 receptors, animal models are available for *in vivo* experiments. In all examined mammalian species, the locations of histaminergic neurons are mainly in the tuberomammillary nucleus (TMN) and/or surrounding regions; only minor differences exist between species (Thakkar, 2011). Therefore, to investigate the sedative effect and sleep-wake cycles related to antihistamines, different animals are used including cat (Lin et al, 1994), rabbit (Monnier et al, 1970), rat (Ahmad et al, 2016; Monti et al, 1986, 1990, 1993, 1994; Shigemoto et al, 2004a, 2004b; Tokunaga et al, 2007; Unno et al, 2012;), mouse (Wang et al, 2015) and dog (Wauquier et al, 1981). Of

all these animal models, rat and mouse are the most commonly used because of their easier accessibility and lower cost.

Although the mouse is cheaper and available in specific gene knockout (KO) models (Wang et al, 2015), the rat is superior for its behavioural characteristics and size in studying sleep-wakefulness (Revel et al, 2009). Specifically, Wistar (Monti et al, 1994; Rojas-Zamorano et al, 2009; Shigemoto et al, 2004a; Tasaka et al, 1988; Tokunaga et al, 2007) and Sprague-Dawley (Kalivas, 1982; Ramesh et al, 2004) rats have been widely used in many studies, which focused on the sleep and wakefulness induced by histamine, its agonists and antagonists. In addition, the Wistar rat has been used to determine the H_1 receptor occupancy in brain homogenate (Midzyanovskaya et al, 2016; Wu et al, 2013). Therefore, in this thesis, the male Wistar rat was chosen as the animal model to study the reason for the purported difference in the CNS sedative side effect of K and N both *in vitro* and *in vivo*.

1.3 Ketotifen and norketotifen

K (Figure 1.1 a and c) and its active metabolite N (by oxidative N-demethylation pathway)(Figure 1.1 b and d) (Aberg et al, 2015; Le Bigot et al, 1987) are both chiral compounds that have S- and R-atropisomers (Breyer-Pfaff and Nill, 2000). Both K and N are relatively lipophilic, basic drugs (Table 1.3). The calculated log P (clog P) of K is reported to be less than that of N even though K has one more methyl group which, theoretically, make its log P value greater by 0.5 (Fujita et al, 1964). The calculated log D (clog D) values of K and N seem to agree with the theory.

The anomaly of clog P of K and N could be due to the following reasons: (a) the deviation of the clog P from the experimental log P as the calculated value does not always in a line with the experimental value, or (b) the deviation of the clog P values caused by different calculation methods as there are several methods for clog P calculation, which may generate different clog P values on the same compound.

Table 1.3 Physicalchemical properties of ketotifen (K) and norketotifen (N) including molecular weight (MW), clog P, log D (pH 7) and pKa values at 25°C obtained from SciFinder Scholar (CAS).

	MW (g/mol)	clog P	clog D (pH = 7)	pKa
K	309.43	2.19 ± 0.73	0.37	8.84 ± 0.20
N	295.40	2.65 ± 0.51	-0.26	10.35 ± 0.20

Oral K has been used in patients with allergic rhinitis, allergic conjunctivitis, atopic dermatitis, urticaria, asthma, mastocytosis, and food allergy in some countries including Canada, Europe, and Mexico. For adult and children more than three years old, the recommended oral does for ketotifen is 1 mg twice a day (Sokol et al, 2013).

After oral delivery, K is readily absorbed from the GI tract and reaches peak plasma/serum concentration (C_{max}) within two to four hours. However, the bioavailability of K is only about 50% because of first-pass metabolism in the liver (Grant et al, 1990; Le Bigot et al, 1987). K is 75% bound to plasma proteins (FDA drug approval package). The clearance of K from plasma is biphasic, with a 3-hour distribution half-life ($t_{1/2}$) and a 22-hour elimination $t_{1/2}$ in adults (Grant et al, 1990). The two main metabolic pathways for K in human are hepatocytes, keto-reduction (reduced K) and N-glucuronidation (K-glucuronide). Traces of N and oxidized K were also found (Figure 1.3) (Le Bigot et al, 1987).

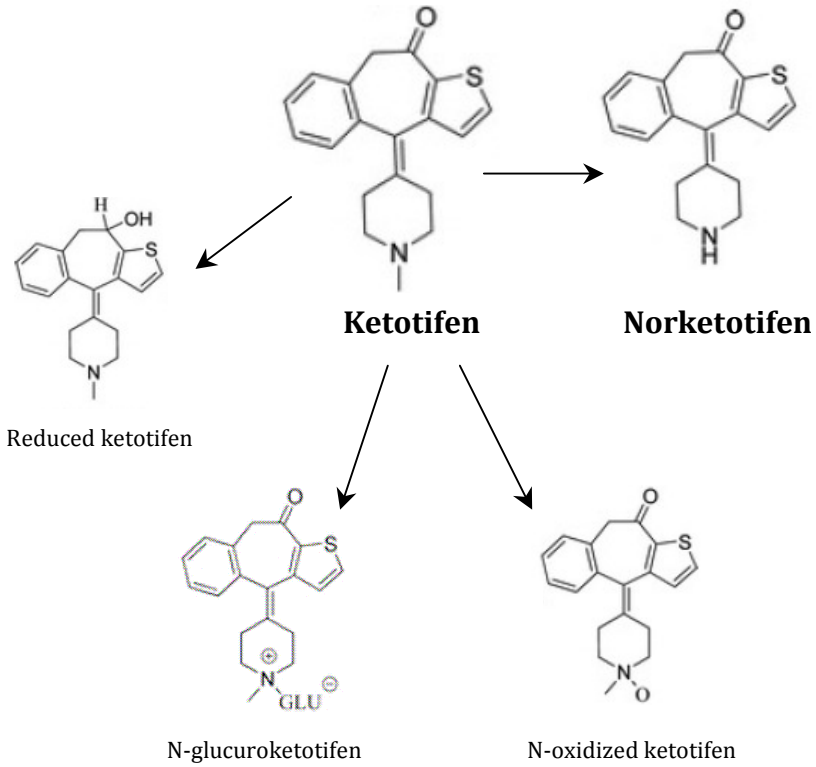

Figure 1.3 Ketotifen and its metabolites including norketotifen.

The enzymes that contribute to the main metabolic routes of K are UDP-glucuronosyltransferase (UGT)2B10, UGT1A4 and aldo-keto reductase (AKR)1C1 for N-glucuronidation and keto-reduction respectively (Kato et al, 2013; Weiner et al, 2006). Although oxidative N-demethylation is not a main route of K metabolism, it contributes to produce the active mebabolite N in human hepatocytes (Le Bigot et al, 1987).

Only two reports have discussed the pharmacokinetic parameters of N, one being a patent and the other one a research study. The patent reported that after dosing N for 28 days (5.6 mg/kg/day) to five male Beagle dogs, N accumulated in skin to a much higher extent than in plasma (Table 1.4) suggesting a possible application of N in skin conditions (Aberg A. K. G, Patent US9439895 B2).

Table 1.4 Pharmacokinetic parameters of N after 28 days dosing (5.6 mg/kg/day) in five Beagle dogs.

	SN		RN		Racemic N	
	Plasma	Skin	Plasma	Skin	Plasma	Skin
AUC*$_{0-\infty}$	1627	25710	1658	20376	3286	54187
$t_{1/2}$ (h)	10.9	162.7	7.7	157.0	10.5	167.6

*AUC: Area under the curve
Patent US9439895 B2

The research paper reported PK parameters of both K and N, in a malarial mouse model (Milner et al, 2012). However, there were calculation and unit errors in this paper making it unreliable.

Pharmacodynamic parameters of K and N have also been investigated in mice (Aberg A. K. G, Patent EP 2911510 A1). The results suggest that K has a higher affinity for the H_1 receptor than N whereas N is more potent as an antiinflammatory agent (Table 1.5).

Table 1.5 Antihistamine and antiinflammatory properties of ketotifen (K) and norketotifen (N) in mice.

	H_1 EC_{50} (nM)*	Inhibition (%)**	EC_{50} (μM)#
K	2.3	98	91
N	11	82	9.2

* *In vitro* experiment using binding assay. EC_{50} values are the concentration that inhibits 50% of specific binding of the ligand.
** *In vivo* experiment calculating inhibition (%) of histaminergic effects after 10mg/kg dosage of K and N in rats.
# Inhibition of inflammatory mediator histamine release from human leukocytes.
Patent EP 2911510 A1

This patent also reported the sedative effects of K and N (racemate and atropisomers) in mice (Table 1.6). The results indicate that N has a lower sedative effect than K and that the sedative effect of N is due to its R-atropisomer (Patent EP 2911510 A1).

Table 1.6 Sedative effects of ketotifen (K), norketotifen (N) and the atropisomers of N (SN and RN) in mice.

	Oral dose (mg/kg)	Sedated mice
K	25	5/10
	50	8/10
	100	10/10
N	100	3/10
	150	3/10
SN	100	0/10
	150	0/10
RN	100	3/10
	150	3/10

Patent EP 2911510 A1

Based on the mechanism of the sedative side effect of antihistamines, there are two potential explanations for the difference in the sedative effects of SN, RN and K:

1. Stereoselective transport by which (a) SN enters the brain to a less extent and/or (b) SN bound to plasma protein/tissue to a greater extent than K and RN, such that there is less SN available for binding to CNS H_1 receptors;
2. Stereoselective binding to H_1 receptors by which SN has a lower affinity for CNS H_1 receptors in than K and RN, such that there is less SN bound to CNS H_1 receptors.

To explore these hypotheses requires an understanding of why stereo-isomers behave differently in bio-systems?

1.4 Chirality

The word "chiral" is derived from the Greek word "cheir", which means, "hand". In 1884 Lord Kelvin introduced the terminology "chiral" and defined it in his Baltimore Lectures as: "*I call any geometrical figure, or any group of points, chiral, and say it has chirality, if its image in a plane mirror, ideally realized, cannot be brought to coincide with itself*". Human hands are the best example of chirality: the left hand is the non-superposable mirror image of the right hand. As antihistamine K and N are both chiral compounds, this section mainly focuses on chirality of antihistamines.

1.4.1 Concepts

There are several important concepts to understand about chirality and they are described in standard textbooks (Solomons et al, 2012):

Enantiomers: Chiral molecules differ in their three-dimensional configurations and exist in two forms, which are the mirror images of each other. These mirror images are called enantiomers. Certain enantiomers can be inverted from one to the other through a series of states.

Atropisomers: The name atropisomer comes from Greek, as "a" (not) and "tropos" (turn) (Bringmann et al, 2005), the ortho-substituents in tetra-substituted biaryls are large enough to hinder the rotation around a C – C single bond. Therefore, interconvertion of atropisomers requires a high energy, which makes it possible for separation and purification for these molecules, though at

higher temperatures interconvertion may occur. As a result, atropisomers is the "grey area" between stereoisomers and conformations (Orchin et al, 2005).
The notation used for atropisomers are R (axially rectus)/P (plus) and S (axially sinister)/M (minus) (Bringmann et al, 2005). The absolute axial configuration can be analysed using the Newman projection along the biaryl axis using the CIP system (Prelog and Helmchen, 1982). In this thesis, the notation R and S are used for K and N atropisomers.
Racemate: an equimolar mixture of opposite enantiomers/atropisomers.

1.4.2 Chirality in biological systems

Chiral compounds have identical molecular formulas. In an achiral environment, the two forms of a chiral compound have the same physical and chemical properties, except for their ability to rotate polarized light. However, in a chiral environment, such as in a biological system, atropisomers sometimes display significant differences in their physicochemical and biochemical properties. Plasma proteins and transporters, which are chiral macromolecules, may form diastereomeric complexes with only one form of the pair of atropisomers (Campo et al, 2009; Lu, 2007). Therefore, it is possible that atropisomers show differences in absorption (Miura and Uno, 2010), protein binding, enzyme interactions, metabolism (Lu, 2007), receptor interactions and DNA binding, etc. (Smith, 2009).
Different binding of atropisomers to chiral macromolecules, for example receptors and transporters, often results in one of the atropisomers being active (eutomer) whereas the other is inactive (distomer). Easson and Stedman (1933) proposed that the eutomer and distomer are differentiated by a three-point attachment model (Figure 1.4). Importantly, the distomer may not simply be ballast but also antagonise the process of the eutomer, or sometimes be toxic (Hassan and Aboul-Enein, 2003; Simith, 2009).

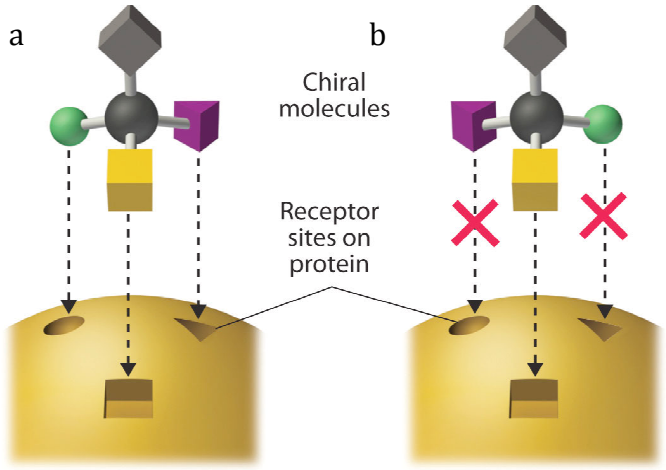

Figure 1.4 Chiral recognition between target and (a) eutomer and (b) distomer.

1.4.3 Chirality in absorption, distribution, metabolism and elimination

Stereochemistry applies to interactions between drug and enzymes, receptors and transporters. In addition, binding to plasma and tissue proteins is crucial to the overall pharmacological activity of a drug, because only the free or unbound drug crosses membranes and participates in receptor interactions. Chirality of binding may influence the pharmacological properties of a drug by affecting the free stereoisomer (eutomer or distomer) concentration (Gupta et al, 2006). As a result, there may be different absorption, distribution, metabolism and excretion behaviours between atropisomers (Table 1.7).

Table 1.7 Examples of stereoselective behaviour in absorption, distribution, metabolism and elimination of chiral antihistamines.

	Drug	Observation of difference	Literature	Mechanism
Absorption	Fexofenadine	Plasma concentration of R-enantiomer is about 2-fold higher than S-enantiomer	Miura and Uno, 2010; Tateishi et al, 2008	Stereoselective P-glycoprotein (P-gp) efflux in intestine
	Cetirizine	Plasma concentration of levocetirizine is 2-fold higher than that of dextrocetirizine	Baltes et al, 2001	
	Terodiline	C_{max} and AUC of R-enantiomer are significantly higher than S-enantiomer	Mann and Andrews, 2007	
Distribution	Cetirizine	Apparent volume of distribution (V_d) of levocetirizine is significantly smaller than that of the distomer	Baltes et al, 2001; Gupta et al, 2006	Higher plasma protein and tissue binding for eutomer
Metabolism	Terodiline	Stereoselective metabolism of R-enantiomer	Mann and Andrews, 2007	Stereoselective metabolism Cytochrome P450 2D6 (CYP2D6) polymorphic metabolism
	Terfenadine	Stereoselective metabolism of R-enantiomer into the carboxylic acid analogue	Blaschke and Terhechte, 1995	
Elimination	Cetirizine	Clearance of dextocetirizine is higher than that of levocetirizine	Baltes et al, 2001; Benedetti et al, 2009	

For pharmaceutical compounds and nutrients, stereoselective transporters express in membrane barriers, such as the intestinal barrier membrane and the blood-brain barrier (BBB), play an important role in the barrier permeability (Chang et al, 2015; He et al, 2010; Makrides et al, 2007; Miura and Uno, 2010; Shen et al, 2007). Understanding of receptors has been derived from research using *in vitro* methods, such as colorectal adenocarcinoma (Caco-2) cell monolayers as a model for the intestinal barrier and brain capillary endothelial cell monolayers as a model for the BBB. Antihistamines have been found to be substrates and/or inhibitors of stereoselective transporters including P-gp, multidrug-resistance protein (MRP), organic anion transporter (OAT), and others. This, therefore, results in different pharmacokinetic and pharmacodynamic properties between antihistamine enantiomers/atropisomers (Akamine, 2015; He et al, 2010; Miura and Uno, 2010; Shen et al, 2007). Several stereoselective transporters have been found at the BBB, thus it is possible that these transporters may contribute to the stereoselective transport of N into the CNS. Therefore, it is important to understand the barriers between the blood and the CNS, transporters expressed on the barrier and which of them may contribute to transport K and/or N into the CNS. These are discussed in the next section (Section 1.5).

1.5 The BBB and its characteristics

1.5.1 What is the BBB?

The brain is protected by the skull and three barriers: the blood-arachnoid barrier (BAB), the blood-cerebrospinal fluid barrier (BCSFB) and the BBB (Davson and Segal, 1995).

The BAB, lying under the dura mater, is a membrane formed by multilayers of epithelial cells completely enclosing the CNS. The inner epithelial cells are connected by tight junctions, which effectively isolate the CNS extracellular fluids from the rest of the body (Abbott et al, 2006). By projecting through the dura mater, the arachnoid villi projects into the sinus but allow only cerebrospinal fluid (CSF) to pass, and is the mechanism by which substances in the CSF move from brain to blood. In addition, the surface area of this passive anatomical

barrier is relatively small; so that the BAB is not an important route for the entry of solutes into the brain (Eyal et al, 2009; Kandel et al, 2000).

The BCSFB is primarily located within the choroid plexus (CP) and projects into brain ventricles. Drug transfer between the blood and CSF is limited by the BSCFB at which CP epithelial cells are sealed by tight junctions (Redzic and Segal, 2004). Although drugs are transferred from blood to brain across the BBB and to CSF through the BCSFB, individual neurons are located closer to brain capillaries (< 20 μm) than to brain ventricles or circumventricular organs (mm or cm) (Schlageter et al, 1999). Therefore, the primary interface for the transfer of drugs between the circulation and the CNS is the BBB (Eyal et al, 2009).

As discussed, the BBB is a delivery route as well as a barrier for most pharmaceutical compounds to enter the brain (Abbott et al, 2010; De Boer and Gaillard, 2007; Kandel et al, 2000). In this thesis, no further interest was taken in the BCSFB and BAB for delivering antihistamines into the CNS and they are not discussed any further in the following sections.

The BBB is the interface between the blood and the brain and it significantly restricts the transport of drugs from cerebral capillaries in the brain. The BBB is formed by the brain capillary endothelial cells and their connecting tight junctions (Figure 1.5) that segregate the circulating blood from interstitial fluid in the brain (Reese and Karnovsky, 1967, Pardridge, 2016, Wilhelm et al, 2016). There are approximately 600 km of cerebral capillaries with an estimated area of almost 20 m^2/ 1300g within the human brain (Kalimo, 2005; Pardridge, 1993). Besides endothelial cells and tight junctions, capillary astrocyte foot processes and pericytes (Figure 1.5) also contribute to BBB functions (Jiang, et al, 2018, Pandey et al, 2016; Pardridge, 1993; Pardridge, 2016; Wilhelm et al, 2016).

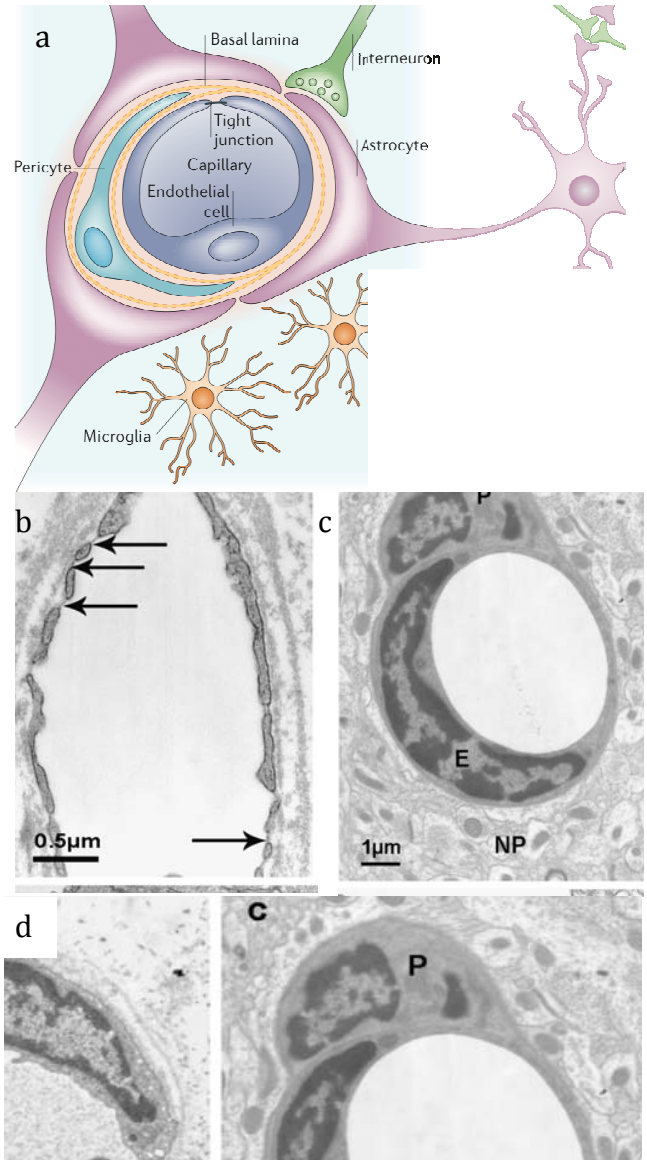

Figure 1.5 A diagram of (a) a brain capillary (the BBB) and comparison of an electron micrograph of (b) a highly permeable fenestrated (arrows) general capillary (c) brain capillary (E: endothelial cells, P: pericyte) and (d) higher magnification part of brain capillary (A: astrocyte foot process, BL: basal lamina and tight junctions: arrow).

(Wolburg et al, 2009; Abbott et al, 2006) (Reproduced with permission)

Compared with the general capillary, the brain capillary is 'wrapped' by several other types of cells including astrocyte foot processes and pericytes (Figure 1.5). The astrocyte foot processes contribute to upregulation of tight junction proteins (both *in vivo* and *in vitro*), the development of polarized transport in the endothelial cell membranes and expression of enzymes (Abbott et al, 2006; DeBault and Cancilla, 1980; Jiang, et al, 2018; Tao-Cheng et al, 1987; Wolburg et al, 2009). The pericytes (Figure 1.5) regulate brain angiogenesis, endothelial cell

tight junction formation and BBB differentiation. They also contribute to microvascular vasodynamic capacity and structural stability (Balabanov and Dore-Duffy, 1998; Jiang et al, 2018).

In addition to astrocytes and pericytes, nerve terminals and microglia (Figure 1.5) are also closely associated with the endothelium. These cells form a second line of defence and play supporting roles in barrier induction, maintenance and function (Abbott et al, 2006; Abbott et al, 2010; Nakagawa et al, 2009; Shimizu et al, 2008).

1.5.2 The BBB function

Although it is only 0.4 μm thick, the BBB is claimed to stop most small molecular weight drugs and 100% of large molecular weight drugs from passing into the brain (Pardridge, 2005). The BBB does this via several mechanisms; by acting as a physical barrier (tight junctions between cells decreasing passive diffusion via the paracellular pathway), a metabolic barrier (enzymes metabolize molecules as they cross), and a transport barrier (efflux transporters) (Abbott et al, 2006). These three mechanisms are discussed in more detail below.

The tight junctions restrict transport by paracellular pathways through the BBB. To measure the "integrity" of the BBB, the transendothelial electrical resistance (TEER, which represents ionic permeability through tight junctions) is used (Claude, 1978). The TEER value of the BBB is approximately 1000 – 5000 Ω cm^2 whereas, in general capillaries, it is about 10 Ω cm^2 (Lo et al, 2001). Because of these complex and restricted tight junctions, only gases and small lipophilic molecules can pass the BBB by passive diffusion (Pardridge, 1993).

To form these endothelial tight junctions, occludin and claudin families are the most important integral membrane proteins with four transmembrane domains and two extracellular loops (Figure 1.7). The occludin and claudin molecules are established in lipid structures where their extracellular loops may interact with each other to form a paracellular barrier (Piontek et al, 2008). Other integral membrane proteins including members of the Ig superfamily, the endothelial cell-selective adhesion molecule (ESAM) and the coxsackie and adenovirus receptor (CAR) also contribute to the "seals" between cells (Gonzalez-Mariscal et al, 2007). In addition, adaptor proteins are part of tight junction components.

First-order adaptors directly associate with Zonula occludens (ZO)-1, ZO-2, and ZO-3, whereas second-order adaptors indirectly associate with cingulin, cingulin-related junction-associated coiled-coil protein. (Wolburg et al, 2009).

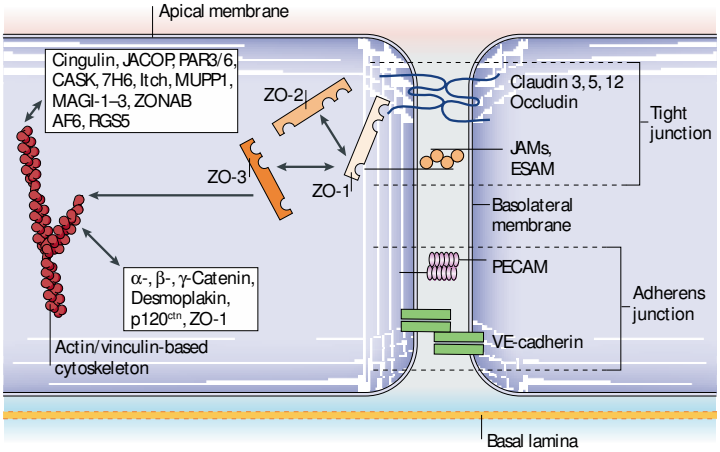

Figure 1.6 Molecular compositions of endothelial tight junctions.

Abbott et al, 2006, reproduced with permission

While the tight junctions form a physical barrier, the BBB is not only a static physical barrier but also a dynamic interface with physiological functions. The high volume of mitochondrial expression (Wolburg et al, 2009) and a variety of enzymes on the cellular plasma membranes (aminopeptidases, carboxypeptidases, endopeptidases, cholinesterases, monoamine oxidase and others) are characteristics of brain capillary endothelial cells (Agundez et al, 2014). Mitochondria and ecto-enzymes deactivate and/or inactive drugs that penetrate the cells of the BBB (Pardridge, 2002). It has been reported that CYP1B1 is the predominant CYP isoform (over 80%) in human brain microvessels (Dauchy et al, 2008). In addition, CYP2U1 and phase II enzymes encoded by GSPT1, GSTM2, 3, 5 and GSTO1 genes, are expressed at the BBB (Shawahna et al, 2011). Among which, glucuronosyltransferase, particularly UGT1A4 contributes to the main metabolic route of K (N-glucuronidation) (Kerdpin et al, 2009; Li et al, 2007). Interestingly, from another aspect, this metabolic barrier is also be used to produce active drugs from pro-drugs (Anderson, 1996).

The last barrier is constituted by efflux transporters, which function as pumps to expel substrates from cells back to the blood. There are three main efflux transporters of the adenosine triphosphate (ATP) binding cassette (ABC)

superfamily have been found at the BBB. They are P-gp, MRPs and breast cancer resistance protein (BCRP). Details of these transporters along with other transporters expressed at the BBB are discussed in below (Section 1.6).

1.5.3 General rules for passage through the BBB

Although BBB permeability is limited for most compounds, there are still some that pass freely through the BBB. Polar lipid soluble small molecules with a molecular weight < 500 Da and surface area < 50 – 100 Å cross the BBB (Fischer et al, 1998). In addition, the number of hydrogen bond donor/acceptor groups of a compound must be < 10. Furthermore, the compound should not be a substrate of BBB enzyme systems or BBB efflux transporters and should not bind excessively to plasma proteins (Pardridge, 2002).

Most of the rules apply to K and N, such as molecular weights are less than 500 Da, surface area (K: 48.6 Å) is less than 50 Å, and sum of hydrogen bond donor and acceptor groups (K: 2 and N: 3) are less than 10. Although 75% K binds to plasma proteins, it is possible that both K and N are transported by passive diffusion if they are not a substrate of BBB enzyme systems or BBB efflux transporters.

1.6 Transporters at the BBB

As discussed in Section 1.5, though restricted permeability caused by the BBB applies to both pharmaceutical compounds and nutrients, the brain must take up nutrients and dispose of metabolic wastes.

There are many transporters that serve important roles in drug delivery into/out of the CNS expressed at the BBB. These include the influx pumps organic anion transporting polypeptide (OATP)1A2, OATP2B1 and efflux pumps P-gp, BCRP, MRP4 and MRP5 (Figure 1.7). Compared with influx transporters, more interest has been focused on the efflux transporters.

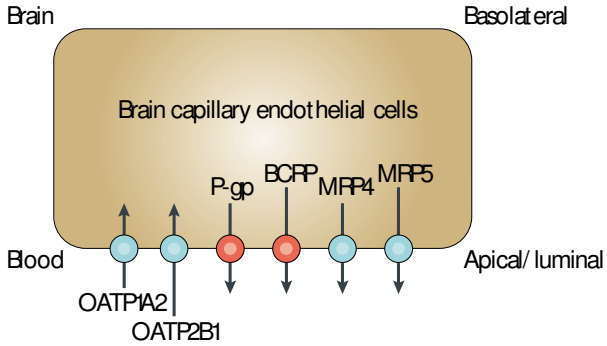

Figure 1.7 Apical (luminal) transport proteins of brain capillary endothelial cells contributing to the function of the blood–brain barrier including the uptake transporters OATP1A2 and OATP2B1, and the efflux pumps P-gp, BCRP, MRP4 and MRP5.

Giacomini et al, 2010, reproduced with permission

1.6.1 Efflux transporters

P-gp:

P-gp belongs to the multiple drug resistance (MDR) family (ABC family, ABCB). It is an active transporter that uses ATP to efflux its substrates independent of concentration gradient, electrochemical transmembrane potential or proton gradient (Konig et al, 2013; Schinkel, 1999). Human P-gp is a large, glycosylated membrane protein, which consists of approximately 1280 amino acids with a molecular weight of about 170 kD. It locates on the luminal membranes of cerebral capillary endothelial cells (Linnet and Ejsing, 2008; Schinkel, 1999). In addition to the BBB, P-gp expressed at organs and tissues such as liver and kidney, where it restricts the penetration of xenobiotics into cells in the small intestine, placenta (Konig et al, 2013), testes (Hughes et al, 1998) and the blood vessels that supply human gliomas and metastatic brain tumours (Gerstner and Fine, 2007).

P-gp recognizes and transports a very wide spectrum of substrates, which molecular weight from approximately 250 Da to more than 1850 Da (Linnet and Ejsing, 2008). It transports cationic and/or zwitterionic compounds (Tamai and Tsuji, 2000) including a wide variety of chemotherapeutic agents of natural origin (anthracyclines, vinca alkaloids, epipodophyllotoxins, and taxanes), peptides (immunosuppressive agents cyclosporine A), cardiac glycosides (digoxin), antipsychotics and antidepressants (risperidone, nortriptyline, and citalopram), HIV protease inhibitors, antibiotics (macrolides), β-blockers (carvedilol), the anthelmintic pesticide ivermectin (Konig et al, 2013; Linnet and

Ejsing, 2008) and antihistamine (fexofenadine) (Miura and Uno, 2010). Therefore, P-gp is important for delivery of pharmaceuticals and critical for transporter-mediated drug-drug interactions (DDIs) (Konig et al, 2013) and moreover, may potentially participate in transport of K and N.

Inhibitors of P-gp are classified based on their specificity and affinity into three generations. First-generation inhibitors are pharmacologically active drugs that include calcium channel blockers (verapamil), immunosuppressants (cyclosporin A), antihypertensives (reserpine, quinidine and yohimbine) and anti-oestrogens (tamoxifen and toremifena). High doses are required to achieve inhibition, which may result in toxicity. Second-generation inhibitors are agents that lack pharmacological activity but usually possess a higher P-gp affinity including non-immunosuppressive analogues of cyclosporin A, PSC 833, the D-isomer of verapamil (dexverapamil) and others such as biricodar (VX-710), GF120918 and MS-209. Because of the non-specific inhibition by this class of inhibitors, complicated DDIs may occur. Third-generation P-gp inhibitors are under development as highly specific inhibitors with low toxicity. Modulators such as LY335979, OC144093 and XR9576 have been shown to be highly potent as well as highly selective inhibitors of P-gp with potency about 10-fold greater than first- and second-generation inhibitors (Eyal et al, 2009; Varma et al, 2003).

MRP:

The human MRP family (ABC Family ABCC) consists of thirteen MRP proteins including one ion channel, two cell surface receptors, a truncated protein that does not mediate transport, and MRP 1 – 9. MRP 1 – 9 are ATP-dependent transporters, some of which require the presence of co-factors for their activity (Deeley et al, 2006). MRPs share approximately 15% amino acid sequence homology with P-gp (Loe et al, 1996). Consequently, there are partial overlaps of selectivity for other ABCC transporters, P-gp, ABCG2 and organic anion transporters (Eyal et al, 2009; Leggas et al, 2004).

MRP1, 2, 4, 5, 8 and 9 have been found in the brain (Dallas et al, 2006). However, only MRP1, 2, 4 and 5 have been detected at the BBB (Eyal et al, 2009; Kusuhara and Sugiyama, 2005; Potschka et al, 2003) and only MRP1, 4 and 5 are confirmed to be located on the luminal membrane of the human BBB (Dallas et al, 2006). More recent research on brain MRP protein quantification using liquid

chromatography-mass spectrometry (LC−MS) suggests that only MRP4 is expressed in quantifiable levels at the human and rodent BBB (Agarwal et al, 2012; Kalvass et al, 2013; Shawahna et al, 2011). Therefore, in respect of transporters in the BBB, MRP4 is the most important in the MRP family.
Substrates of MRP4 include a variety of mono-phosphorylated compounds, cyclic nucleotides (cyclic adenosine monophosphate and cyclic guanosine monophosphate), nucleotide analogs (9-(2-phosphonylmethoxyethyl)adenine) and azidothymidine monophosphate and purine analogs (6-mercaptopurine and 6-thioguanine) (Chen et al, 2001; Dallas et al, 2006; Lai and Tan, 2002; Reid et al, 2003; Schuetz et al, 1999; Wielinga et al, 2003).
Although MRP4 plays an important role in BBB function, it is predominantly an organic anion transporter, also transporting neutral organic compounds. Therefore, it is unlikely to participate in transport of K and not discussed further.
BCRP:
BCRP (ABC family, ABCG) is one of the luminal/apical localized ABC transporters present in human brain microvessels (Cooray et al, 2002; Dauchy et al, 2008; Zhang et al, 2003). This so-called half-size ABC transporter (consists of only 655 amino acids, half the size of P-gp and MRP2) has been found at almost twice the concentration of P-gp in brain microvessels (Shawahna et al, 2011).
Substrates of BCRP include antivirals (acyclovir), statins (Matsushima et al, 2005) and antibiotics (ciprofloxacin and ofloxacin), as well as diclofenac, sulfasalazine, cimetidine, endogenous substances and metabolites (vitamin K3), and uric acid. The substrate specificity of BCRP partially overlaps with that of P-gp. Compounds efflux by both P-gp and BCRP including zidovudine, lamivudine, prazosin, pantoprazole, and the chemotherapeutic agents methotrexate, doxorubicin, daunorubicin, mitoxantrone, topotecan, irinotecan, imatinib (Gleevec) and gefitinib (Iressa) (Eyal et al, 2009).
Inhibitors of BCRP include GF 120918 (also inhibits P-gp), fumitremorgi C (FTC) and FTC analogues such as Ko132, Ko134, and CI1033 (Wolfgang and Heidrun, 2005), cyclosporine, tacrolimus, omeprazole and pantoprazole and saquinavir (Konig et al, 2013). BCRP protects the brain against toxicants, xenobiotic, and their metabolites.

1.6.2 Other transporters (influx transporters)

In addition to the three main efflux transporters, other drug transporters have been found at the BBB. Transporters of the solute carrier (SLC) superfamily include facilitated transporters and ion-coupled transporters and exchangers that do not require ATP. Over 360 human SLC transporters have been identified (Hediger et al, 2004). The SCL family plays an important role especially in organic anions transport (Kusuhara and Sugiyama, 2005). The organic anion transporting polypeptides and organic anion/cation/zwitterion transporter families have an important role in drug transport into the brain (Eyal et al, 2009). They are divided into the following subfamilies: OAT, OATP, organic cation transporter (OCT), organic cation/zwitterion transporter (OCTN), concentrative nucleoside transporter (CNT), the equilibrative nucleoside transporter (ENT), multidrug and toxin extrusion transporter (MATE), and others (Bauer et al, 2005). Transporters that are not expressed in brain or at the BBB are not covered in this section.

OATPs:

There are eleven members in the human OATP family (SLC21/SLCO). Based on amino acid sequence similarities, they are divided into six subfamilies OATP1 – 6 (Hagenbuch and Meier, 2004). The OATPs are sodium-independent, multi-specific anion exchangers. They mediate bidirectional transport that depends on local substrate gradients. In this family, three transporters (OATP1A2, OATP2B1 and OATP1C1) have been identified on human brain endothelial cells (Giacomini et al, 2010; Lai, 2013).

Substrates of OATPs are anionic amphipathic molecules with molecular weights > 450 Daltons and a high degree of albumin binding. These consist of a broad range of drugs including antibiotics, chemotherapeutic agents, antihistaminic drugs, diuretics (fexofenadine, digoxin, and methotrexate) and several endogenously synthesized metabolites such as bile acids, thyroid hormones, or hormone conjugates (Konig et al, 2013; Lai, 2013).

OAT:

OATs do not require energy for transporting substrates. They are anion exchangers, which take up an organic anion into a cell and release another organic anion from the cell, or vice versa (Koepsell and Endou, 2004).

OATs consist of OAT1 – 4 (Konig et al, 2013). The summary of this transporter family is listed below (Table 1.8).

Table 1.8 Summary of organic anion transporter.

OAT family	Expression location	Substrate* examples	Inhibitor* examples	Reference
OAT1 (SLC22A6)	It is highly expressed in basolateral membrane of proximal tubule cells in kidney. It is also expressed in the brain (cerebellum, choroid plexus, hippocampus and hypothalamus) and the placenta.	Substrates include angiotensin-converting enzyme (ACE) inhibitors (captopril), diuretics (bumetanide and furosemide), antibiotics (ceftibuten) and antivirals (ganciclovir).	Statins are OAT1 inhibitors.	Lopez-Nieto et al, 1997; Cihlar and Ho, 2000; Sweet et al, 2002; Khamdang et al, 2004; Giacomini et al, 2010
OAT2 (SLC22A7)	It is highly expressed in human liver. It is also expressed on basolateral membrane of proximal tubule cells in kidney.		Statins are OAT2 inhibitors.	Sekine et al, 1997; Enomoto et al, 2002a; Khamdang et al, 2004
OAT3 (SLC22A8)	It is expressed in basolateral membrane of proximal tubule cells in kidney.	Substrates include ACE inhibitors (quinapril) angiotensin II receptor blockers (olmesartan) several diuretics, and antibiotics (rosuvastatin and pravastatin) and nonsteroidal antiinflammatory drugs (cefaclor, ceftizoxime, furosemide and bumetanide).	Inhibitors include atorvastatin, fluvastatin, pravastatin, rosuvastatin, simvastatin, probenecid and novobiocin.	Kusuhara et al, 1999; Hasegawa et al, 2002; Khamdang et al, 2004; Windass et al, 2007; Yuan et al, 2009; Yamada et al, 2007; Giacomini et al, 2010
OAT4 (SLC22A11)	It is expressed in the luminal membrane of proximal tubule cells in kidney.	Substrates include diuretics (bumetanide), torasemide and antineoplastic agent (methotrexate).		Babu et al, 2002; Hasannejad et al, 2004; Hagos et al, 2007; Takeda et al, 2002

* Detailed spectra of substrates and inhibitors are summarised in a book (Lai, 2013)

OCT and OCTN:

Organic cation transporters (OCTs) are sensitive to potential. They are facilitated uniporters that are independent of Na+ (Koepsell et al, 2007). OCTs include OCT1 – 3 and 6, and mediate the absorption, distribution and excretion of cationic drugs (Ciarimboli et al, 2016). A summary of this transporter family is listed in the table below (Table 1.9).

Table 1.9 Summary of organic cation transporters.

	Expression location	Substrate* examples	Inhibitor* examples	Reference
OCT1 (SLC22A1)	It is strongly expressed in the sinusoidal membrane of hepatocytes and has a weaker expression in small intestine, lung, heart, kidney, skeletal muscle, brain, placenta, eye, adrenal gland, immune cells, and skin.	Endogenous compounds monoamine and neurotransmitters (serotonin, dopamine, and agmatine), etc. Drugs such as metformine, lamivudine, acyclovir, oxaliplatin, picoplatin and sorafenib. Toxins such as aflatoxin B1 or ethidiumbromide etc.	Common inhibitors for both OCT1 and OCT2 include proton pump inhibitors (PPI, such as omaprazol and lansoprazole) tetrapropylammonium, tetrapentylammonium and desipramine, etc. EC_{50} for procainamide is 68-fold lower for OCT1 compared with OCT2	Arndt et al, 2001; Koepsell, 2013; Ciarimboli et al, 2016; Nies et al, 2011; Urtti, 2011
OCT2 (SLC22A2)	It is strongly expressed in the basolateral membrane of kidney proximal tubules and has a weaker expression in lung, placenta, brain (hippocampus, choroid plexus), small intestine, thymus, and inner ear	The substrate specificity of OCT2 is broadly overlapping with OCT1, with some exceptions such as histamine, epinephrine and norepinephrine, etc.	Common inhibitors for both OCT1 and OCT2 include PPI (omaprazol and lansoprazole etc.), tetrapropylammonium, tetrapentylammonium and desipramine, etc. EC_{50} for corticosterone is 38-fold lower for *OCT2* compared to rOCT1	Arndt et al, 2001; Busch et al, 1998; Koepsell, 2013; Ciarimboli et al, 2016; Lai, 2013; Nies et al, 2011; Urtti, 2011
OCT3 (SLC22A3)	It is expressed in brain (cortex, hippocampus, and substantia nigra), heart, skeletal muscle, liver, lung, kidney, small intestine, skin, mammary gland, and placenta	Endogenous compounds such as neurotransmitters, epinephrine, norepinephrine, histamine and agmatine. Drugs such as metformin, oxaliplatin, lamivudine, lidocaine, quinidine, etilefrine, etc.	Inhibitors include PPI (omaprazol and lansoprazole etc.)	Koepsell et al, 2007, Koepsell, 2013; Nies et al, 2011; Urtti, 2011
OCT6 (SLC22A19, CT2)	It is expressed in testis and epididymis, expressed at lower level in embryonic liver, hematopoietic cells, and several cancer cells	It has a high affinity for carnitine.		Koepsell, 2013; Enomoto et al, 2002b

* Detailed spectra of substrates and inhibitors are summarised in a book (Lai, 2013).

It is reported that OCT1 and 2 may be involved in transport of cationic drugs through the BBB (Koepsell, 2013; Volk, 2014). However, literature suggests OCT is unlikely to be the transporter that participates in transport of K (Ishiguro et al, 2004).

OCTN depend on membrane potential and/or concentration gradient for cation translocation (Lai, 2013). This transporter family incudes OCTN 1 – 3 (Volk, 2014). A summary of this transporter family is listed in the table below (Table 1.10).

Table 1.10 Summary of organic cation and zwitterion transporters (OCTNs).

	Expression location	Substrate* examples	Inhibitor* examples	Reference
OCTN1 (SLC22A4)	It is expressed in kidney, intestine, spleen, heart, skeletal muscle, brain, mammary gland, thymus, airways, and male reproductive tract.	Physiologically, OCTN1 is an ergothioneine transporter. Substrates include quinidine, verapamil, gabapentin, and oxaliplatin, etc. It has a low affinity to carnitine.	Inhibitors include cimetidine, cisplatin, clonidine etc.	Lai, 2013; Tamai, 2013; Volk, 2014
OCTN2 (SLC22A5)	It is expressed in kidney, skeletal muscle, placenta, heart, prostate, and thyroid. It is also expressed at lower level in small intestine, liver, lung, or brain.	Physiologically, OCTN2 is a carnitine transporter. Substrates include carnitine, TEA, choline, verapamil, or spironolactone, etc.	Inhibitors include acetylcholine, cefadroxil, ipratropium, etc.	Koepsell, 2013; Lai, 2013; Tamai, 2013
OCTN3	Not detected in human			

* Detailed spectra of substrates and inhibitors are summarised in a book (Lai, 2013).

Monocarboxylic acid transport systems (MCT):

MCT1 (SCL16A1) present on both luminal and abluminal sides of brain capillary endothelial cells and it may be responsible for the transport of some organic anions from brain to endothelial cells and then to blood (Tamai and Tsuji, 2000). Substrates of MCT1 include lactate, pyuvate and the ketone bodies acetoacetate and β-hydroxybutyate (Galic et al, 2003).

1.7 Stereoselective transporters and receptors at the BBB

Stereoselective absorption, disposition, metabolism and elimination can result from stereoselective transport and/or receptor activity (Table 1.7). Similarly, the difference in sedative effects of K and N atropisomers could also be due to their different affinities for BBB transporters and/or CNS H_1 receptors.

P-gp plays an important role in minimizing the sedative effects of second-generation antihistamines including fexofenadine, cetirizine, loratadine, ebastine (Ecker and Chiba, 2009; Miura et al, 2007; Miura and Uno, 2010). Moreover, P-gp has been reported to be stereoselective for some second-generation antihistamines (fexofenadine) and other drugs (citalopram, mefloquine, loperamide, tacrolimus, pioglitazone and ivermectin) (Chang et al, 2015; Choong et al, 2010; Miura et al, 2007; Miura and Uno, 2010). S-Fexofenadine has been reported to have a higher P-gp affinity than the R-enantiomer (Miura et al, 2007). Sakugawa et al indicated that in the presence of verapamil (a P-gp inhibitor), the pharmacokinetics of S-fexofenadine showed a greater change than that of R-fexofenadine. With verapamil, the AUCs of the S- and R-enantiomers were 3.5- and 2.2-fold higher respectively compared with the AUCs without verapamil (Sakugawa et al, 2009). Interestingly, P-gp can be regulated stereoselectively by cetirizine enantiomers (Shen et al, 2007).

Not only P-gp, but the MCT has also been reported to be highly stereospecific for substrates and show evidence of selectivity for amino acids (Bickel et al, 2001). The glucose transporter (GLUT)-1 is stereoselective for the D-glucose stereoisomer (McAllister et al, 2001).

However, some publications indicate that investigating stereoselective transport using total brain-to-plasma (B/P) ratio could be misleading. Gupta et al reported that the stereoselective transport of S-cetirizine results from stereoselective plasma protein and brain tissue binding (Gupta et al, 2006). This suggests it is important and necessary to determine the free B/P ratio to study stereoselective transport (Chapter 7).

Stereoselective transporters and enzymes contribute to chiral drug delivery and stereoselective receptors also play an important role. For instance, Gustavo et al reported stereoselectivity of the H_3 receptors based on the different affinity and

potency of the ligand enantiomers of R-α-methylhistamine (H_3 receptor agonist) and thioperamide (H_3 receptor antagonist) (Gustavo et al, 2016). More examples are shown in Table 1.11 (Smith and Jakobsen, 2007).

Table 1.11 Examples of stereoselective receptors in the central nervous system. Data were summarised from a review paper.

Receptors	Preferred enantiomer/atropisomer	Reference
Muscarinic acetylcholine receptor	[^{123}I]4-iododexetimide was a high affinity antagonist whereas [^{123}I]4-iodolevetimide was inactive	Muller-Gartner et al, 1992
α2-Noradrenergic receptor	Accumulation of S-[^{11}C]mirtazapine was greater than that of R-[^{11}C]mirtazapine	Smith et al, 2006
D_1-dopamine receptor	D_1-dopamine receptor was selectively inhibited by R-NNC 122 whereas S-NNC 122 lacks affinity for this receptor.	Anderson et al, 1992
Opiate receptor	The (5R,6R)-cyclofoxy has high affinity at μ- and κ- receptors (*in vitro*), whereas (5S,6S)-cyclofoxy has virtually no affinity for opiate receptors.	Ostrowski et al, 1987

Smith and Jakobsen, 2007

1.8 Aim of this thesis

Enzymes, transporters, receptors and protein binding can contribute to the stereoselective delivery of chiral compounds through the BBB. In this thesis, the reason for the lower sedative effect of SN than of SK, RK and RN was investigated. The following questions were posed and consequent investigations performed.

Is there stereoselective transport of K and/or N into/through brain capillary endothelial cells? Immortalized rat brain endothelial (RBE4) and Caco-2 cell models were used for uptake and permeability studies respectively (Chapter 5);

Is there stereoselective binding of K and/or N to the CNS H_1 receptor? CNS H_1 receptor occupancy assay was used (Chapter 6);

Is there stereoselective transport at the BBB? Rat tail vein injection technique was used to investigate the total and free B/P ratios of K and N (Chapter 7).

To aid understanding and interpretation of *in vitro* and *in vivo* results, log P, log D of racemic K and N by different systems at different temperatures (4, 25 and 37°C) were determined (Chapter 3).

To analyse samples in bio-matrices from *in vitro* and/or *in vivo* studies, chiral and nonchiral high-performance liquid chromatography (HPLC) assays were developed and validated (Chapters 2 and 4).

Chapter 2 Nonchiral HPLC assay development and validation

2.1 Introduction

As HPLC is one of the most robust and widely used analytical techniques, it was chosen to be the basis for both a nonchiral assay to simultaneously determine racemic K and N and chiral assays to determine K and N atropisomers. Previous publications have reported nonchiral assays to determine racemates of K by HPLC (Le Bigot et al, 1983, 1987; Yagi et al, 2002; Nnane et al, 1998) and LC–MS (Tashiro et al, 2005) and nonchiral LC–MS assays to determine K and N (Mey et al, 1999; Milner et al, 2012) in various matrices. Although the LC–MS assay of Milner et al. (2012) determined both K and N in mouse plasma, it was decided to develop a less complex HPLC assay for their determination in RBE4 cell homogenate.

In developing an HPLC assay to simultaneously determine K and N racemates, the choice of stationary phase (SP) is crucial. In this regard Yagi et al, (2002) reported a C_8 SP gave better separation of K from endogenous peaks in plasma than a C_{18} SP despite having little effect on its retention time (Rt). Thus, a C_8 column was used here to develop the nonchiral HPLC assay for simultaneous determination of K and N.

2.2 Materials

2.2.1 Chemicals and reagents

RBE4 cells were kindly provided by Professor Michael Aschner (Vanderbilt University, Nashville, TN, USA). Sodium dihydrogen phosphate monohydrate (99%) and potassium dihydrogen orthophosphate (≥ 99.5%) were purchased from BDH Laboratory Supplies (England). Racemic K and N fumarates (> 98%) were provided by GL Synthesis Inc. (MA, USA) through the kind offices of Dr Gunnar Aberg, BridgePharma, Sarasota, FL, USA. Acetonitrile (ACN), methanol, isopropanol and n-hexane were purchased from Merck (Darmstadt, Germany). HEPES (≥ 99.6%), anhydrous calcium chloride (≥ 96%) and Krebs-Ringer

bicarbonate buffer were obtained from Sigma (Auckland, New Zealand). The BCA™ protein assay kit was purchased from PIERCE (Rockford, IL, USA).

2.2.2 Instrumentation (HPLC system)

The HPLC system (Shimadzu Prominence series) consisted of a degasser (DGU-20A5), pump (LC-20AD), autosampler (SIL-20AC), C_8 column (Luna 5 µm, 150 × 4.6 mm, Phenomenex), column oven (CTO-20A) and diode array detector (SPD-M20A). The software used for data analysis was CLASS-VP7.4 SP4. C_{18} guard cartridges, 0.45 µm nylon filter membranes, 100 µl HPLC inserts (PP LV, 5 × 32 mm) and liners (PTFE/SIL, 8 mm) were purchased from Grace Davison Discovery Science (Deerfield, IL, USA).

2.3 Assay development and validation

2.3.1 Chromatagraphy

Separation of K and N was assessed in terms of the separation factor α, a higher α value indicating better separation. The α value was calculated using Equation 2.1:

$$\alpha = (Rt_2 - Dt) / (Rt_1 - Dt) \qquad 2.1$$

where Rt_1 and Rt_2 are the retention times of the first and second peak respectively, and Dt is the column dead time (time to the solvent front).

As part of assay development, factors potentially affecting the separation of K and N including mobile phase composition, mobile phase pH, column temperature and flow rate were investigated as follows:

Mobile phase composition: Flow rate 1 ml/min, column temperature 30°C, mobile phase ACN:50 mM phosphate buffer pH 6; 30:70, 40:60 and 50:50.

Mobile phase pH: Flow rate 1 ml/min, column temperature 30°C, mobile phase 30:70 ACN:50 mM phosphate buffer; pH 4, 5 and 6.

Column temperature: Flow rate 1 ml/min, mobile phase 30:70 ACN:50 mM phosphate buffer pH 6; column temperature 20, 25, 30 and 40°C.

Flow rate: Mobile phase 30:70 ACN:50 mM phosphate buffer pH 6, column temperature 30°C; flow rate 1.0, 1.2 and 1.5 ml/min.

Detection was at 310 nm despite the fact that the wavelength of maximum absorption of both K and N is at 295 nm (Yagi et al, 2002). This is because the

peak due to K was subject to interference from an endogenous peak, which was not detected at 310 nm. In addition, the absorption of K and N at 310 nm was only slightly lower than at 295 nm. Quantitation was based on determination of peak areas.

Another factor considered was whether to include an internal standard (IS). It was decided an IS was not necessary because sample preparation involved simple protein precipitation, recovery was consistently > 90% and accuracy and precision were acceptable based on the Bioanalytical Method Validation, Guidance for Industry of U.S. Food and Drug Administration (FDA) (2001).

2.3.2 Sample preparation

RBE4 cell monolayers in 75 cm^2 collagen coated cell culture flask (BD BioCoat™, England) were washed with 5 ml Ringer-HEPES buffer (10 mM HEPES 1.2 mM calcium chloride, pH 7.4). Milli-Q water (5 ml) was added to each flask and incubated at 4°C overnight to lyse cells. Cell suspensions were collected by pipetting up and down several times and transferred to 1.7 ml centrifuge tubes. Glass beads were added and sample mixtures homogenised at speed 7 for 3 min using a Bullet Blender® (NEXT >>>ADVANCE, NY, USA). All homogenates were mixed together and protein concentration determined using 50 µl aliquots of homogenate in the BCA™ protein assay. The final protein concentration in quality control (QC) samples was approximately 250 µg/ml.

Sample preparation of RBE4 cell homogenate (or calibration standards or QC samples) involved protein precipitation using 2 volumes ACN (180 µl sample plus 360 µl ACN) followed by vortexing and centrifuging (Eppendorf AG, Hamburg, Germany) at 10,000 rpm for 10 min. Supernatant (510 µl) was transferred into a clean tube and dried under vacuum at room temperature (Speed Vac Concentrator and Refrigerated Vapor Trap RVT4104, SAVANT) overnight. The residue was reconstituted in mobile phase (60 µl) followed by vortexing and centrifuging at 10,000 rpm for 10 min. Finally 55 µl supernatant was transferred into an HPLC insert and 50 µl injected into the HPLC system.

2.3.3 Validation

Stock and standard solutions: K and N racemates (1 mg/ml) were dissolved in methanol. Further dilutions were made using Milli-Q water to give standard solutions with concentrations in the range 1 – 5 µg/ml.

Calibration standards and QC samples: Mixed calibration standards containing 20, 40, 80, 125 and 200 ng/ml K and N racemates (Table 2.1) and low, medium and high mixed QC samples (QCL, QCM and QCH) containing 25, 50 and 100 ng/ml K and N racemates respectively (Table 2.2) were freshly prepared on each assay day by spiking RBE4 cell homogenate with K and N standard solutions.

Table 2.1 Preparation of mixed calibration standards for K and N racemates in RBE4 cell homogenate.

Final concentration (ng/ml)	Standard solution concentration (µg/ml)	Standard solution (µl) (for both K and N)	Milli-Q water (µl)	Cell homogenate (µl)
20	1	16	84	700
40	1	32	68	700
80	2	32	68	700
125	2	50	50	700
200	5	32	68	700

Table 2.2 Preparation of mixed QC samples for K and N racemates in RBE4 cell homogenate.

Final concentration (ng/ml)	Standard solution concentration (µg/ml)	Standard solution (µl) (for both K and N)	Cell homogenate (µl)
25	1	225	8775
50	2	225	8775
100	4	225	8775

Linearity and lower limit of quantitation (LLOQ): Linearity was determined based on construction of three calibration curves in the concentration range 20 – 200 ng/ml. The LLOQ was taken as the concentration with a signal-to-noise ratio of 5 to 1 (FDA 2001).

Recovery: Recovery (%) was determined using triplicate QC samples as the peak area of the compound after sample preparation compared with the peak area of

the compound at the same concentration in mobile phase without sample preparation.

Accuracy and precision: Intra- and inter-day accuracy (as percent relative error, RE) and precision (as percentage coefficient of variation, CV) were determined by analysis of 5 replicates of QC samples on 3 different days. Intra- and inter-day values are calculated according to Equations 2.2 and 2.3 respectively:

$$\textbf{Accuracy (\%)} = (\sum |Di - S| \times 100) / N \qquad \textbf{2.2}$$

$$\textbf{Precision (\%)} = (SD / mean) \times 100 \qquad \textbf{2.3}$$

where Di is the determined concentration, S is the nominal concentration, SD is the standard deviation and N is the number of determinations.

For intra-day accuracy and precision, calculation was based on data from individual days (n = 5) while for inter-day values, a combination of data for all three days (n = 15) were used.

Stability: Stability of racemic K and N in QC samples and in processed samples in the autosampler were investigated. The storage conditions are shown in Table 2.3. The remaining concentration (recovery) after storage was calculated using Equation 2.4.

$$\textbf{R (\%)} = (Di/C_0) \times 100 \qquad \textbf{2.4}$$

where R is the percentage of remaining stable compound, Di is the determined concentration after storage and C_0 is the determined concentration of fresh made QC sample.

Table 2.3 Conditions of storage to determine stability of racemic K and N in RBE4 cell homogenate and processed samples.

Conditions	Storage temperature (°C)	Storage time
Bench top	25 ± 1	4 h
Autosampler (processed samples)	4	24 h
3 Freeze-thaw cycles (- 80 to 25°C)	N/A	N/A
Long-term storage	- 80	2 months

2.4 Results and discussion

2.4.1 Assay development

Different HPLC conditions were tested to achieve the best separation of K and N, in addition, intensity of responses of these two compounds were also considered. Figure 2.1 showed the elution order of K and N on a C_8 column in the optimized conditions. The tested HPLC conditions are shown in the following sections.

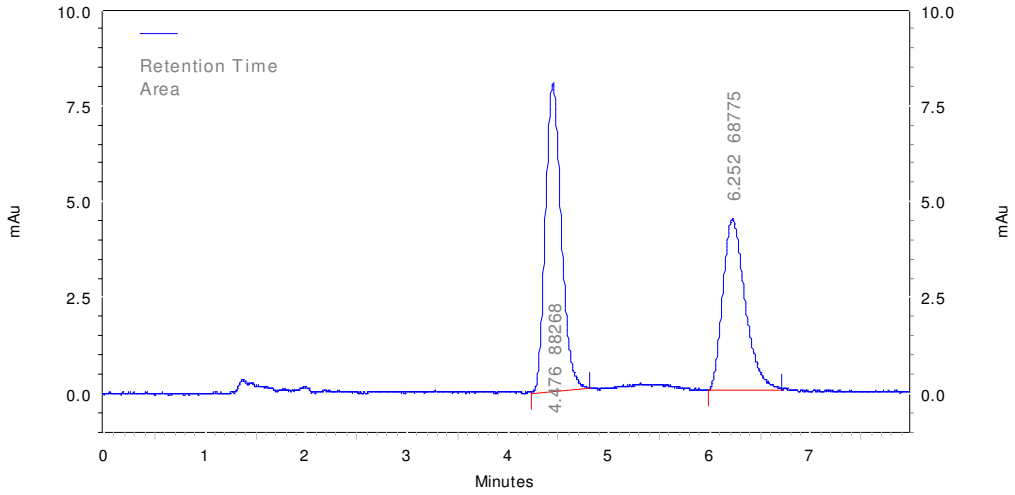

Figure 2.1 Chromatograph of 125 ng/ml racemic ketotifen (6.25 min) and norketotifen (4.47 min) in mobile phase.

Mobile phase composition: Increasing the ACN percentage in the mobile phase from 30% to 50% decreased the Rt of both K and N but had no effect on α (Figure 2.2 a).

Mobile phase pH: Increase in mobile phase pH from 4 to 6 increased the Rts of both K and N and, because the Rt of K increased more than that of N, increased α particularly from pH 5 to 6 (Figure 2.2b).

Column temperature: Increasing the column temperature from 20 to 40°C decreased the Rts of both K and N but had little effect on α (Figure 2.2c).

Effect of flow rate: Increasing the flow rate from 1.0 to 1.5 ml/min decreased the Rts of both K and N and slightly decreased α (Figure 2.2d).

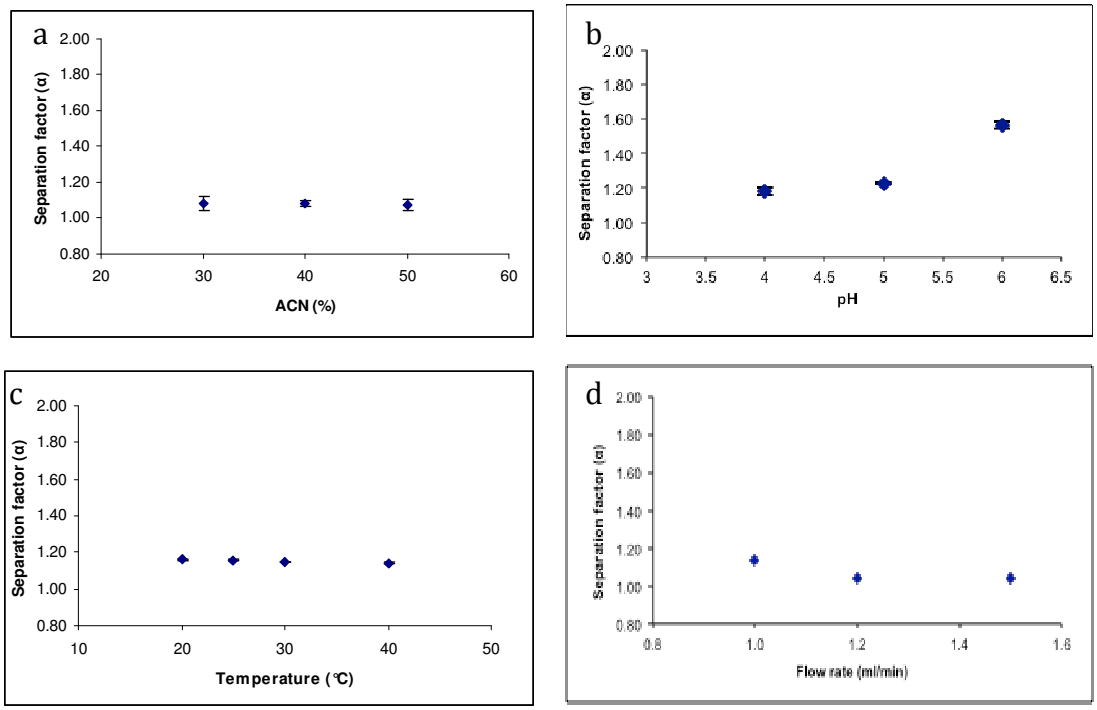

Figure 2.2 Effects of changing HPLC conditions on the separation factor (α) of racemic K and N; (a) mobile phase composition, (b) mobile phase pH, (c) column temperature and (d) flow rate (for conditions of each chromatograph see Section 2.3).

The factor causing most change in the separation of K and N in RBE4 cell homogenate was the mobile phase pH. With increasing pH (from 4 to 6), the Rt of K increased from 5.43 min to 6.98 min while that of N increased only slightly from 4.76 min to 4.89 min such that separation between K and N increased. This is presumably because of the increasing difference in degree of ionization between K and N as pH increases from 4 to 6. The result is contrary to the findings of Galaon and David (2012) who found that as pH increased from 7 to 8.5, the retention of N increased more than that of K such that their separation decreased.

This discrepancy arises because, in changing form pH 4 to 6, the percent unionized K (pKa 8.8) increases from 0.002% to 0.2% whereas that of N (pKa 10.4) increases from 0.00004% to 0.004%. In changing from pH 7 – 8.5, the percent unionized K increases from 1.6% to 33.4% whereas that of N increases from 0.04% to 1.3%.

The optimized conditions for the assay were mobile phase 30:70 ACN:50 mM phosphate buffer pH 6 delivered at a flow rate of 1 ml/min through a column maintained at 30°C. A chromatograph of K and N under these conditions is shown in Figure 2.3.

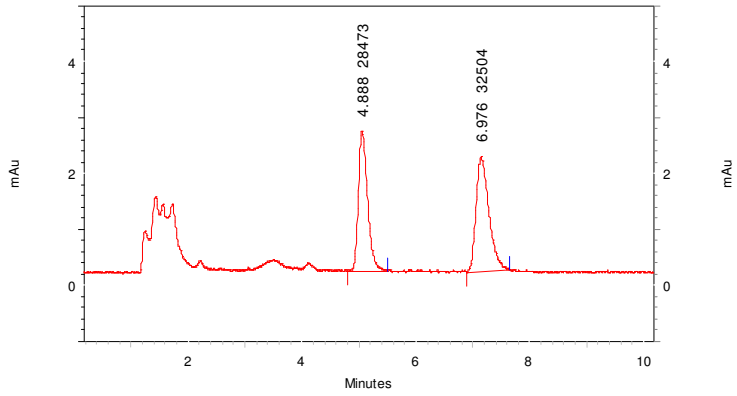

Figure 2.3 HPLC of 80 ng/ml racemic ketotifen (6.98 min) and norketotifen (4.89 min) in RBE4 cell homogenate (α = 1.6) using the optimized condition for the assay.

2.4.2 Assay validation

Linearity and LLOQ: The assay was linear ($R^2 > 0.999$) for both K and N (Figure 2.4) in the concentration range tested. The LLOQ for both K and N was 20 ng/ml.

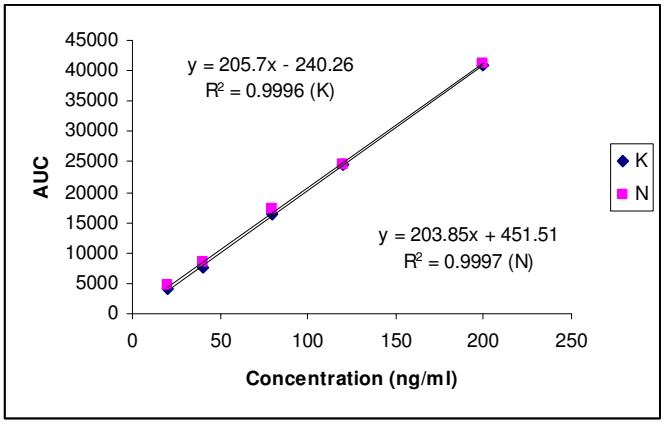

Figure 2.4 Calibration curves of racemic K and N in RBE4 cell homogenate (data are means ± SD, *n* = 3).

Recovery: The recovery was > 90 % at all three QC concentrations.

Accuracy and precision: Intra- and inter-day accuracies were satisfactory with concentrations ± 8 % of the nominal values at all QC concentrations. Intra- and inter-day precisions were < 19% for QCL and < 9% for QC M and QC H samples

(Table 2.4). These results indicate that the accuracy and precision of the assay meet the requirements of the FDA guidelines (2001).

Stability: Under all storage conditions (Table 2.5), the concentrations of K and N racemates in QC samples remained ± 10 % of the nominal concentrations (Table 2.5). This shows K and N are stable in RBE4 cell homogenate under the tested storage conditions.

In conclusion, the nonchiral HPLC assay is a simple, reliable and accurate tool to determine racemic K and N in RBE4 cell homogenate and buffer solutions in log P and log D determinations.

Table 2.4 Accuracy and precision of the HPLC assay for racemic ketotifen (K) and norketotifen (N) in RBE4 cell homogenate (data are means ± SD for assay of 5 replicates on 3 different days).

		Theoretical QC concentration (ng/ml)	Determined QC concentration (ng/ml)	Accuracy RE (%)	Precision CV (%)
K	Intra-day 1	L (25)	25.1	6.0	6.6
		M (50)	50.1	0.9	3.5
		H (100)	96.4	4.0	4.9
	Intra-day 2	L (25)	26.1	4.8	12.1
		M (50)	51.2	3.5	5.4
		H (100)	104.7	4.7	3.0
	Intra-day 3	L (25)	24.8	4.0	15.2
		M (50)	48.9	4.0	8.9
		H (100)	101.3	2.0	2.5
	Inter-day	L (25)	25.3	5.1	10.6
		M (50)	50.1	2.8	5.7
		H (100)	100.8	3.8	3.5
N	Intra-day 1	L (25)	22.8	7.3	18.0
		M (50)	49.1	2.3	4.3
		H (100)	101.2	4.3	2.6
	Intra-day 2	L (25)	24.4	4.8	12.9
		M (50)	51.1	3.5	5.4
		H (100)	103.3	4.7	3.1
	Intra-day 3	L (25)	25.2	4.7	18.7
		M (50)	49.8	4.0	8.7
		H (100)	101.2	2.0	2.5
	Inter-day	L (25)	24.1	5.7	15.6
		M (50)	50.0	3.3	5.6
		H (100)	101.9	3.9	2.8

Table 2.5 Stability of racemic ketotifen (K) and norketotifen (N) in RBE4 cell homogenate stored under different conditions (data are means ± SD, *n* = 3 for percent compound remaining).

	QC concentration (ng/ml)	Recovery (%) under different storage conditions			
		25°C (4 h)	4°C (24 h) (processed)	Freeze- thaw (3 cycles)	-80°C (2 months)
K	25	91.3 ± 3.8	109.2 ± 5.5	101.6 ± 4.7	106.4 ± 3.3
	50	90.8 ± 2.5	103.9 ± 2.8	98.5 ± 3.2	100.9 ± 3.0
	100	94.6 ± 5.0	102.7 ± 2.4	106.2 ± 1.8	102.8 ± 2.7
N	25	92.7 ± 4.5	99.6 ± 1.3	101.1 ± 1.3	97.0 ± 2.7
	50	95.2 ± 2.1	102.1 ± 3.5	97.7 ± 3.9	99.5 ± 0.4
	100	99.9 ± 4.5	100.1 ± 2.8	105.5 ± 2.0	105.2 ± 2.4

Chapter 3 Partition and distribution coefficients of ketotifen and norketotifen

3.1 Introduction

The partition coefficient P of a drug is usually determined in octanol/water (log P) as a measure of its relative lipophilicity. If the compound is ionised at or close to physiological pH (7.4), the distribution coefficient D is determined in octanol/buffer (log D). Log D at a particular pH is a measure of the relative lipophilicty of the compound at that pH. Generally log D < log P since the ionised form of the drug has low solubility in octanol. This is the case with K and N which exist as equilibrium mixtures of free base and positively charged conjugate acid. The calculated log P values of K and N (Table 3.1) from SciFinder Scholar (CAS) indicate K is less lipophilic than N, which is contrary to expectation based on their structures. However, the calculated log D values (octanol/buffer pH 7) are in the opposite order and are much lower than the corresponding log P values.

Table 3.1 Calculated log P and log D (pH 7) of ketotifen and norketotifen at 25°C obtained from SciFinder Scholar (CAS).

	Log P	Log D (pH 7)
K	2.19 ± 0.73	0.37
N	2.65 ± 0.51	-0.26

Log P and log D values are useful in predicting the passive diffusion of drugs through cell membranes in cell uptake and permeability studies. However, effect of temperature on log D measurement is a complex interplay between multiple factors, such as distribution, pKa of drug and buffer. Therefore, to better interpret results from cell experiments (Chapter 5), it is important to determine log P and log D at certain temperatures, at which experiments were carried out. This chapter reports the determination of log P and log D of K and N at temperatures (4°C, 25°C and 37°C) relevant to such studies in Chapter 5 (REB4 cell uptake at 4°C and 37°C and Caco-2 cell permeability at 37°C).

Although log D in an octanol/buffer system is a convenient measure of relative lipophilicity, it does not necessarily reflect distribution across a cell membrane. A

more valid measure of this distribution can be obtained using liposomes because, like cells, they possess lipid bilayers with similar negative charges on their surfaces. This chapter also reports log D values of K and N in the liposome/Ringer-HEPES buffer pH 7.4 system at 37°C.

3.2 Materials

Soy lecithin phospholipid was obtained from Lipoid (GmbH, Ludwigshafen, Germany). Cholesterol (approx. 95%) was obtained from Sigma (USA). Other materials and chromatographic conditions are described in Section 2.2.

3.3 Methods

3.3.1 Assay

The nonchiral HPLC assay (Chapter 2) was used to analyse samples from partition and distribution studies. Samples from octanol/water and octanol/buffer systems were dried under vacuum at room temperature to remove any residual octanol after which residues were reconstituted in mobile phase and analysed by HPLC. Both buffer and octanol phases were analysed whereas in the liposome/buffer system, only the buffer was analysed.

3.3.2 Log P octanol/water: Effect of temperature

For log P measurements, octanol-saturated water and water-saturated octanol were equilibrated at 4°C, 25°C and 37°C in a cold room (4°C), at room temperature and in a water bath (37°C) respectively. To obtain K and N free bases, 150 µl racemic K and N stock solutions (fumarate salt equivalent to 1 mg/ml K and N in methanol) were evaporated at room temperature and 1.5 ml NaOH solution in water (pH 13) added. K and N free bases were then extracted into 3 ml water-saturated octanol after which aliquots (0.3 ml) of these solutions (50 µg/ml) together with 3 ml octanol-saturated water were added to a Mixor (Wu et al, 2004; Yang et al, 2009) (5 ml) and mixed 30 times to reach equilibrium. Finally aliquots (180 µl) of both the aqueous and octanol phases were collected, evaporated at room temperature, reconstituted in 60 µl mobile phase (30:70 ACN:50 mM phosphate buffer, pH = 6) and injected into the HPLC system.

Log P was calculated using Equation 3.1:

$$\textbf{Log P} = \textbf{Log}_{10} (C_{oct} / C_{wat}) \qquad \textbf{3.1}$$

where C_{oct} and C_{wat} are the concentrations of K or N in octanol phase and in aqueous phase at equilibrium respectively.

3.3.3 Log D octanol/buffer: Effect of temperature

Log D of K and N in octanol/Ringer-HEPES buffer pH 7.4 (10 mM HEPES and 1.2 mM calcium chloride) was also determined at 4°C, 25°C and 37°C. In this case, 150 µl racemic K and N stock solutions (fumarate salts equivalent to 1 mg/ml K and N in methanol) were evaporated to dryness and reconstituted in 30 ml octanol-saturated Ringer-HEPES buffer. An aliquot (3 ml) of this solution together with Ringer-HEPES buffer-saturated octanol (0.3 ml) were added to a Mixor (5 ml) and mixed 30 times to reach equilibrium. The two phases were then analysed for K and N as described above. Log D was calculated using Equation 3.1 where C_{wat} was replaced by the concentration of K or N in buffer (C_{buf}).

3.3.4 Log D liposome/buffer

3.3.4.1 Liposome preparation

Liposomes were prepared by the thin film hydration method and extruded to decrease particle size and obtain a narrow size distribution. Soy lecithin phospholipid (100 mg) and cholesterol (25 mg) were dissolved in 5 ml chloroform-methanol (3:1, v/v) in a round-bottomed flask. The thin film was formed by rotary evaporation (Rotavapor R110) at 35°C under vacuum for 30 min, then kept under vacuum overnight to remove traces of organic solvent. Ringer-HEPES buffer pH 7.4 (5 ml) and 0.5 g glass beads were added and the film hydrated by rotary evaporation without vacuum for 30 min. After hydration the liposomal suspension was sonicated (bath sonicator, RK100H) for 10 min and then extruded sequentially ten times through 200 nm Nucleopore Track-Etch membranes using a liposome extruder (Lipex Extruder, NORTHERN LIPIDS INC, Burnaby, Canada). Finally liposomes were suspended in Ringer-HEPES buffer pH 7.4 containing 1.5×10^{-3} mg/ml (5 µM) racemic K or N to a concentration of 10 mg/ml lipid.

3.3.4.2 Liposome characterization

The concentration of phospholipid in the liposomal suspension was determined using the Stewart assay (Stewart, 1980). Particle size was determined by dynamic light scattering (DLS) using a Zetasizer (ZS90, Malvern Instrument, Worcestershire, UK). The liposomal suspension (20 µl) and Ringer-HEPES buffer pH 7.4 (1980 µl) were mixed in the cuvette and placed in the Zetasizer using a refractive index (RI) of 1.335, viscosity of 1.02 mPa.s and temperature of 25°C.

3.3.4.3 Log D determination

The liposome suspension containing 5 µM racemic K or N (0.5 ml) was injected into the donor side of an equilibrium dialysis device (10000 Da) and Ringer-HEPES buffer pH 7.4 (0.5 ml) injected into the receptor side. The device was switched on and maintained at 37°C for 4 h to reach equilibrium. A sample (180 µl) was removed from the receptor side and analysed for K or N. Liposome/Ringer-HEPES buffer apparent distribution coefficient (D) was calculated using Equation 3.2 (Plemper van Balen et al, 2004):

$$\mathbf{D = V_B \times (C_{ini} - 2C_B) / (V_{lipo} \times C_B) + 1} \qquad \mathbf{3.2}$$

where C_{ini} and C_B are the concentrations of K or N on the receptor side initially and at equilibrium respectively, V_B is the volume in buffer compartment and V_{lipo} is the volume of phospholipid used (calculated using the lipid concentration assuming a density of 1 g/ml).

3.3.5 Statistic analysis

Statistical analysis was carried out using GraphPad Prism (GraphPad Software, San Diego, CA, USA). One-way ANOVA with post-hoc Bonferroni testing was used to compare selected data sets for log P and log D values at different temperatures. Unpaired two-tailed t-test (with Welch's correction) was used to compare the difference in log D values between liposome/buffer and octanol/buffer systems. Results are presented as means ± SD. Differences for which $p < 0.05$ were taken as significant.

3.4 Results

3.4.1 Log P octanol/water: Effect of temperature

The experimental log P values are larger for K than for N at all temperatures contrary to the calculated values in Table 3.1. Experimental Log P values of K and N increase significantly with increasing temperature (from 4°C to room temperature)(Table 3.2 and Figure 3.1) indicating K and N partition more extensively into octanol with increasing temperature. Although the differences in log P values of neither K nor N between room temperature and 37°C was significant, this could be due to insufficient sample number used in the experiment. As power of statistical analysis increases with increasing sample size, by using more replicates in determination in future studies, a significant difference might be found in K and N log P values between room temperature and 37°C.

Table 3.2 Log P of ketotifen (K) and norketotifen (N) in the octanol/water system at different temperatures (data are means ± SD, *n*= 5).

	Log P in the octanol/water system		
	4°C	Room Temperature*	37°C
K	2.24 ± 0.13	2.89 ± 0.33	3.23 ± 0.16
N	1.48 ± 0.21	1.78 ± 0.06	1.92 ± 0.06

*25 ± 2°C

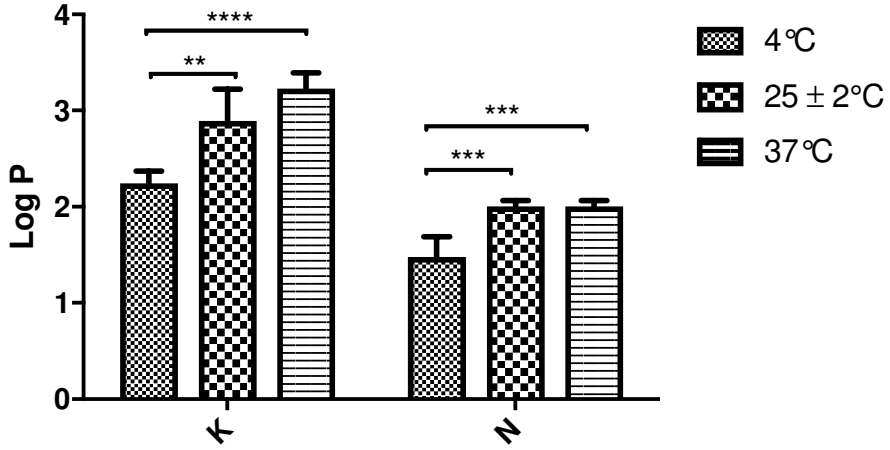

Figure 3.1 Log P values of ketotifen (K) and norketotifen (N) measured in the octanol/water system at different temperatures (data are means ± SD, *n* = 5, **P<0.002, ***P<0.001, ****P<0.0001).

According to the π system for calculating log P values, K with one more methyl group than N (Figure 1.1) should have a log P that is higher than that of N by

approximately 0.5. However, the results (Table 3.2) indicate the difference is more than 0.5 at all temperatures. This is presumably because the π system does not fully take into account the structural differences between the two compounds. More recent methods for estimating log P take into account other factors such as atomic contributions and topological indices (Erica et al, 2011). The effect of temperature on log P is elucidated as follows (Equation 3.3):

$$\textbf{Log P} = \Delta S^\circ/2.303R - \Delta H^\circ/2.303RT \qquad \textbf{3.3}$$

where T is temperature (Kelvin), ΔH^o and ΔS° is the enthalpy and entropy change in distribution respectively, and R is the gas constant.

It suggests with increasing temperature, log P can be increasing or decreasing depending on whether the distribution procedure is endothermic (H > 0) or exothermic (H < 0). According to our result (Table 3.2 and Figure 3.1), log P increased with increasing temperature thus the distribution procedure of K and N between octanol and water is endothermic.

3.4.2 Log D octanol/buffer: Effect of temperature

As found with log P values, Log D values in the octanol/buffer pH 7.4 system show K distributes more extensively into octanol at all temperatures. As expected, the log D values are always less than their corresponding log P values and increase with increasing temperature although at a slower rate than the log P values. However, only the difference log D values between 4°C and 37 °C is significant (Table 3.3 and Figure 3.2), which may be due to insufficient sample number used in determination as discussed in Section 3.4.1.

Table 3.3 Log D of ketotifen (K) and norketotifen (N) in the octanol/Ringer-HEPES buffer pH 7.4 system at different temperatures (data are means ± SD, *n* = 5).

	Log D in the octanol/buffer pH 7.4 system		
	4°C	Room Temperature *	37°C
K	2.08 ± 0.43	2.49 ± 0.07	2.68 ± 0.02
N	0.99 ± 0.02	1.01 ± 0.43	1.62 ± 0.45

* 25 ± 2°C

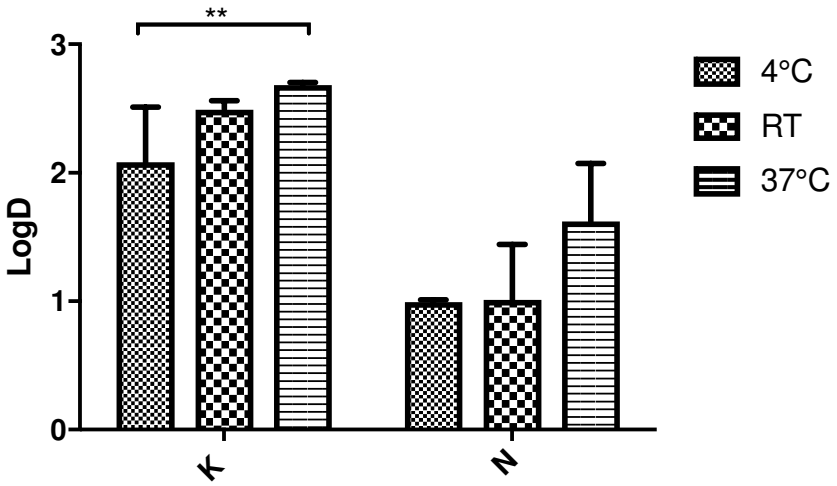

Figure 3.2 Log D values of ketotifen (K) and norketotifen (N) measured in the octanol/ Ringer-HEPES buffer pH 7.4 system at different temperatures (data are means ± SD, *n* = 5, **P<0.002).

The changes with temperature presumably reflect the complex interplay between log P, which increases with temperature and pKa, pH of buffer, which are discussed in the following paragraphs.

Effect of temperature on partition coefficient was discussed in last section (Section 3.4.1); however, temperature affects not only log P but also pKa.

The effect of temperature on pKa can be elucidate using the following equation (Equation 3.4):

$$pKa = \Delta H°/2.303RT - \Delta S°/2.303R \qquad 3.4$$

where T is temperature (Kelvin), ΔH^o and $\Delta S°$ is the enthalpy and entropy change in disassociation respectively, and R is the gas constant.

Effect of temperature on pKa, similar to log P, depends on ΔH^o. With increasing temperature, pKa increases when the dissociation is exothermic but decreases when dissociation procedure is endothermic.

This effect of temperature on pKa not only applies to K and N but also applies to buffer used in log D measurement. As a result of temperature-dependent pKa, the pH of buffer solution used decreases with increasing temperature for exothermic dissociation, vice versa. It has been reported that for bases generally decrease by 0.3 pH units for every 10°C rise in temperature (Perrin et al, 1981). As a result, effect of temperature on log D measurement is a complex interplay between multiple factors, such as distribution, pKa of drug and buffer. Therefore, to better interpret results from cell experiments (Chapter 5), it is important to determine log P and log D at certain temperatures, at which experiments were

carried out. In our case, we are going to use these log P and log D values at 4 and 37° to interpret REB4 cell uptake and Caco-2 cell permeability results of K and N in Chapter 5.

3.4.3 Log D liposome/buffer

Log D values were found to differ between the octanol/buffer (log $D_{o/b}$) and liposome/buffer (log $D_{l/b}$) systems (Table 3.4). Log $D_{o/b}$ values indicate K distributes more extensively into octanol than N, whereas log $D_{l/b}$ values indicate K distributes less extensively into liposomes.

Table 3.4 Summary of calculated and experimental (data are means ± SD) log D values for ketotifen and norketotifen at 37°C (There was a significant difference in log D values of N between liposome/buffer and octanol/buffer systems (***P<0.0002)).

	Log D		
	Liposome/buffer pH 7.4 (*n* = 3)	Octanol/buffer pH 7.4 (*n* = 5)	Octanol/buffer pH 7.4*
K	2.63 ± 0.04	2.68 ± 0.02	2.15
N	3.64 ± 0.01	1.62 ± 0.45	0.92

*Unpublished results from Aberg A. K. G. using phosphate-buffered saline (PBS) buffer pH 7.4.

Compared with the octanol/aqueous system, the liposomes/aqueous system is a better model to determine the interaction between compound and cells. This is because the drug-membrane interaction involves both partitioning and binding (Plemper van Balen et al, 2004). Instead of using octanol as lipid phase, liposome/aqueous system uses liposomes, to be specific, phospholipid bilayers as lipid phase. These lipid bilayers are similar to cell membranes and contribute to the partitioning part of the drug-membrane interaction. In addition, the polar head of phospholipid on liposome bilayers carries charges, which depend on phospholipids used to make liposomes. The charge on liposomes provides a chance for ionic bonds or ion exchange between membrane and ionized compounds to take place, thus contribute to the binding part of the drug-membrane interaction (Plemper van Balen et al, 2004). Therefore, compared with octanol/aqueous system, distribution of drug between liposome/aqueous system helps to better elucidate the behaviours of a compound at the target membrane.

In our log $D_{l/b}$ determination, liposomes (mean particle size approximately 200 nm) used were made from soy lecithin phospholipid and cholesterol. This

combination produces a negative surface charge (zeta potential ~-2 mV) at lipid bilayers. Both K and N at pH 7.4 are positively charged but K (pKa = 8.8) is less ionized than N (pKa = 10.3), such that liposomes would be expected to interact and bind more strongly to N than to K. A similar result has been described elsewhere where binding was probably due to ion exchange or ionic bond on lipid membranes (Klein et al, 2001, Plemper van Balen et al, 2004; Yang et al, 2011). Future work could be done to investigate the effect of physiochemical properties liposome to log D measurement by using a positively charged liposomes/buffer system to determine log D of K and N. The electric force between positively charged liposome membrane and positively charged compound may result in a lower log $D_{l/b}$.

3.5 Discussion

Experimental log $D_{l/b}$ and log $D_{o/b}$ values at 37°C for K and N trend in opposite directions. Thus whereas log $D_{l/b}$ values indicate that K distributes less into liposomes than N, the log $D_{o/b}$ and Aberg A. K. G log $D_{o/b}$ values both indicate K distributes more into octanol than N (Table 3.4). As discussed in Section 3.4.3, the difference may be related to binding between K and N and liposomes.
Log P results showed the temperature effect on partition of K and N between octanol and water. Log $D_{o/b}$ results demonstrated the complex interplay between multiple factors for K and N partitioning between octanol and Ringer-HEPES buffer at 4°C and 37°C. These results are useful for interpretation of cell culture work, which were carried out under the same conditions (Section 5.4.3). Log $D_{l/b}$ results represent drug-membrane interaction in both distribution and binding aspects, which elucidated the K and N interactions with cell membranes at 37°C (Section 5.4.3 and 5.4.4).

Chapter 4 Chiral HPLC assay development and validation

4.1 Introduction

There are a number of separation techniques by which chiral separation can be achieved: capillary electrophoresis (CE) (Alessandro et al, 2014; Beibei et al, 2014; Elena et al, 2016; Gerald and Martin, 2000; Salvatore, 2009), gas chromatography (GC) (Beibei et al, 2014; Malgorzata and Alina, 2014; Schurig, 1994), supercritical fluid chromatography (Eric and Caroline, 2015; Kveta et al, 2014; Michael et al, 1994), counter-current chromatography (Xin-Yi and Duo-Long, 2015), LC–MS (Sian and Barbara, 2014), HPLC and ultra-high performance liquid chromatography (UHPLC) (Beibei et al, 2014; Jun et al, 2014; Ola et al, 2010; Szabolcs et al, 2014). LC–MS methods are known to be highly sensitive and selective, and asymmetric molecules with different m/z values do not require separation. However, for atropisomers or enantiomers which have the same m/z values, they do require separation which tends to extend chromatographic run times. LC–MS also suffers from high maintenance cost and the need for volatile buffers. Given that in this study anticipated levels of K and N in biological samples are above the detection limit of HPLC, it was used to develop chiral assays to determine K and N atropisomers in RBE4 cell homogenate, rat plasma and rat brain homogenate.

A chiral HPLC assay has been reported for the determination of K atropisomers in liver microsomes (Breyer-Pfaff and Nill, 2000) but no studies have reported the separation of N atropisomers using HPLC alone.

In this thesis, a chiral HPLC was carried out on a column containing a β-cyclodextrin-bound silica chiral stationary phase (CSP). The assay was validated and used to determine single atropisomers of K and N in different matrices, such as buffer, cell homogenate, human plasma and rat brain homogenate. In addition, it was used to determine atropisomers in racemates and in the single

atropisomers where it allowed assessment of atropisomeric purity and detection of any racemization or inversion in the presence of RBE4 cells and Caco-2 cells.

4.2 Materials

Human plasma was kindly provided by SCL lab, Dunedin hospital. Caco-2 cells were purchased from European Collection of Cell Culture (Sigma Aldrich, New Zealand). RS-Metoprolol (±)-tartrate (≥ 98%), RS-atenolol (≥ 98%), cyproheptadine hydrochloride (100%), (R)-(+)-propranolol hydrocloride (≥ 98%), sodium bicarbonate (cell culture tested) and Hank's Balanced Salt Solution (HBSS) were purchased from Sigma (Auckland, New Zealand). Methanol were purchased from Merck (Darmstadt, Germany). Sodium dihydrogen orthophosphate monohydrate (99%) and potassium dihydrogen orthophosphate (≥ 99.5%) were purchased from BDH Laboratory Supplies (England). Anhydrous disodium hydrogen orthophosphate (99%) was purchased from Asia Pacific Specialty Chemicals Ltd. RS-pizotifen was provided by GL Synthesis Inc. (MA, USA) through the kind offices of Aberg, A. K. G BridgePharma, Sarasota, FL, USA. Other materials are given in Chapters 2 (Section 2.2) and 3 (Section 3.2).

4.3 Assay development

4.3.1 Methods of assay development

4.3.1.1 Chiral separation

First attempts were made to develop a chiral HPLC method for the simultaneous determination of the atropisomers of K and N. However, this was not successful because it was impossible to obtain baseline separation of all four peaks of K and N. Thus, separate chiral HPLC methods were developed for K and N atropisomers.

A β-cyclodextrin-bonded silica chiral column (CDB-453 HQ, 4.6 × 150 mm, Phenomenex) maintained at 30°C was used for the chiral assay with the

remainder of HPLC system being the same as for the nonchiral assay (Chapter 2). The separation of K atropisomers was used to optimize the conditions for chiral resolution based on the following investigations.

Mobile phase composition: Flow rate 0.5 ml/min, mobile phase ACN:50 mM phosphate buffer pH 6 10:90, 20:80 and 30:70.

Mobile phase pH: Flow rate 0.5 ml/min, mobile phase 10:90 ACN:50 mM phosphate buffer; pH 3.5, 5 and 7.

Flow rate: Mobile phase 10:90 ACN:50 mM phosphate buffer pH 6; flow rates 0.4, 0.5 and 0.6 ml/min.

Buffer concentration: Flow rate 0.5 ml/min, mobile phase 10:90 ACN:phosphate buffer pH 6; buffer concentration 50 mM and 100 mM.

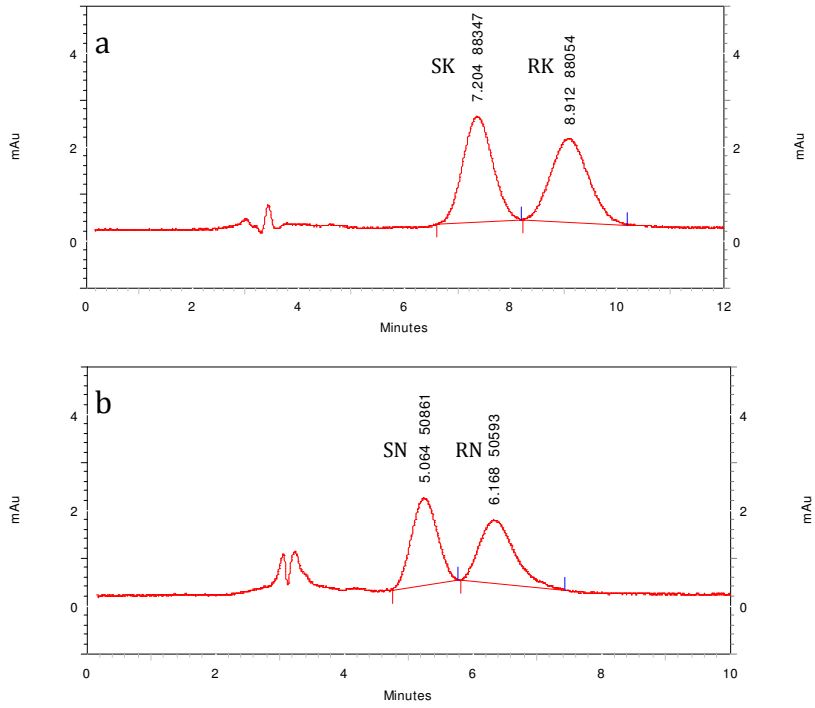

Figure 4.1 Chiral HPLC of 50 ng/ml racemic ketotifen (K) and norketotifen (N) showing separation of (a) K atropisomers and (b) N atropisomers in RBE cell homogenate at 310 nm.

Matrices used for method development and validation were prepared as follow: RBE4 cells (Yang et al, 2011) and Caco-2 cells (Yang et al, 2009) were grown, detached from the incubation flask, and homogenized using a Bullet Blender® tissue homogenizer (Next Advance, NY, USA) (refer to Section 2.3.2 for details).

The homogenate was further diluted with Milli-Q water to a final protein concentration of 250 µg/ml (measured using the BCA™ protein assay kit).
Wistar rats for brain matrix were purchased from the animal facility of Otago University. Rat brains were collected, weighed and homogenized in two volumes of Milli-Q water (w/v). The brain homogenate was further diluted to 1 in 10 diluted brain homogenate to prepare calibration standards and QC samples. The unused aliquots of 1 in 3 diluted brain homogenate samples were stored at -80°C until required.
For RBE4 cell homogenate samples prepared as for the nonchiral assay, SN which has the shortest Rt was subject to interference from an early eluting peak but this was eliminated by simply changing the detection wavelength from 295 nm to 310 nm (Figure 4.1). No IS was needed for the assay of RBE4 cell homogenate for the same reasons as for the nonchiral assay (refer to Section 2.3.1).
However, liquid-liquid extraction (LLE) was an absolute requirement for assay of plasma and brain homogenate, and detection at 295 nm was then free of interference. An IS was included in this assay.

4.3.1.2 Selection of IS

The IS was selected on the basis of an investigation into the suitability of the following five compounds: pizotifen, atenolol, metoprolol, cyproheptadine and propranolol (Figure 4.2). The compounds were examined in terms of their MW, calculated partition coefficient (Clog P), pKa, and Rt (Table 4.1). There was no clear correlation between the clog P and Rt of the compounds tested ($r^2 = 0.35$) suggesting separation by the CSP depends less on hydrophobicity and more on the size of the compound and electrostatic interactions in the cavity of the β-cyclodextrin (Lammerhofer, 2010). The deeper a compound inserts into the cavity, the stronger the interaction (Chankvetadze et al, 2000). It has been reported that, to some extent, a compound with a chiral centre (enantiomer)

gains a better separation than one without chiral centre (atropisomers) on the β-cyclodextrin matrix stationary phase. However, the separation also depends on interaction with the cavity mouth of the β-cyclodextrin (Armstrong et al, 1986; Stalcup et al, 1991). Therefore, the interactions of β-cyclodextrin and K and N may be come from the interaction of the β-cyclodextrin cavity mouth, as K and N do not have a chiral centre.

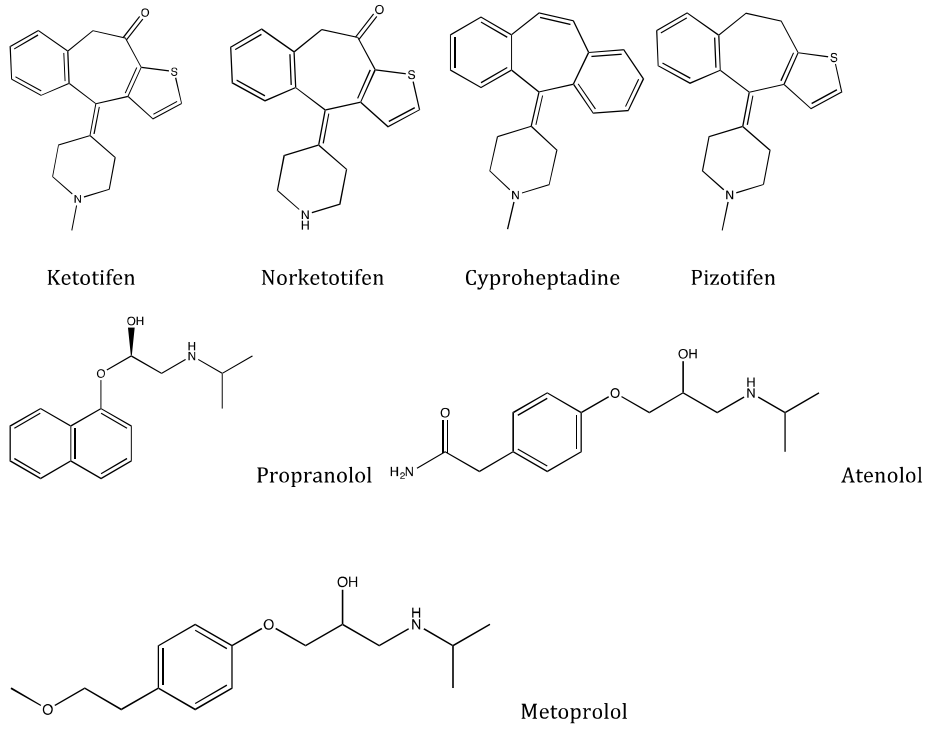

Figure 4.2 Structures of ketotifen, norketotifen and the five compounds tested as internal standards in the chiral assays of ketotifen and norketotifen.

Table 4.1 Properties of ketotifen, norketotifen and the five compounds evaluated as internal standards in the chiral assays of ketotifen and norketotifen (clog P and pKa were obtained from SciFinder Scholar).

	MW	clog P	pKa	Rt (min)
K	309	2.19 ± 0.73	8.84 ± 0.20	6.9 (SK) 9.1 (RK)
N	295	2.65 ± 0.51	10.4 ± 0.2	5.6 (SN) 6.5 (RN)
Pizotifen	295	2.71 ± 0.67	9.04 ± 0.20	> 100
Atenolol	266	0.34 ± 0.28	9.43 ± 0.10	3.3
Metoprolol	267	1.63 ± 0.26	9.43 ± 0.10	4.9
Cyproheptadine	287	5.82 ± 0.76	8.95 ± 0.20	> 100
Propranolol	259	2.90 ± 0.25	9.50 ± 0.30	61

Although pizotifen and cyproheptadine are similar to K in structure and pKa, their values of Rt are much longer than those of both K and N. Again this cannot be due to hydrophobicity since the clog Ps for the compounds are very similar. The only explanation is that the ketone group in K and N reduces greatly the interaction with the CSP but the detailed reason for the difference is unknown. RS-Metoprolol was finally chosen as IS because (a) it eluted before K and N atropisomers with an Rt long enough to avoid interference from matrix peaks but still baseline resolved from the first atropisomer peaks of SK and SN and (b) as metoprolol elutes before K and N atropisomers, it results in a shorter total run-time without any separation of its enantiomer peaks. The maximum absorbance of metoprolol was at 220 nm and, accordingly, the diode array detector was programmed to switch from 220 nm to 295 nm after its elution.

4.3.1.3 Sample preparation

Sample preparation of RBE4 cell homogenate was as described in Chapter 2 (Section 2.3.2). For human plasma and rat brain homogenate samples, 10 µl IS solution (10 µg/ml) was added to 0.5 ml sample (or calibration standard or QC sample) to give a final concentration of 200 ng/ml. An aliquot of 1M NaOH (30 µl) was added after which 1 ml 60:40 diethyl ether:n-hexane was added to

plasma samples and 1 ml 10:90 dichloromethane:n-hexane added to brain homogenate samples. Mixtures were vortexed for 30 s and centrifuged at 10,000 g for 10 min. The upper organic phase (0.95 ml) was then transferred into clean tubes and 0.3 ml 0.0036% HCl added for back extraction. Tubes were vortexed for 30 s and centrifuged for 10 min at 10,000 g after which 0.27 ml aliquots of aqueous phase were transferred to clean tubes and evaporated to dryness under vacuum at room temperature overnight. Dried samples were reconstituted in 60 µl mobile phase followed by vortexing and centrifuging at 10,000 g for 10 min. Finally, 55 µl supernatant was transferred into HPLC inserts and 50 µl injected into the HPLC system.

4.3.2 Results and discussionof assay development

Mobile phase composition: Increasing the ACN percentage in the mobile phase above 20% decreased the Rt of K atropisomers and decreased the separation factor (Figure 4.3a).

Mobile phase pH: Increasing the mobile phase pH increased the Rt of K atropisomers and decreased the separation factor (Figure 4.3b).

Flow rate: Increasing the flow rate decreased the Rt of K atropisomers but had no effect on the separation factor (Figure 4.3c).

Phosphate buffer concentration: Increasing the phosphate buffer concentration caused a slight decrease in the Rt of K atropisomers and a slight increase in the separation factor (Figure 4.3d).

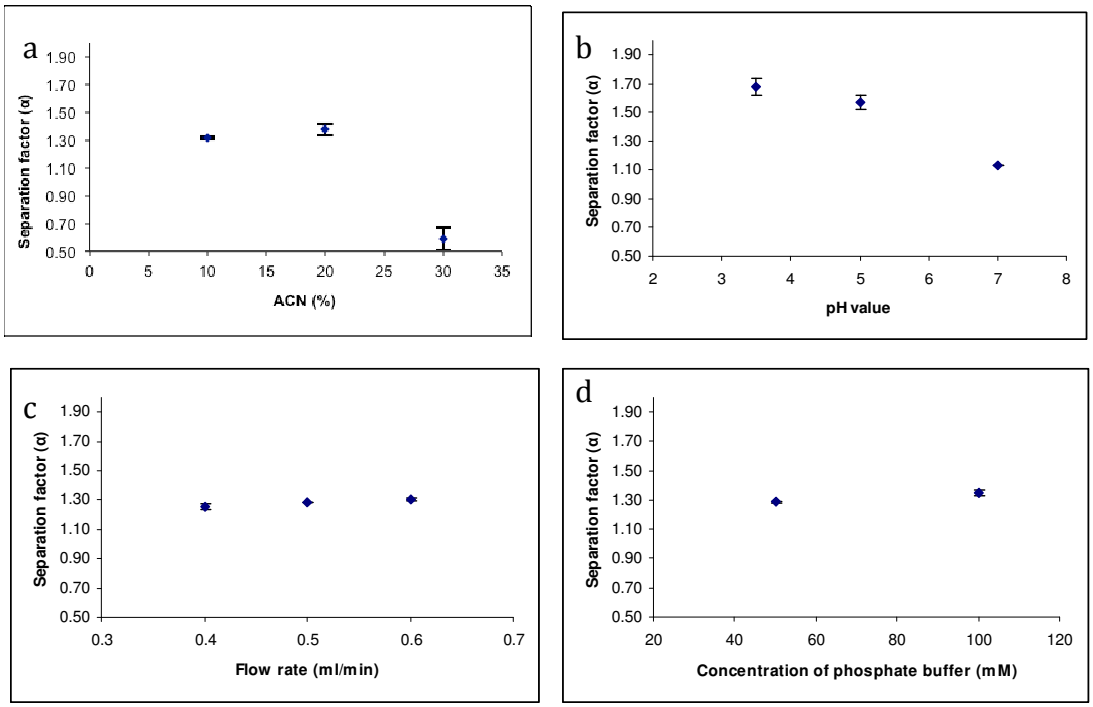

Figure 4.3 Effects of changing chiral HPLC conditions on the separation factor of K atropisomers: (a) mobile phase composition, (b) mobile phase pH, (c) flow rate, and (d) phosphate buffer concentration (for conditions of each chromatograph, see Section 4.3.1).

The factors causing most change in the separation of K atropisomers were the mobile phase composition and pH. The effect of increasing ACN in the mobile phase to decrease Rt and separation arises because ACN reduces the affinity between CSP and analytes (Ferguson et al, 1996). The effect of increasing mobile phase pH to increase Rt and decrease separation is presumably due to the change in ionization degree of K. Cyclodextrin predominantly interacts with uncharged molecules (Lutka and Golda, 2006) so that, as the proportion of unionized K increases with increasing of pH, the interaction between both atropisomers and CSP increases. This may increase the retention of both atropisomers thereby reducing the separation between K atropisomers. Similar procedures were carried out to obtain the optimized conditions for separation of N atropisomers (results are not shown here).

The optimized conditions for the chiral HPLC assays were mobile phases of ACN:100 mM phosphate buffer pH 3.2 6:94 for K and 12:88 for N delivered at a flow rate of 0.5 ml/min through the column maintained at 30°C. Chromatographs of K and N racemates rat plasma and rat brain homogenate under these conditions are shown in Figure 4.4.

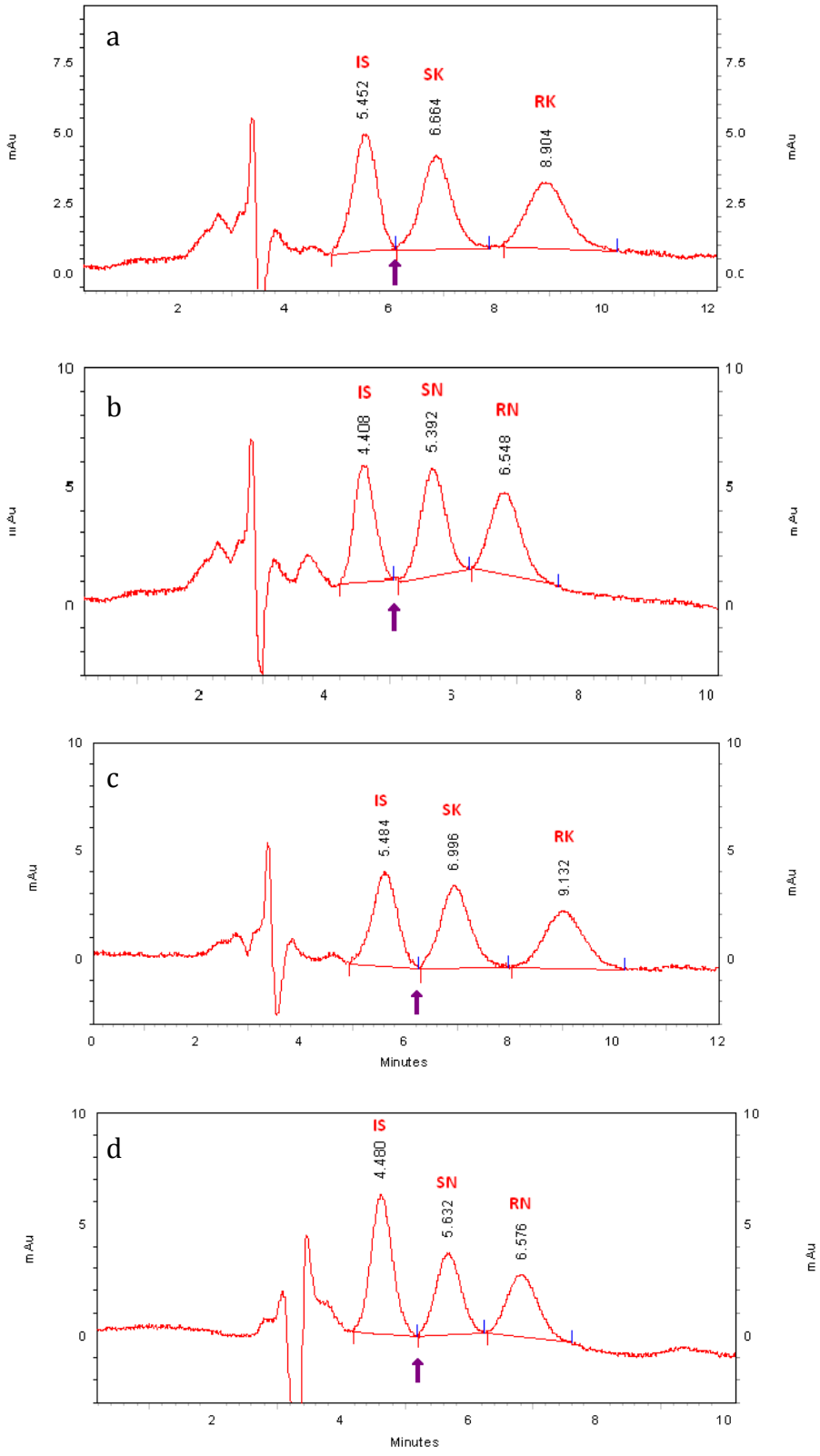

Figure 4.4 Chiral HPLC of racemic ketotifen (K) and racemic norketotifen (N) showing separation of (a) K atropisomers and (b) N atropisomers in human plasma and (c) K atropisomers and (d) N atropisomers in rat brain homogenate.

Assay of plasma and brain homogenate included an internal standard (RS-metoprolol) which elute first and is detected at 220 nm after which detection wavelength is changed to 295 nm at the time indicated by the arrow.

4.4 Assay validation

4.4.1 Methods of assay validaiton

4.4.1.1 Human plasma versus rat plasma

In this chapter, plasma QC samples were prepared using human plasma instead of rat plasma. This was due to following reasons:

First, the LLOQ of chiral assay requires a 0.5 ml plasma sample for sample extraction. Consequently a relatively large amount of rat plasma is needed for QC sample preparation. However, one rat (200 g body weight) only has 12 ml blood, which is approximately 6 ml of plasma. Moreover, it is impossible to collect all of the 6 ml plasma from a rat. In this case, plasma from one rat is just enough to make a standard curve let alone all of the QC samples for precision and accuracy tests and stability tests. Thus to validate this assay using rat plasma requires killing too many rats, which is not ethical.

Second, although there was no proper cross-validation done between human plasma and rat plasma in this thesis, tests were performed to compare these two plasma samples. Results from human plasma and rat plasma were very similar, in both chromatograph and standard curve.

Third, species difference of esterase expression and activity do happen between human and rat plasma (Bahar et al, 2012), however, different esterase expression does not affect K and N metabolic route (Figure 1.2).

As discussed above, there was no clear evidence that suggesting difference between using rat plasma and human plasma occurs during K and N HPLC assay validation. Moreover, using human plasma avoids ethical issue caused by using

rat plasma. As a result, human plasma was used in this validation instead of rat plasma.

4.4.1.2 Preparation of calibration standards and QC samples

Calibration standards were prepared freshly each assay day by spiking RBE4 cell homogenate or plasma or rat brain homogenate (diluted 1 in 10 with Milli-Q water) with aqueous solutions of K or N racemates to give final atropisomer concentrations in the range 20 – 500 ng/ml. Low, medium and high QC samples were prepared in the same way at concentrations of 30, 60 and 120 ng/ml.

4.4.1.3 Linearity, LLOQ, recovery, accuracy and precision

Linearity, LLOQ, recovery, accuracy and precision: These were determined as described for the nonchiral assay (Chapter 2, Section 2.3.3).

4.4.1.4 Stability

This was assessed using QC samples of racemates (in REB4 cell homogenate, human plasma, and rat brain homogenate) stored under the same conditions as for the nonchiral assay (Section 2.3.3, Table 2.3) except that long-term stability at -80°C was for one month.
Stability of atropisomers in racemate K and N in RBE4 cells, human plasma and rat brain homogenate was calculated using Equation 2.4.

4.4.2 Results and discussion of assay validation

4.4.2.1 Linearity

The assays for both K and N atropisomers in all matrices were linear ($R^2 > 0.999$) in the concentration range used (Figure 4.5) and in all cases the LLOQ was 20 ng/ml.

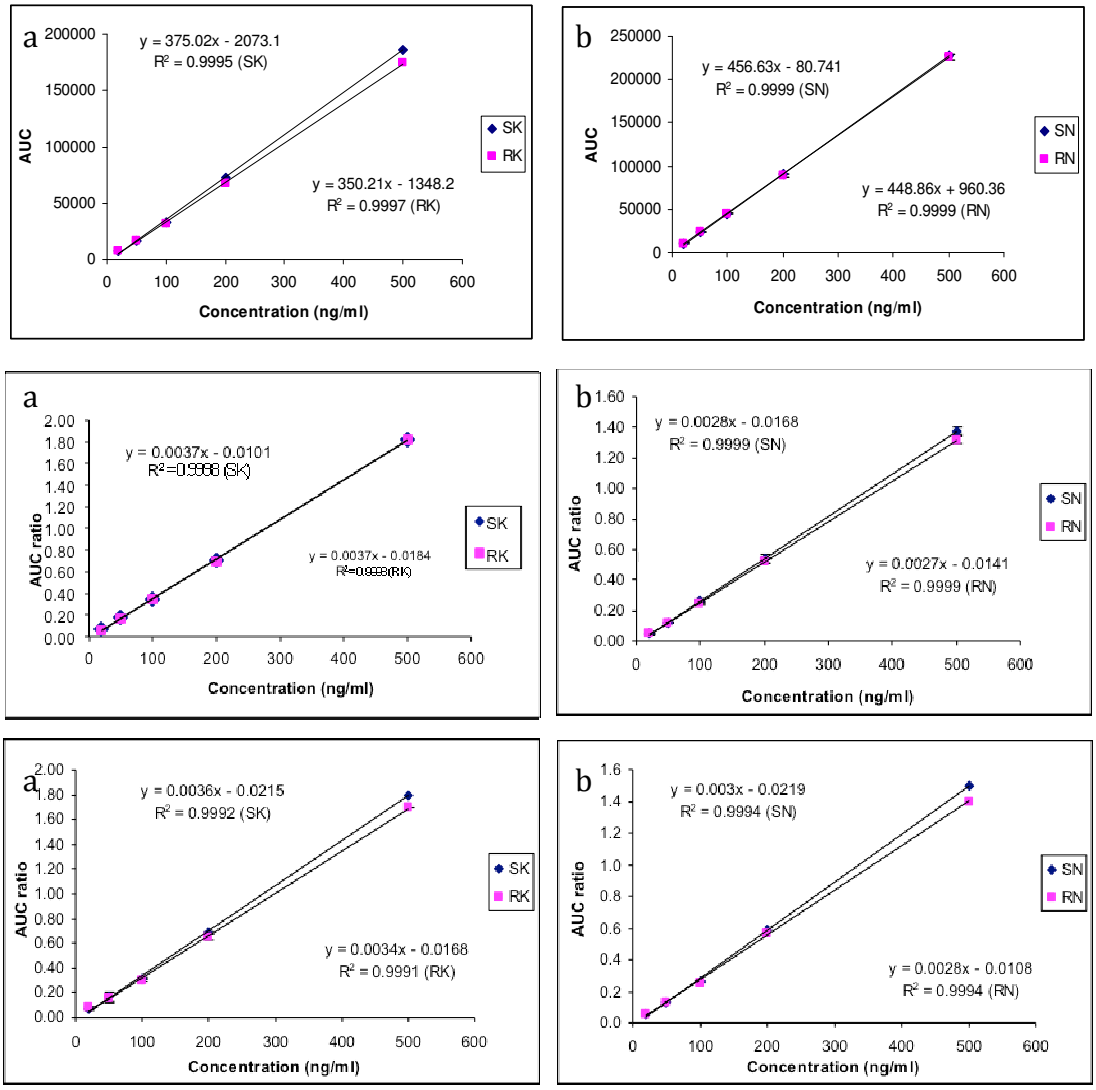

Figure 4.5 Calibration curves for (a) K atropisomers and (b) N atropisomers in TOP RBE4 cell homogenate, MIDDLE human plasma, and BOTTOM rat brain homogenate (data are means ± SD, *n* = 3). Assay of RBE4 cell homogenate used external standards, whereas assays of plasma and rat brain homogenate used an internal standard.

4.4.2.2 Recovery

The recovery was > 90% for assay of RBE4 cell homogenate and > 80% for human plasma and rat brain homogenate.

4.4.2.3 Accuracy and precision

Intra-day and inter-day accuracy of K and N atropisomers in RBE4 cell homogenate, human plasma and rat brain homogenate were within ± 15% at all QC concentrations. The corresponding intra-day and inter-day precisions were < 10% at all QC concentrations (Table 4.2 to 4.7). These results indicate the assays fully meet the requirements of the FDA Guidelines (2001).

Table 4.2 Accuracy and precision of the chiral HPLC assays for ketotifen (K) atropisomers in RBE4 cell homogenate (data are means ± SD for assay of 5 replicates).

		Theoretical QC concentration (ng/ml)	Determined QC concentration (ng/ml)	Accuracy RE (%)	Precision CV (%)
SK	Inter-day 1	L (30)	28.4 ± 1.0	5.5	3.5
		M (60)	60.6 ± 2.8	3.6	4.6
		H (120)	117.6 ± 5.0	3.7	4.3
	Inter-day 2	L (30)	27.9 ± 2.2	8.2	7.8
		M (60)	63.2 ± 1.7	5.3	2.8
		H (120)	119.6 ± 8.3	6.1	7.1
	Inter-day 3	L (30)	29.6 ± 0.5	1.5	1.6
		M (60)	61.2 ± 1.9	2.9	3.2
		H (120)	116.0 ± 5.9	4.4	5.1
	Intra-day	L (30)	28.6 ± 1.5	5.1	5.2
		M (60)	61.7 ± 2.4	4.0	5.8
		H (120)	116.8 ± 6.1	4.7	5.2
RK	Inter-day 1	L (30)	31.4 ± 1.0	4.6	3.2
		M (60)	68.8 ± 2.3	14.6	3.4
		H (120)	137.5 ± 1.8	14.5	1.3
	Inter day 2	L (30)	28.7 ± 1.8	6.5	6.4
		M (60)	65.4 ± 2.4	9.0	3.6
		H (120)	122.1 ± 8.5	5.6	7.0
	Inter-day 3	L (30)	27.7 ± 1.0	7.8	3.4
		M (60)	63.0 ± 2.8	5.3	4.5
		H (120)	119.3 ± 3.8	2.4	3.2
	Intra-day	L (30)	29.2 ± 2.0	6.3	7.0
		M (60)	65.7 ± 3.4	11.0	5.2
		H (120)	126.3 ± 9.7	10.1	7.0

Table 4.3 Accuracy and precision of the chiral HPLC assays for norketotifen (N) atropisomers in RBE4 cell homogenate (data are means ± SD for assay of 5 replicates).

		Theoretical QC concentration (ng/ml)	Determined QC concentration (ng/ml)	Accuracy RE (%)	Precision CV (%)
SN	Inter-day 1	L (30)	29.4 ± 1.5	4.6	5.2
		M (60)	58.6 ± 2.1	3.2	3.6
		H (120)	121.7 ± 5.7	4.0	4.7
	Inter-day 2	L (30)	25.9 ± 0.4	13.6	1.5
		M (60)	55.6 ± 2.3	7.3	4.1
		H (120)	116.4 ± 2.7	3.0	2.3
	Inter-day 3	L (30)	30.8 ± 0.7	2.9	2.3
		M (60)	63.4 ± 1.4	5.7	2.2
		H (120)	127.3 ± 3.1	6.1	2.4
	Intra-day	L (30)	28.7 ± 2.3	7.0	7.0
		M (60)	52.9 ± 3.8	5.4	5.4
		H (120)	121.8 ± 5.9	4.4	4.4
RN	Inter-day 1	L (30)	31.2 ± 2.0	6.4	6.5
		M (60)	59.1 ± 2.1	2.8	3.6
		H (120)	127.8 ± 2.5	6.5	2.0
	Inter-day 2	L (30)	25.5 ± 0.8	14.9	3.3
		M (60)	53.3 ± 2.0	11.2	3.8
		H (120)	113.4 ± 3.5	5.5	3.1
	Inter-day 3	L (30)	29.6 ± 2.6	6.3	8.7
		M (60)	60.5 ± 3.0	4.2	4.9
		H (120)	114.3 ± 3.6	4.8	3.1
	Intra-day	L (30)	28.8 ± 3.0	9.2	9.2
		M (60)	57.6 ± 3.9	6.1	6.1
		H (120)	118.5 ± 7.5	5.6	5.6

Table 4.4 Accuracy and precision of the chiral HPLC assays for ketotifen (K) atropisomers in human plasma (data are means ± SD for assay of 5 replicates).

		Theoretical QC concentration (ng/ml)	Determined QC concentration (ng/ml)	Accuracy RE (%)	Precision CV (%)
SK	Inter-day 1	L (30)	31.5 ± 1.5	5.7	4.9
		M (60)	60.5 ± 1.6	2.1	2.6
		H (120)	117.2 ±1.7	2.4	1.4
	Inter-day 2	L (30)	30.9 ± 1.7	5.2	5.6
		M (60)	61.1 ± 4.5	6.1	7.3
		H (120)	120.5 ± 2.0	1.3	1.7
	Inter-day 3	L (30)	31.3 ± 0.6	4.3	1.8
		M (60)	62.6 ± 2.0	4.3	3.1
		H (120)	116.0 ± 1.1	3.3	1.0
	Intra-day	L (30)	31.2 ± 1.3	5.1	4.1
		M (60)	61.4 ± 2.9	4.2	4.7
		H (120)	117.9 ± 2.5	2.3	2.1
RK	Inter-day 1	L (30)	30.1 ± 1.7	4.1	5.6
		M (60)	62.3 ± 0.7	3.9	1.1
		H (120)	116.7 ± 3.6	3.5	3.1
	Inter-day 2	L (30)	29.0 ± 1.3	5.1	4.6
		M (60)	61.7 ± 4.7	6.9	7.5
		H (120)	120.0 ± 3.2	1.9	2.7
	Inter-day 3	L (30)	31.4 ± 0.7	4.8	2.2
		M (60)	61.2 ± 1.5	2.6	2.5
		H (120)	115.3 ± 0.2	3.9	1.7
	Intra-day	L (30)	30.2 ± 1.6	4.6	5.3
		M (60)	61.7 ± 2.7	4.5	4.3
		H (120)	117.4 ± 3.5	3.1	2.9

Table 4.5 Accuracy and precision of the chiral HPLC assays for norketotifen (N) atropisomers in human plasma (data are means ± SD for assay of 5 replicates).

		Theoretical QC concentration (ng/ml)	Determined QC concentration (ng/ml)	Accuracy RE (%)	Precision CV (%)
SN	Inter-day 1	L (30)	30.9 ± 1.6	4.1	5.2
		M (60)	60.8 ± 4.4	6.0	7.3
		H (120)	120.1 ± 3.0	1.9	2.5
	Inter-day 2	L (30)	29.2 ± 1..6	4.3	5.6
		M (60)	57.9 ± 2.3	4.5	4.0
		H (120)	116.3 ± 1.9	3.0	1.6
	Inter-day 3	L (30)	34.0 ± 0.6	13.2	1.6
		M (60)	61.4 ± 3.1	3.2	5.0
		H (120)	111.4 ± 6.8	7.2	6.1
	Intra-day	L (30)	31.0 ± 2.8	6.3	7.4
		M (60)	59.8 ± 2.5	4.7	5.9
		H (120)	116.6 ± 4.9	3.6	4.2
RN	Inter-day 1	L (30)	29.2 ± 1.0	3.6	3.5
		M (60)	61.4 ± 3.4	5.0	5.6
		H (120)	120.7 ± 4.2	2.3	3.4
	Inter-day 2	L (30)	31.1 ± 0.8	3.9	2.5
		M (60)	59.4 ± 2.0	2.8	3.4
		H (120)	118.4 ± 4.1	1.4	0.9
	Inter-day 3	L (30)	33.2 ± 1.3	10.5	4.0
		M (60)	60.7 ± 2.9	3.8	4.8
		H (120)	111.1 ± 8.8	7.5	7.9
	Intra-day	L (30)	30.9 ± 1.8	5.3	5.9
		M (60)	60.5 ± 2.8	3.9	4.6
		H (120)	117.6 ± 5.8	3.2	5.0

Table 4.6 Accuracy and precision of the chiral HPLC assays for ketotifen (K) atropisomers in rat brain homogenate (Brain) (1 to 10 diluted with Milli-Q water) (data are means ± SD for assay of 5 replicates).

		Theoretical QC concentration (ng/ml)	Determined QC concentration (ng/ml)	Accuracy RE (%)	Precision CV (%)
SK	Inter-day 1	L (30)	29.2 ± 1.8	4.9	6.1
		M (60)	57.3 ± 1.4	4.5	2.4
		H (120)	114.6 ± 2.4	4.5	2.1
	Inter-day 2	L (30)	31.2 ± 2.3	6.4	7.3
		M (60)	62.8 ± 4.1	4.7	6.5
		H (120)	126.1 ± 7.4	5.6	5.9
	Inter-day 3	L (30)	29.2 ± 1.8	4.9	6.1
		M (60)	57.4 ± 1.3	4.4	2.2
		H (120)	114.6 ± 2.4	4.5	2.1
	Intra-day	L (30)	29.9 ± 2.1	5.4	6.9
		M (60)	59.2 ± 3.6	4.5	6.1
		H (120)	118.4 ± 7.1	4.9	6.0
RK	Inter-day 1	L (30)	31.4 ± 1.4	6.0	4.6
		M (60)	61.4 ± 2.8	3.3	4.6
		H (120)	118.6 ± 2.8	2.0	2.3
	Inter-day 2	L (30)	30.3 ± 0.6	1.7	1.9
		M (60)	61.8 ± 3.6	4.3	5.8
		H (120)	126.8 ± 7.7	6.2	6.1
	Inter-day 3	L (30)	31.2 ± 1.5	5.4	4.8
		M (60)	61.7 ± 2.5	2.9	4.1
		H (120)	118.6 ± 2.8	2.0	2.3
	Intra-day	L (30)	30.9 ± 1.2	4.4	4.0
		M (60)	61.6 ± 2.8	3.5	4.5
		H (120)	121.3 ± 6.1	3.4	5.0

Table 4.7 Accuracy and precision of the chiral HPLC assays for norketotifen (N) atropisomers in rat brain homogenate (Brain) (1 to 10 diluted with Milli-Q water) (data are means ± SD for assay of 5 replicates).

		Theoretical QC concentration (ng/ml)	Determined QC concentration (ng/ml)	Accuracy RE (%)	Precision CV (%)
SN	Inter-day 1	L (30)	31.0 ± 1.7	5.5	5.4
		M (60)	61.4 ± 1.7	3.3	2.8
		H (120)	120.7 ± 4.1	2.9	3.4
	Inter-day 2	L (30)	31.7 ± 1.0	5.7	3.2
		M (60)	60.3 ± 2.5	3.0	4.1
		H (120)	119.1 ± 5.1	3.6	4.3
	Inter-day 3	L (30)	29.9 ± 1.6	4.1	5.4
		M (60)	58.0 ± 2.3	4.1	3.9
		H (120)	118.0 ± 3.9	2.9	3.3
	Intra-day	L (30)	30.8 ± 1.6	5.1	5.1
		M (60)	59.9 ± 2.5	3.4	4.2
		H (120)	119.3 ± 4.2	3.2	3.6
RN	Inter-day 1	L (30)	31.1 ± 1.0	4.5	3.3
		M (60)	58.5 ± 2.3	3.5	3.9
		H (120)	116.6 ± 4.3	3.5	3.7
	Inter-day 2	L (30)	30.5 ± 2.4	5.9	8.0
		M (60)	60.9 ± 2.0	3.0	3.2
		H (120)	121.1 ± 6.2	4.2	5.2
	Inter-day 3	L (30)	30.5 ± 0.8	2.8	2.8
		M (60)	59.8 ± 2.1	2.7	3.5
		H (120)	1117.4 ± 2.5	2.4	2.2
	Intra-day	L (30)	30.7 ± 1.5	4.4	5.0
		M (60)	59.7 ± 2.2	3.1	3.7
		H (120)	118.4 ± 4.7	3.4	4.0

4.4.2.4 Stability in plasma and rat brain homogenate

For racemates in human plasma (Table 4.8) and rat brain homogenate (Table 4.9), the changes in K and N atropisomer concentrations indicate the atropisomers are stable under all the tested storage conditions.

Table 4.8 Stability of ketotifen (K) and norketotifen (N) atropisomers to decomposition in human plasma under different storage conditions (data are means ± SD, *n* = 5).

	QC sample concentrations (ng/ml)	Compound remaining after storage (%)			
		25°C (4 h)	4°C (24 h)	Freeze-thaw (3 cycles)	-80°C (1 month)
SK	L (30)	96.0 ± 2.9	104.0 ± 0.7	97.0 ± 5.1	102.3 ± 3.6
	M (60)	95.5 ± 1.5	95.8 ± 4.1	95.4 ± 2.1	96.3 ± 1.1
	H (120)	100.2 ± 4.2	93.6 ± 3.6	95.1 ± 2.5	96.3 ± 3.2
RK	L (30)	100.2 ± 2.2	104.7 ± 3.1	102.4 ± 4.8	98.7 ± 1.7
	M (60)	96.3 ± 4.8	92.2 ± 4.8	98.0 ± 1.6	101.2 ± 2.1
	H (120)	98.7 ± 2.9	98.5 ± 4.9	95.7 ± 1.3	97.4 ± 2.1
SN	L (30)	101.0 ± 3.9	94.4 ± 7.5	107.8 ± 5.4	98.0 ± 0.2
	M (60)	100.5 ± 5.7	98.4 ± 1.5	95.5 ± 7.8	105.0 ± 6.0
	H (120)	103.4 ± 2.7	97.1 ± 1.7	101.4 ± 4.12	103.2 ± 4.2
RN	L (30)	101.1 ± 3.8	96.2 ± 1.4	102.5 ± 8.4	104.6 ± 6.3
	M (60)	98.8 ± 4.9	95.3 ± 2.8	92.7 ± 4.2	100.1 ± 6.7
	H (120)	100.4 ± 3.0	96.6 ± 2.5	95.2 ± 2.4	106.5 ± 1.7

Table 4.9 Stability of ketotifen (K) and norketotifen (N) atropisomers to decomposition in rat brain homogenate (1 in 10 diluted with Milli-Q water) (data are means ± SD, *n* = 5).

	QC sample concentrations (ng/ml)	Compound remaining after storage (%)			
		25°C (4 h)	4°C (24 h)	Freeze-thaw (3 cycles)	-80°C (1 month)
SK	L (30)	99.1 ± 4.1	102.8 ± 6.4	101.7 ± 3.8	101.2 ± 7.0
	M (60)	95.2 ± 2.5	100.7 ± 1.6	101.7 ± 1.5	104.4 ± 4.1
	H (120)	95.2 ± 2.0	104.7 ± 2.4	100.1 ± 5.6	100.8 ± 6.5
RK	L (30)	103.9 ± 5.2	101.9 ± 8.5	102.5 ± 5.5	107.2 ± 7.0
	M (60)	95.3 ± 3.7	100.3 ± 1.8	98.5 ± 2.3	107.0 ± 1.3
	H (120)	93.7 ± 1.6	104.0 ± 2.1	99.7 ± 6.3	102.7 ± 8.4
SN	L (30)	96.3 ± 8.5	99.6 ± 4.6	103.2 ± 3.2	94.1 ± 4.0
	M (60)	97.7 ± 1.6	97.8 ± 2.0	98.9 ± 2.7	104.7 ± 6.2
	H (120)	100.3 ± 5.2	97.4 ± 1.2	97.0 ± 1.6	95.2 ± 3.4
RN	L (30)	94.3 ± 9.3	95.3 ± 2.5	102.1 ± 2.5	101.9 ± 7.0
	M (60)	97.0 ± 1.0	105.3 ± 5.3	107.0 ± 1.9	103.1 ± 6.8
	H (120)	101.7 ± 3.3	102.8 ± 1.7	103.0 ± 1.2	100.3 ± 4.4

4.5 Atropisomeric purity of single atropisomers

After validation of the chiral HPLC assay, atropisomeric purity of the single atropisomers was determined. Results (Figure 4.6) indicate that all atropisomers were contaminated to different extents with their antipodes.

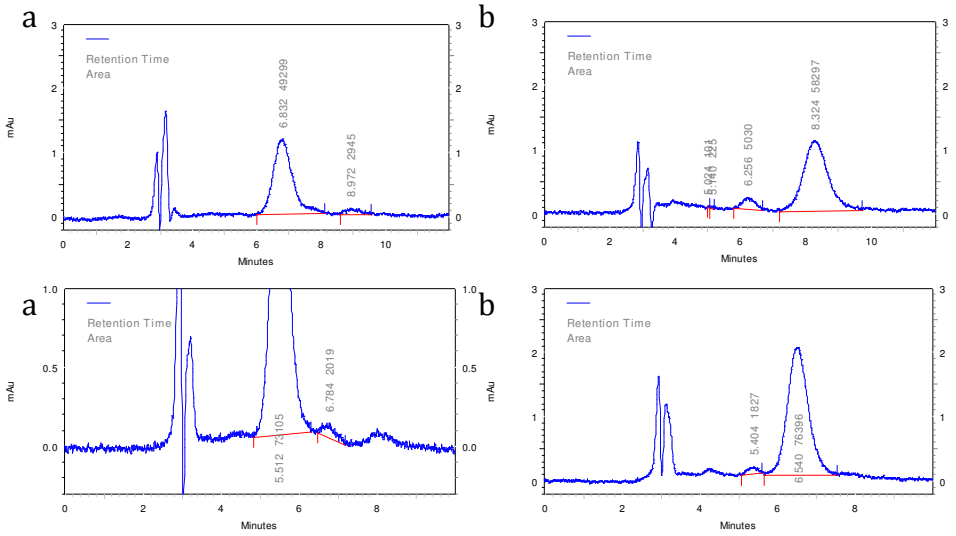

Figure 4.6 Chromatographs showing the presence of the antipode of the predominant atropisomer in single atropisomers of (TOP) ketotifen (K) and (BOTTOM) norketotifen (N) in Ringer-HEPES buffer (pH 7.4); (a) R in S, (b) S in R.

The antipode of the predominant atropisomer was found to be present in all compounds, that is, the compounds are not atropisomerically pure. The atropisomeric purity of SK, RK, SN and RN are approximately 92%, 88%, 95% and 97% respectively. To ensure the absence of inversion during uptake and permeation studies, racemization of atropisomers in the presence of RBE4 and Caco-2 cells under different conditions was investigated

4.5.1 Methods

Racemization of single atropisomer was assessed in the presence of RBE4 and Caco-2 cells and their respective culture buffer to investigate cell-mediated racemisation or inversion. Ringer-HEPES buffer pH 7.4 was used for RBE4 cells

and HBSS-HEPES buffer pH 7.4 for Caco-2 cells. In both cases, incubations were carried out in 12-well plates at 37 ℃ under 5% CO_2 for 6 h in (a) buffer only, (b) buffer pre-incubated with cell monolayers for 2 h, and (c) buffer in the presence of cell monolayers previously washed 3 times with 0.5 ml buffer. In all cases 2.2 ml K or N atropisomer solutions (2 µM) were added to each well and incubations carried out in triplicate. Buffer samples (180 µl) were removed at times 0, 10, 30, 60, 120, 240, 360 and 480 min and then dried under vacuum at room temperature. Dried samples were reconstituted with 60 µl mobile phase and subjected to chiral assay.

Racemization of single atropisomers of K and N in the presence of RBE4 and Caco-2 cells and their respective culture buffer was calculated using Equation 4.1.

$$\mathbf{A\ (\%) = (C_{anti}/C_{nor}) \times 100} \qquad \mathbf{4.1}$$

where A is the percentage from the antipode, C_{anti} is the determined concentration of the antipode and C_{nor} is the nominal concentration of the atropisomer used for stability test.

4.5.2 Results and discussions

4.5.2.1 Racemization of single atropisomers in RBE4 cell culture medium

As shown in Figure 4.7, the single atropisomers of K and N were stable to racemization or inversion (a) in Ringer-HEPES buffer pH 7.4, (b) Ringer-HEPES buffer pH 7.4 pre-incubated with RBE4 cell monolayers and (c) in Ringer-HEPES buffer pH 7.4 in the presence of RBE4 cell monolayers.

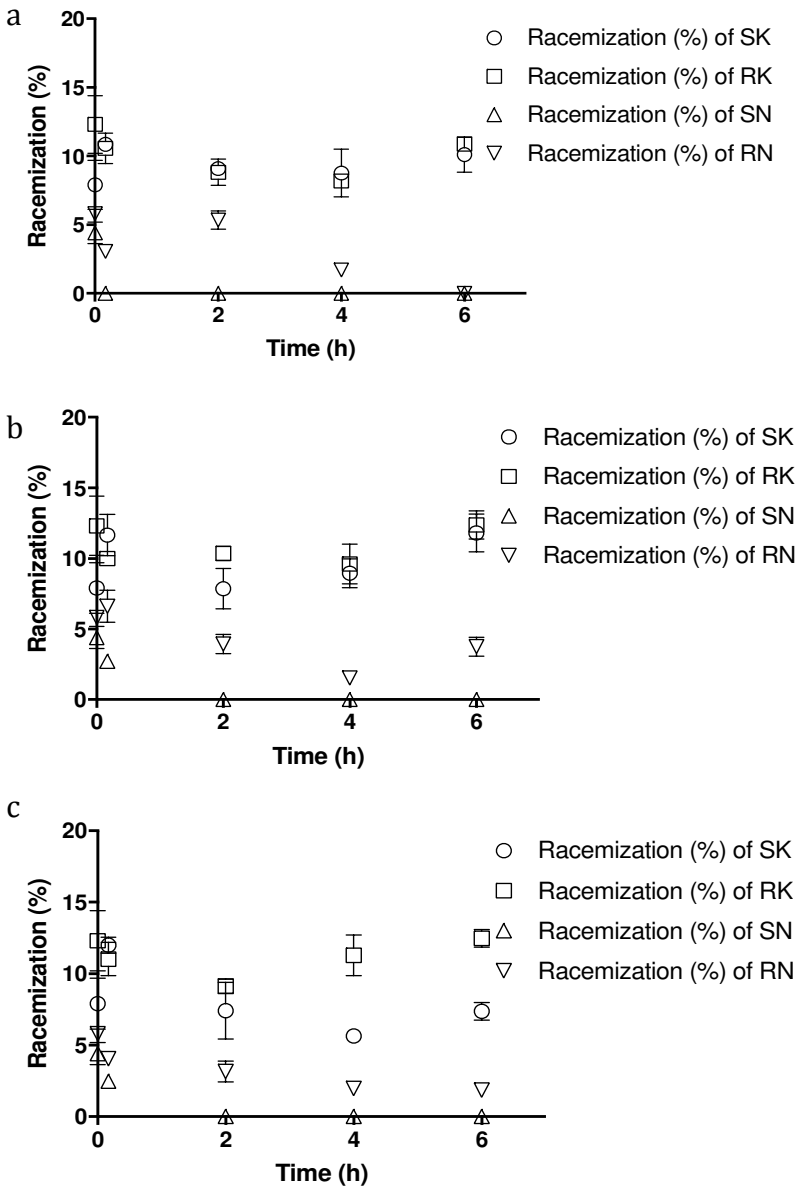

Figure 4.7 Stability of single atropisomers of ketotifen (K) and norketotifen (N) at 37°C over 6 h in (a) Ringer-HEPES buffer pH 7.4 (b) Ringer-HEPES buffer pre-incubated with RBE4 cell monolayers for 2 h, and (c) Ringer-HEPES buffer in the presence of RBE4 cell monolayers (data are means ± SD, *n* = 3).

4.5.2.2 Racemization of single atropisomers in Caco-2 cell culture medium

As shown in Figure 4.8, the single atropisomers of K and N were stable to racemization or inversion in (a) HBSS-HEPES buffer pH 7.4, (b) HBSS-HEPES

buffer pH 7.4 pre-incubated with Caco-2 monolayers for 2 h, and (c) in HBSS-HEPES buffer in the presence of Caco-2 cell monolayers.

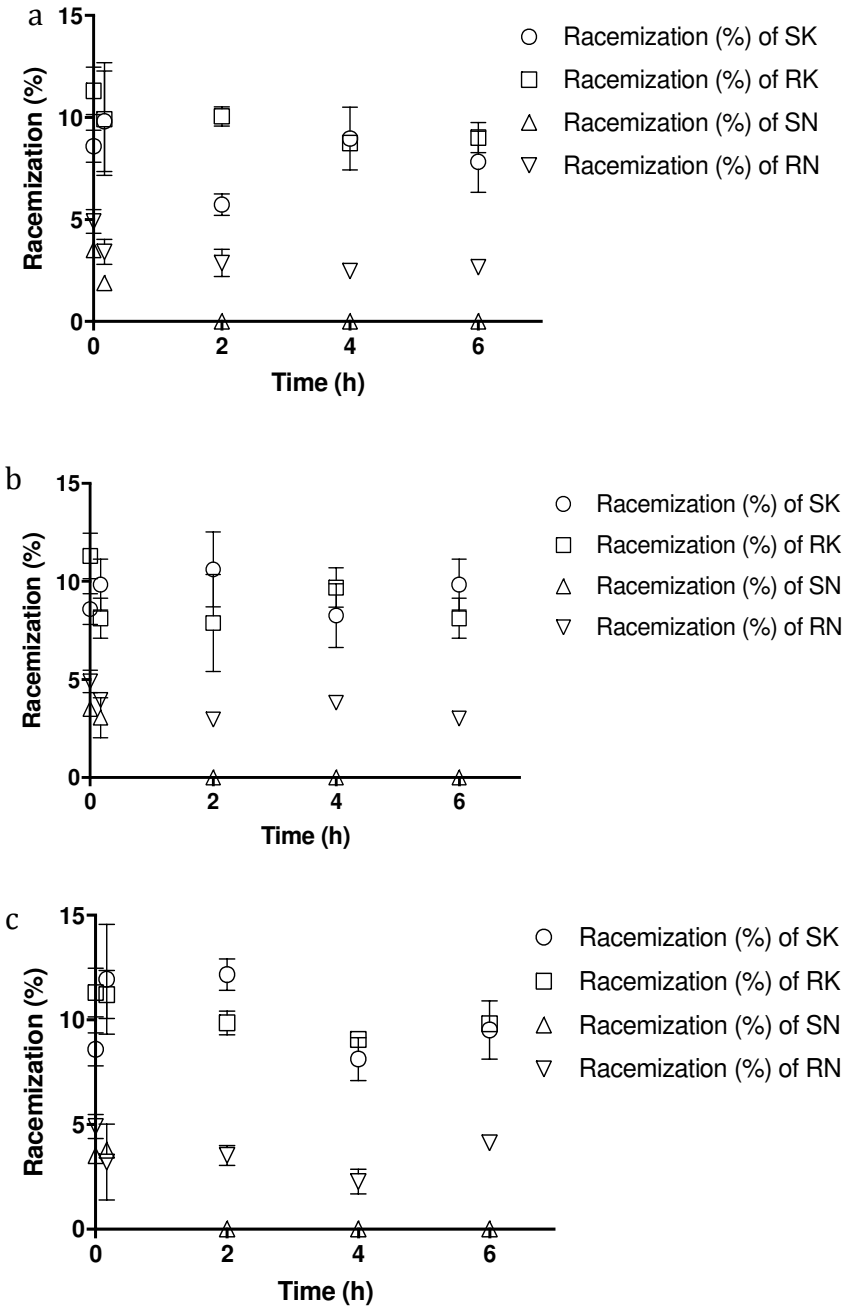

Figure 4.8 Stability of single atropisomers of ketotifen (K) and norketotifen (N) at 37°C over 6 h in (a) HBSS-HEPES buffer pH 7.4, (b) HBSS-HEPES buffer pre-incubated with Caco-2 cell monolayers for 2 h, and (c) HBSS-HEPES buffer in the presence of Caco-2 cell monolayers (data are means ± SD, n = 3).

As shown above, atropisomers of K and N were stable to racemization or inversion under different conditions (Figure 4.7 and 4,8) but the existing counter

atropisomers (5 to 10%) could be a potential problem when we assume pure atropisomers were used. Thus it is necessary to investigate the uptake of K and N into RBE4 cells using both atropisomers (with antipodes) and racemates (50% of each atropisomers) by using both nonchiral (Chapter 2) and chiral assays to investigate the effect of existing antipodes on the uptake of K and N atropisomers in RBE4 cells.

Chapter 5 Uptake and permeation studies of ketotifen and norketotifen in cell models of the BBB

5.1 Introduction

The isolation of cerebral capillaries by Joo and Karnushina (1973) initiated a new generation of *in vitro* studies of the BBB. Recently, investigation of the barrier functions at the cellular and molecular levels has involved *in vitro* models of the BBB such as primary and immortalised capillary endothelial cell lines of human, bovine, porcine and rat brain (Naik and Cucullo 2012; Roux and Couraud 2005) .

The immortalized rat brain endothelial cell line, RBE4, is one of the most well characterized models of the BBB. The cells, immortalized using a plasmid containing the E1A adenovirus gene (Yang et al, 2001), retain many characteristics of their *in vivo* capillary endothelial cells including enzymes, glial factors (Calhau et al, 2002; Roux et al. 1994) and a wide range of transporters. These include P-gp (Babakhanian et al, 2007; Begley et al, 1996), BCRP (Lee et al, 2007), MRP (Regina et al, 1998), GLUT (Regina et al, 1997, 2001) OCTN-2 (Friedrich et al, 2003) and L-amino acid transporter (LAT) (Reichel et al, 2002). For this reason, RBE4 cells are widely used to investigate drug transport across the BBB.

Early studies of K transport in RBE4 cells implicated an influx transporter (Ishiguro et al, 2004), later shown to be a common transporter of cationic H_1 antagonists (Suzuki et al, 2010). This suggests that both K and N are substrates of this transporter but nothing is known about whether it is stereoselective. The first aim of the work reported in this chapter was to determine whether the uptake of K and N by RBE4 cells is stereoselective using single atropisomers (nonchiral assay) and racemates (chiral assays). A non-linear fitting model (Michaelis-Menten), which consists both passive (linear) and active (non-linear) components, was used to estimate kinetic parameters in the uptake.

Although the RBE4 cell line has been widely used for uptake studies, it cannot be used for transendothelial permeability studies because monolayers of REB4 cells do not form complete tight junctions thus do not generate the necessary

restrictive paracellular barrier properties (Rist et al, 1997; Tsukita and Furuse, 2000). Barrier properties can be improved by co-culture of RBE4 cells with astrocytes (or astrocyte-conditioned medium) (Balbuena et al, 2010; 2011) or cortical neurons (Cestelli et al, 2001) but the integrity of the membranes produced remains poor.

An alternative strategy is to use the Caco-2 cell line, an immortalized heterogeneous human epithelial adenocarcinoma cell line which forms complete tight junctions and shares some transporters with rat brain endothelial cells. It has been reported that as endothelial and epithelial cells share similarity in organization and regulation, cultured epithelial cell lines such as Caco-2 are appropriate to investigate generic regulatory mechanisms (Abbott, 2005).

The second aim of the work reported in this chapter was to investigate whether transport of K and N across Caco-2 cell monolayers is stereoselective. This was done using racemates (chiral assays).

5.2 Materials

TrypLE™ Express, MEM non-essential amino acids, F-10 nutrient mixture (Ham) (1×), MEM alpha (1×) minimum essential medium, Dulbecco's Modified Eagle Medium, L-glutamine 200 mM, penicillin-streptomycin (10,000 U/ml), fetal bovine serum (FBS), selective antibiotic (Geneticin® G418 Sulphate) and Dulbecco's phosphate buffered saline were purchased from Gibco® (Invitrogen, New Zealand). Basic bovine fibroblast growth factor (FGF) (156Aa) was purchased from Roche (Mannheim, Germany). Cell proliferation assay using CellTiter 96® AQueous One solution was obtained from Promega Corporation (USA). [^{14}C]Mannitol (58.8 mCi/mmol (2.176 GBq/mmol), OPTIPHASE 'HISAFE' 2 scintillation cocktail and miniature 6 ml polyethylene vials were purchased from PerkinElmer (Waltham, USA). DMSO was purchased from Merck (New Zealand).

12-well, 24-well (MULTIwell™), and 96-well (MICROTEST™) plates, 15 ml and 50 ml high-clarity polypropylene conical tubes, 10 ml and 25 ml serological pipettes were obtained from BD FALCON™ (USA). Collagen coated 12-well plates and 75 cm^2 flasks were purchased from BD BioCoat™ (England). VacuCap® 60 filter units (0.2 μm) were purchased from PALL Life Sciences (Auckland, New Zealand). Cell

culture flasks (25 cm^2) and Transwell® permeable supports (0.4 μm PCmembranes, COSTAR®), were purchased from Corning Inc. (NY, USA). Rapid equilibrium dialysis devices (8K MWCO) (RED, Pierce) were purchased from ThermoFisher Scientific (Taiwan).
Other materials were obtained and described in Section 2.2 and 4.2.

5.3 Methods

5.3.1 Studies in RBE4 cells

5.3.1.1 RBE4 cell culture techniques

Medium preparation: RBE4 cell culture medium was prepared by mixing MEM-alpha and F-10 (1× Hams) medium in a 1:1 ratio and adding 10% FBS, 2 mM L-glutamine, 300 μg/ml G418, 1% penicillin-streptomycin and 1 ng/ml FGF. The medium was sterilized by filtering through a 0.2 μm filter (Aspiration Station GILSON, Switzerland) in a laminar flow hood (HERA Safe KS 12, Thermo Electron Corp. Germany).
Cell thawing: Frozen cells were thawed in a 37°C water bath (Julabo TW20, John Morris Scientific Pty Ltd, Austria) and transferred to a 15 ml centrifuge tube containing 8 ml culture medium. The suspension was centrifuged (KUCOTA 5930, Japan) at 1000 rpm for 5 min, the supernatant removed and the cells resuspended in 10 ml culture medium. The cell suspension was then added to a 75 cm^2 flask along with another 5 ml culture medium and incubated at 37°C under 95% O_2, 5% CO_2 (HERA cell 150, Thermo Electron Corp., Germany). Medium (15 ml) was renewed every two days until confluence.
Cell subculture: After carefully removing culture medium, 1.5 ml TrypLE™ was added and the flask left in the laminar flow hood at room temperature for 10 min to allow cells to detach. Cell culture medium (12 ml) was added and pipetted up and down several times to retrieve most cells. Finally, the cell suspension was equally divided into three clean flasks to which more cell culture medium was added to ensure 15 – 20 ml medium was present in each flask.
Cell freezing: RBE4 cells were detached as described above after which 10 ml cell culture medium was pipetted up and down several times to retrieve most cells.

The cell suspension was transferred to a 15 ml tube and centrifuged at 1000 rpm for 5 min. The supernatant medium was then removed and 10 ml freezing medium (10% DMSO, 90% cell culture medium) added to the cell pellet. Cells were resuspended and divided into 5 freezing tubes, which were stored at -80°C for short-term storage and in liquid nitrogen for long-term storage.
Seeding for uptake studies: RBE4 cells were seeded into a 12-well collagen-coated culture plate at a concentration of 50,000 cells/ml (1.5 ml cell suspension per well) and incubated at 37°C under 95% O_2, 5% CO_2. Medium was changed every 2 days and cells reached confluence in 2 – 3 days.

5.3.1.2 Binding to RBE4 cell membranes (chiral assays)

In cell uptake, before being taken up into cells, compound binds specifically and non-specifically to cell membranes to different extents (Chapter 3). Since cell membranes are a chiral environment (with three-dimensional proteins such as receptors and transporters), it is possible for a chiral compound to stereoselectively bind to cell membranes. However, after homogenizing cells, it is impossible to tell whether the compound concentration determined is from cell membranes (binding) or inside cells (uptake). Therefore, in order to interpret the cell uptake result correctly, it is important to investigate (a) whether the compound binds to cell membrane, and (2) whether the compound binds stereoselectively to cell membranes. In this study, binding of K and N single atropisomers to RBE4 cell membranes was determined using RED.
RBE4 cells were harvested and suspended in water for 4 h at 4°C to allow cells to swell before being subjected to three freeze-thaw cycles (from -80 to 25°C). The suspension was then probe-sonicated for 3 × 10 s with 10 s intervals and centrifuged at 1000 rpm for 10 min to remove unbroken cells and nuclei. The supernatant was further centrifuged (OPTMA™ L Preparative Ultracentrifuge Class R, Beckman and 60 Ti Rotor, Backman, USA) at 22,300 rpm for 10 min (Anthes et al, 2002) and the pellet resuspended and centrifuged again. The final pellet was resuspended in 10 ml Ringer- HEPES buffer pH 7.4 with K or N atropisomers (2 or 10 μM). An aliquot (0.5 ml) of the suspension was added to the RED unit and subjected to orbital shaking (Orbital Mixer Incubator, Ratex) at 250 rpm for 4 h. Aliquots (180 μl) from both the buffer and cell membrane sides

were collected for chiral analysis. Results were analysed and compared using one-way ANOVA with Bonferroni's multiple comparison post hoc test (GraphPad Prism5) to investigate whether the binding of K and N atropisomers to RBE4 cell membranes was stereoselective.

Binding was calculated using Equation 5.1

$$\textbf{Binding (\%)} = (C_{cell} - C_{buffer}) \times 100 / C_{cell} \qquad \textbf{5.1}$$

where C_{cell} is the concentration of compound in cell compartment, C_{buffer} is the concentration of compound in the buffer compartment.

Mass balance (recovery) was calculated using Equation 5.2

$$\textbf{Mass balance (\%)} = (M_{cell} + M_{buffer}) \times 100 / M_{loading} \qquad \textbf{5.2}$$

where M_{cell} is the mass of compound in cell compartment, M_{buffer} is the mass of compound in the buffer compartment, $M_{loading}$ is the mass of compound loaded at the beginning of the experiment.

5.3.1.3 Cytotoxicity to RBE4 cells

The CellTiter 96® AQ_{ueous} One Solution Cell Proliferation Assay, a colorimetric method for determining the number of viable cells, was used in this experiment. This assay reagent is bio-reduced to a coloured formazan product by reduced forms of nicotinamide adenine dinucleotide phosphate or nicotinamide adenine dinucleotide, which is produced by living cells. Therefore, the darker the colour after incubation indicates more formazan product, which is directly proportional to the number of living cells.

RBE4 cells were seeded into 96-well plates at 50,000 cell/ml and allowed to reach confluence over 2 – 3 days. The monolayers were washed three times with 0.2 ml Ringer-HEPES buffer pH 7.4 at 37°C before an experiment.

Aliquots (100 µl) of K or N atropisomer solutions (0 – 100 µM) in Ringer-HEPES buffer pH 7.4 were added to the monolayers after which CellTiter 96® AQueous One Solution (20 µl) (reagent) was added into each well and the plate incubated at 37°C under 5% CO_2 for 2 h. The absorbance of each well was then determined at 490 nm using a plate reader (SPECTRA MAX 340, Molecular Devices).

The strongest colour was produced by wells with cell monolayers only ($A_{control}$), this absorbance representing 100% living cells. To exclude interference absorbance from reagent and buffer, absorbance of wells without cell monolayer

but with reagent and buffer were measured (A_{Blank}) and subtracted from $A_{control}$. Thus, the percentage of living cells remaining after incubation with K and N can be calculated using Equation 5.3:

$$\textbf{Cell Proliferation (\%)} = A_{sample} \times 100 / (A_{Control} - A_{Blank}) \quad \textbf{5.3}$$

where A_{sample} is the absorbance of sample, $A_{Control}$ is the absorbance of the cell monolayer containing buffer and reagent (no drug) and A_{Blank} is the absorbance of buffer and reagent (no cell monolayer or drug).

5.3.1.4 Initial uptake studies

Experiment 1: Time course of uptake of K and N atropisomers

The first experiment involved incubation of single atropisomers of K or N at various time points with RBE4 cell monolayers and analysis of K and N using the nonchiral assay to determine the appropriate time for the concentration-dependent uptake studies.

RBE4 cell monolayers were washed with 0.5 ml Ringer-HEPES buffer pH 7.4 after which 1.5 ml 5 µM solutions of SK, RK, SN or RN were added to wells in triplicate and incubated at 37°C for 1, 2, 3, 5, 10, 15, 20, 30, 60 and 120 min. Incubations were terminated by washing monolayers three times with 0.5 ml ice-cold Ringer-HEPES buffer after which 0.5 ml Milli-Q water was added to each well and incubated at 4°C overnight to detach and briefly lyse cells. The suspensions thus produced were collected by pipetting up and down several times and transferred to 1.7 ml centrifuge tubes. Glass beads were added and sample mixtures homogenised at speed 7 for 3 min using a Bullet Blender®. Finally, 180 µl aliquots of homogenates were processed and subjected to nonchiral analysis (Chapter 2). As each well contains different numbers of cells and compound concentration may vary during detaching and homogenization, all of which may affect measured K and N concentrations. To solve this problem, protein concentration of each homogenate sample was determined to normalise K and N atropisomer concentrations as nmol per mg of protein (nmol of compound per mg of protein in homogenate) instead of nmol. To determine protein concentration of each cell homogenate sample, 50 µl aliquots of homogenates were subjected to BCA™ protein assay. Normalised concentrations

of K and N atropisomers were plotted against time and the linear portion used to determine initial uptake rates.

The time course of uptake of K and N atropisomers from 5 μM solutions at 37°C by RBE4 cells is shown in Figure 5.1. The results indicate that uptake was approximately linear over the first 2 min and this duration was used for subsequent uptake studies (Ishiguro et al, 2004).

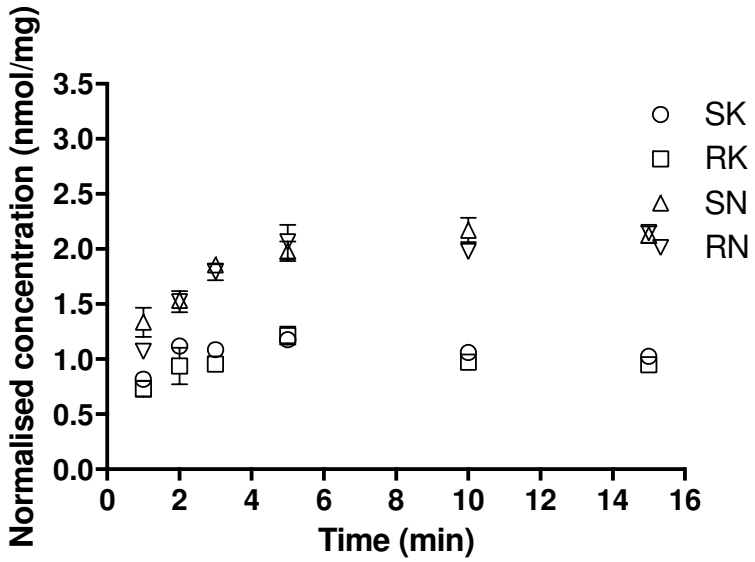

Figure 5.1 Time course of ketotifen (K) and norketotifen (N) atropisomer uptake from 5 μM solutions by RBE4 cells at 37°C (data are means ± SD, *n* = 3).

Experiment 2: Effect of concentration on uptake of K and N atropisomers (incubating with single K or N atropisomers)

The second experiment involved incubation of single atropisomers of K or N at various concentrations with RBE4 cell monolayers for 2 min (based on experiment 1) and analysis of K and N using the nonchiral assay to determine the effect of concentrations on uptake studies.

RBE4 cell monolayers were washed three times with 0.5 ml Ringer-HEPES buffer pH 7.4 and then incubated with 1.5 ml of SK, RK, SN or RN solutions (0.2 – 50 μM) in Ringer-HEPES buffer at 37°C for 2 min. Uptake was terminated, suspensions collected, homogenates prepared and analysed, as described above in Experiment 1. Results were plotted as loading concentration (μM) vs. normalised uptake rate (nmol/mg/min) over 2 min and fitted to a model incorporating passive and active transport (Equation 5.4) using GraphPrism 5.

$$\mathbf{V = (V_{max} \times S)/(K_m + S) + k \times S} \qquad \mathbf{5.4}$$

where V is the reaction rate, K_m is the Michaelis-Menten constant, V_{max} is the maximum reaction velocity of active transport, V contributes most at lower concentrations before the transporter is saturated as indicated by the V_{max} plateau in the active transport curve. S is concentration and k, the rate constant for passive diffusion, becomes important at higher concentrations where V_{max} is reached. The linear part of the curve at high substrate concentration gives the k value. The best-fit values of V_{max}, K_m and k were obtained from the model.

Experiment 3: Effect of temperature and ATP depletion on concentration-dependent uptake of K and N atropisomers (incubating with racemic K and N)

The third experiment involved incubation of racemates of K and N at various concentrations with RBE4 cell monolayers for 2 min (based on experiment 1) and analysis of K and N by atropisomers using the chiral assays to determine the effect of concentrations, temperatures and ATP depletion on uptake studies (mechanism of uptake).

At 4°C, the active transport was eliminated by cutting off the ATP required, as enzymes involved in ATP production are not functioning at 4°C. However, the lower temperature not only reduces the enzyme activity but also alters other parameters such as pH of buffer used during uptake studies, pKa and distribution coefficient of K and N (Chapter 3), cell membrane structures and, consequently, passive diffusion constant. Thus, the reduction of uptake at 4°C may not simply a result from reduced active transport. It is necessary to investigate the role of active transport played in cell uptake of K and N. To exclude the interference from passive diffusion, NaN_3, an ATP depleter, was used. This is because as an ATP depleter, NaN_3 eliminates active transport without changing other variables.

Both the 4°C and ATP depleter methods provide information on uptake of K and N in different aspects under different conditions. As a result, comparing data from these studies may provide more information and help with interpreting uptake results.

To investigate the effect of temperature, RBE4 cell monolayers were washed three times with 0.5 ml Ringer-HEPES buffer pH 7.4 and then incubated with 1.5 ml of racemic K or racemic N solutions (0.5 – 100 μM) in Ringer-HEPES buffer for 2 min.

For the uptake at 37°C, experiments were performed as described above in Experiment 2. For the uptake at 4°C, uptake of racemic K and N was investigated in a cold-room maintained at 4°C to eliminate active transport. Uptake rate (nmol/mg/min) over 2 min time versus concentration (μM) of K and N atropisomers was interpreted by linear regression (ie. Equation5.4 collapses to: $V = k \times S$) and taken as the passive diffusion constant for the determined compound.

To investigate the effect of ATP depletion, RBE4 cell monolayers were washed and incubated with 1.5 ml 10 mM NaN_3 solution in Ringer-HEPES buffer pH 7.4 at 37°C for 30 min. After removal of the NaN_3 solution, 1.5 ml racemic K and N solutions at various concentrations (0.5 – 100 μM) containing 10 mM NaN_3 in Ringer-HEPES buffer pH 7.4 were added and incubated for 2 min at 37°C. Uptake was terminated by washing three times with ice-cold Ringer-HEPES buffer, and samples subjected to chiral analysis. Uptake with or without 10 mM NaN_3, rate (nmol/mg/min) at 37°C over 2 min versus concentration (μM) of K or N atropisomers was determined by nonlinear regression using GraphPrism 5 (Equation 5.4).

Statistical analysis was carried out by one-way ANOVA with post-hoc Bonferroni testing to compare selected data sets. Results are presented as means ± SD. Differences for which $p < 0.05$ were taken as significant.

5.3.2 Studies in Caco-2 cells

5.3.2.1 Caco-2 cell culture techniques

Medium preparation: Caco-2 cell culture medium was prepared by mixing DMEM with 10% FBS, 1% penicillin-streptomycin and 1% MEM-NEAA in the laminar flow hood.

Cell thawing: Frozen Caco-2 cells were equilibrated at 40°C and transferred into a 15 ml centrifuge tube containing 8 ml culture medium. The suspension was centrifuged at 1000 rpm for 5 min and the cells resuspended in 7 ml culture medium before being transferred to a 25 cm^2 flask. Cells were then placed in an incubator at 37°C under 95% O_2, 5% CO_2 and 7 ml culture medium added every two days until reaching confluence.

Cell subculture: After removing medium from the flask, 0.5 ml TrypLE™ was added to cover the cell monolayer and the flask left in the laminar flow hood at room temperature for 10 min to allow cells to detach. Cell culture medium (6 ml) was added and pipetted up and down several times to retrieve most cells after which the cell suspension was divided into three clean flasks and cell culture medium added to ensure 7 – 8 ml medium was present in each flask.
Cell freezing: Caco-2 cells were detached and collected by pipetting up and down several times. The cell suspension was transferred to a 15 ml tube and centrifuged at 1000 rpm for 5 min. After removal of supernatant, 6 ml freezing medium (10% DMSO, 90% cell culture medium) was added and cells resuspended and divided into three freezing tubes. Tubes were stored at -80°C for short-term storage and in liquid nitrogen for long-term storage.
Cell seeding for permeability studies: Aliquots (0.5 ml) of Caco-2 cell suspension were added to a 12-well transwell plate at a concentration of 100,000 cells/well. Cell culture medium (1.5 ml) was added to each well and changed every two days. TEER was measured every two days until it reached a constant value of around 300 – 400 $\Omega*cm^2$ after about 21 days.

5.3.2.2 TEER measurement

The TEER instrument described was switched on and probes were equilibrated in warmed sterilized PBS (37°C) for 5 min in the laminar flow hood. The TEER probes were then carefully inserted into each well with the short probe in the insert and the longer probe in the well. After measurement, probes were left in PBS solution for short-term storage.

5.3.2.3 Permeability of K and N atropisomers

Solutions of K and N racemates (5 µM) were prepared containing 3×10^5 dpm/ml [^{14}C]mannitol in HBSS-HEPES buffer pH 7.4. Caco-2 cell monolayers were washed with HBSS-HEPES buffer at 37°C for 3 × 5 min before recording the TEER value.
Caco-2 cell monolayers were incubated with test solutions in triplicate. For study of A (apical) to B (basolateral) transport, 0.5 ml drug solution was added to

inserts and 1.5 ml HBSS-HEPES buffer added into wells below inserts. For B to A studies, 1.5 ml drug solution was added to wells below inserts while 0.5 ml buffer was added to inserts. Plates were incubated at 37°C for 2 h during which 0.4 ml samples were taken from the receptor side after 10, 20, 30, 60, 90 and 120 min and immediately replaced with 0.4 ml 37°C HBSS-HEPES buffer.

After collecting the last sample, TEER values were measured taking care to wash probes after use to remove radioactivity. All solutions from donor and receptor sides were transferred to labelled 1.7 ml centrifuge tubes and the filter membranes washed with ice-cold HBSS-HEPES buffer and cut off from inserts. Caco-2 cells on these membranes were transferred to 1.7 ml centrifuge tubes and homogenized in 0.5 ml Milli-Q water containing glass beads using a Bullet Blender® at speed 7 for 3 min.

Samples from the donor and receptor sides as well as loading solutions and cell monolayer homogenates were subjected to chiral analysis. To determine permeability of [^{14}C]mannitol, 100 µl samples were mixed with 5 ml scintillation cocktail for scintillation counting. Samples of cell monolayer homogenates were used to analyse protein concentration using BCA protein assay. P_{app} values of [^{14}C]mannitol, K and N racemates were calculated using Equation 5.5:

$$\mathbf{P_{app} = (dQ/dt) / (A \times C_0)} \qquad \mathbf{5.5}$$

where dQ/dt is the rate of permeation (µmol/s) obtained from the slope of the linear portion of the Q versus time data, A is the surface area of the membrane (1.12 cm^2) and C_0 is the initial concentration in the donor solution (µM). The equation assumes that the donor concentration is essentially constant over the time of the study and Q versus t is linear.

The mass recovered (%) of K and N atropisomers was calculated using Equation 5.6:

$$\mathbf{Mass\ recovered\ (\%) = (MS + MD + MC + MR) \times 100/MT} \qquad \mathbf{5.6}$$

where MS is the mass of compound in collected samples, MD is the mass of compound in the donor side after 2 h incubation, MC is the mass of compound in the cell monolayer homogenate, MR is the mass of compound in the receptor side after 2 h incubation and MT is the mass added to the donor side at beginning of the study (time 0).

Statistical analysis was carried out by one-way ANOVA with post-hoc Bonferroni testing to compare selected data sets using GraphPad Prism (GraphPad Software, San Diego, CA, USA). Results are presented as means ± SD. Differences for which $p < 0.05$ were taken as significant.

5.4 Results

5.4.1 Binding of K and N atropisomers to RBE4 cell membranes

There was no significant difference between binding of SK and RK or between SN and RN to RBE4 cell membranes at the tested concentrations. The results suggest that binding of K and N atropisomers to RBE4 cell membranes is not stereoselective. However, binding of SN and RN was significantly higher than that of SK and RK at both concentrations (Figure 5.2).

Mass balance of K and N atropisomers (Table 5.1) was in the range 78.5 – 110% of the concentration of the loading solution.

The concentrations 2 μM and 10μM of K and N atropisomers were chosen as low and high concentrations of K and N before saturation of active transport (Figures 5.5 and 5.6). That is, the concentration used for these binding studies was sufficient to detect binding but not high enough to saturate the binding sites.

Table 5.1 Mass balance (recovery) for binding of ketotifen (K) and norketotifen (N) atropisomers to RBE4 membranes racemates as determined by rapid equilibrium dialysis at 37°C for 4 h (data are means, *n* = 3).

	Loading (μM)	Cell (%)	Buffer (%)	Recovery (%)
SK	2	44.1	34.5	78.5
RK		50.7	35.1	85.8
SN		75.4	35.4	110.8
RN		67.8	32.7	100.6
SK	10	59.0	40.9	99.9
RK		63.9	43.6	107.5
SN		65.9	29.4	95.3
RN		65.1	25.0	90.2

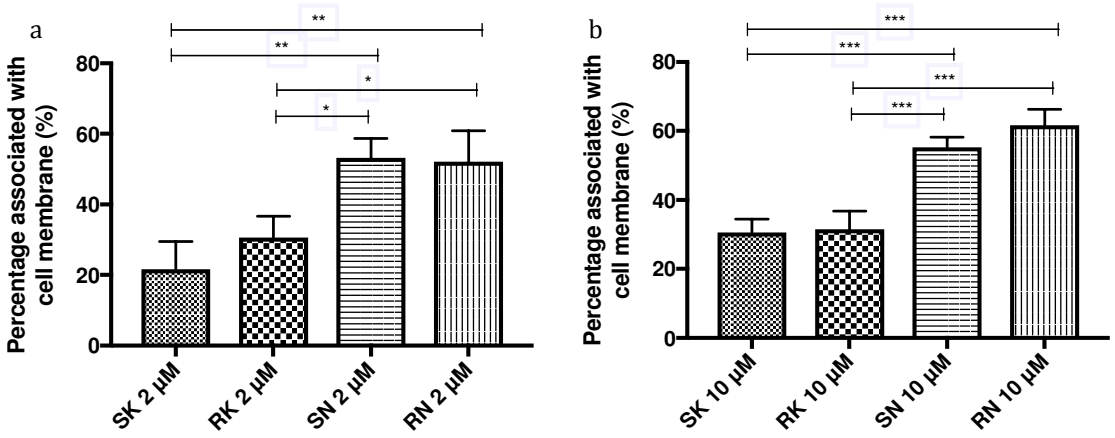

Figure 5.2 Binding of ketotifen (K) and norketotifen (N) atropisomers (a) 2 µM and (b) 10 µM to RBE4 cell membranes after 4 hours at 37°C (data are means ± SD, *n* = 3) (* P < 0.05, ** P < 0.01 and *** P < 0.001).

5.4.2 Cytotoxicity of K and N to RBE4 cell monolayers

K and N were non-cytotoxic to RBE4 cells over 2 h in the tested concentration range (Figures 5.3 and 5.4) as the number of viable cells changed by < 10%. The slight increase in living cell percentage over time is probably due to medium evaporation during incubation.

Based on these results, concentrations up to 100 µM were deemed safe to use in RBE4 uptake experiments.

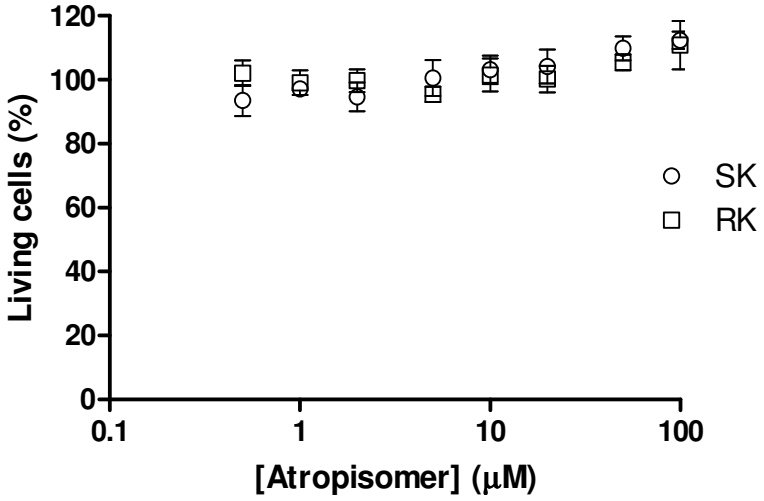

Figure 5.3 Cytotoxicity of ketotifen (K) atropisomers to RBE4 cell monolayers after 2 h at 37°C (data are means ± SD, *n* = 4).

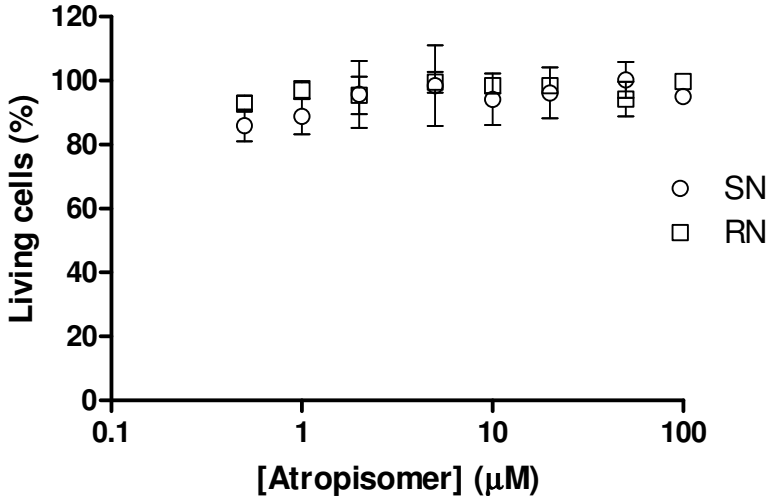

Figure 5.4 Cytotoxicity of norketotifen (N) atropisomers to RBE4 cell monolayers after 2 h at 37°C (data are means ± SD, *n* = 4).

5.4.3 Initial uptake experiments

Concentration dependence (Experiment 2, loading single atropisomers):

The concentration dependence of uptake of K (Figure 5.5) and N (Figure 5.6) atropisomers (loaded as single atropisomers) into RBE4 cell monolayers over 2 min at 37°C shows a combination of both active and passive transport. The presence of active uptake is consistent with previous studies, which suggested K is transported by an unidentified influx transporter (Ishiguro et al, 2004; Suzuki et al, 2010).

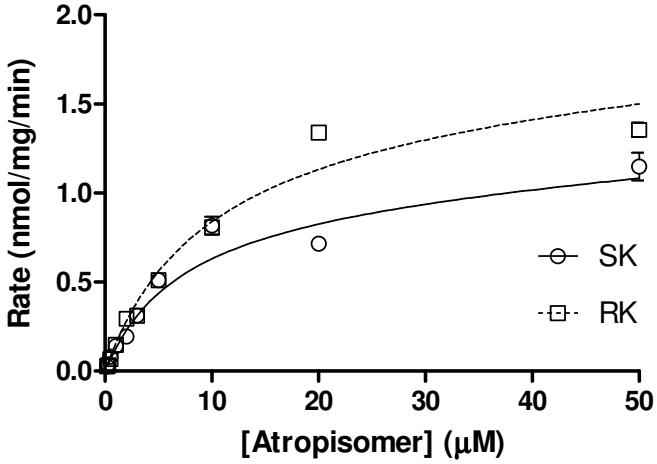

Figure 5.5 Initial rate of uptake of S-ketotifen (SK) and R-ketotifen (RK) atropisomers after loading single atropisomers into RBE4 cell monolayers over 2 min at 37°C (data are means ± SD, *n* = 3). The non-linear regression is based on Equation 5.4.

There are small differences between the rate of uptake of SK and RK (Figure 5.5) and SN and RN (Figure 5.6), but the differences are not significant (Table 5.2). The small differences may be due to inter-well variation arising from the loading of individual atropisomers into different wells. The results indicate that uptake of K and N atropisomers into RBE4 cell monolayers is not stereoselective under the tested conditions.

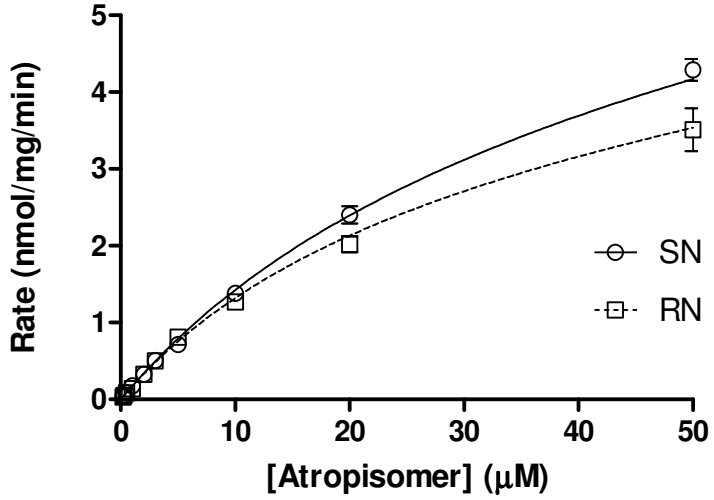

Figure 5.6 Initial rate of uptake of S-norketotifen (SN) and R-norketotifen (RN) atropisomers after loading single atropisomers into RBE4 cell monolayers over 2 min at 37°C (data are means ± SD, *n* = 3). The non-linear regression is based on Equation 5.4.

Table 5.2 Parameter estimates based on Equation 5.4 for uptake of ketotifen (K) and norketotifen (N) atropisomers loaded as single atropisomers over 2 min at 37°C (data are means ± SD, *n* = 3).

	V_{max} (nmol/mg/min)	K_m (μM)	k (μL/mg/min) (shared)
SK	1.02 ± 0.31	7.24 ± 2.69	3.84 ± 6.10
RK	1.55 ± 0.41	9.45 ± 2.68	
SN	5.78 ± 4.25	35.6 ± 19.5	15.9 ± 36.5
RN	4.15 ± 2.73	25.8 ± 12.3	

Although non-stereoselective, the results show that the uptake of N atropisomers is higher than that of K atropisomers by both active transport and passive diffusion (Table 5.2). The latter is unexpected since the Log D (octanol/buffer pH 7.4) of K (2.68 ± 0.02) is higher than that of N (1.62 ± 0.45) (Table 3.4) but it is

consistent with the greater binding of N to RBE4 cells as revealed in the binding studies (Figure 5.2). In addition, the result is also consistent with the Log D (liposome/buffer pH 7.4 at 37°C) of K (2.63 ± 0.04), which is lower than that of N (3.64 ± 0.01) (Table 3.4). This provides further evidence that the higher concentration of N determined was a result from association with cell membranes.

Concentration, temperature and ATP dependence (Experiment 3, loading racemates):

The concentration dependence of the rates of uptake of K (Figure 5.7) and N (Figure 5.8) atropisomers loaded as racemates also shows a combination of active and passive transport.

The data for SK and RK and for SN and RN are almost superimposable, indicating the uptake is not stereoselective.

In addition, the uptake of N is much higher than that of K by both active and, especially, by passive transport mechanisms.

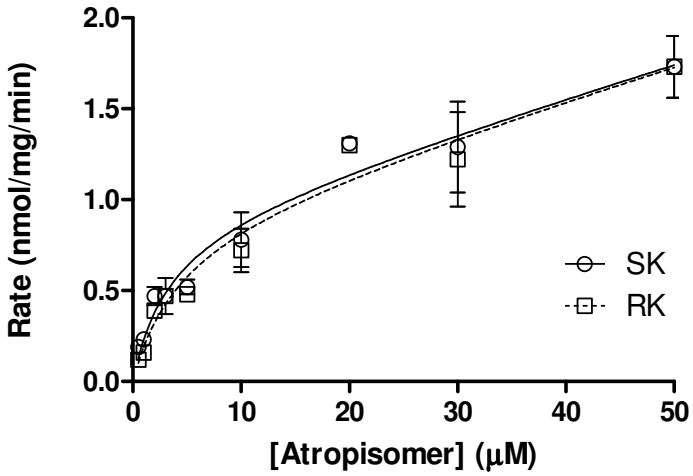

Figure 5.7 Initial rate of uptake of S-ketotifen (SK) and R-ketotifen (RK) atropisomers into RBE4 cell monolayers after loading racemic ketotifen (K) over 2 min at 37°C (data are means ± SD, *n* = 3).

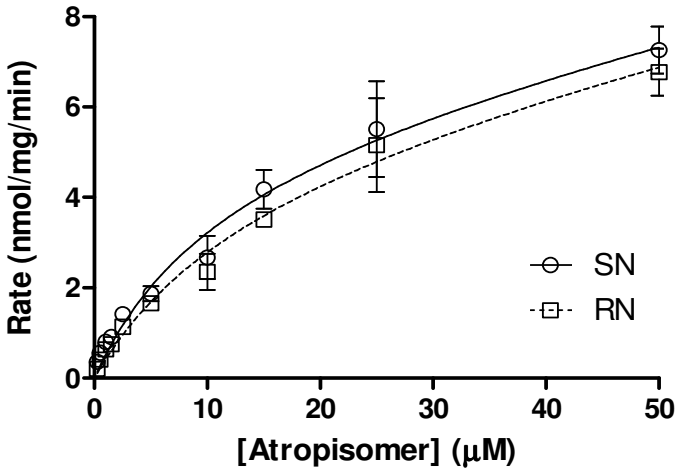

Figure 5.8 Initial rate of uptake of S-norketotifen (SN) and R-norketotifen (RN) atropisomers into RBE4 cell monolayers after loading racemic norketotifen (N) over 2 min at 37°C (data are means ± SD, *n* = 3).

The uptake rates of K atropisomers at 4°C and in the presence of NaN_3 at 37°C are shown in Figures 5.9 and 5.10, and the corresponding uptake rates for N atropisomers are shown in Figures 5.12 and 5.13.

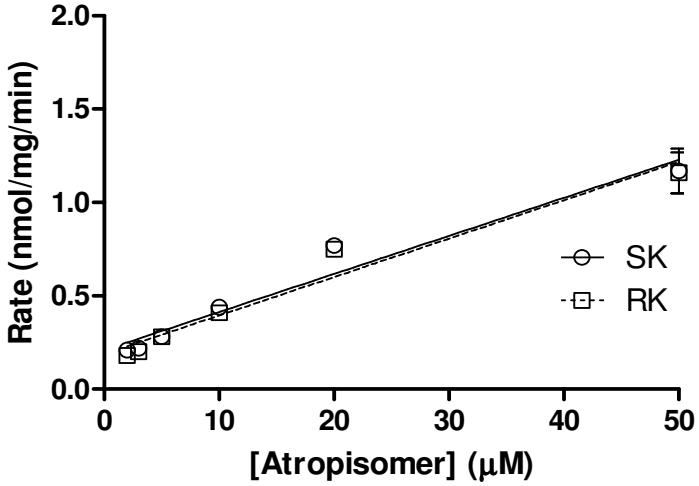

Figure 5.9 Initial rate of uptake of S-ketotifen (SK) and R-ketotifen (RK) atropisomers after loading racemic ketotifen (K) into RBE4 cell monolayers over 2 min at 4°C (data are means ± SD, *n* = 3).

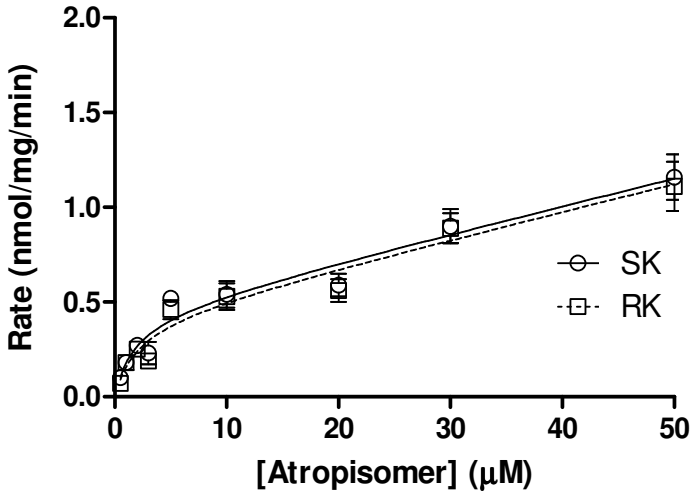

Figure 5.10 Initial rate of uptake of S-ketotifen (SK) and R-ketotifen (RK) atropisomers after loading racemic ketotifen (K) and 10 mM NaN_3 into RBE4 cell monolayers over 2 min at 37°C (data are means ± SD, *n* = 3).

The rates of uptake of K atropisomers in the absence and presence of NaN_3 is shown in Figure 5.11 and those for N atropisomers in Figure 5.14.

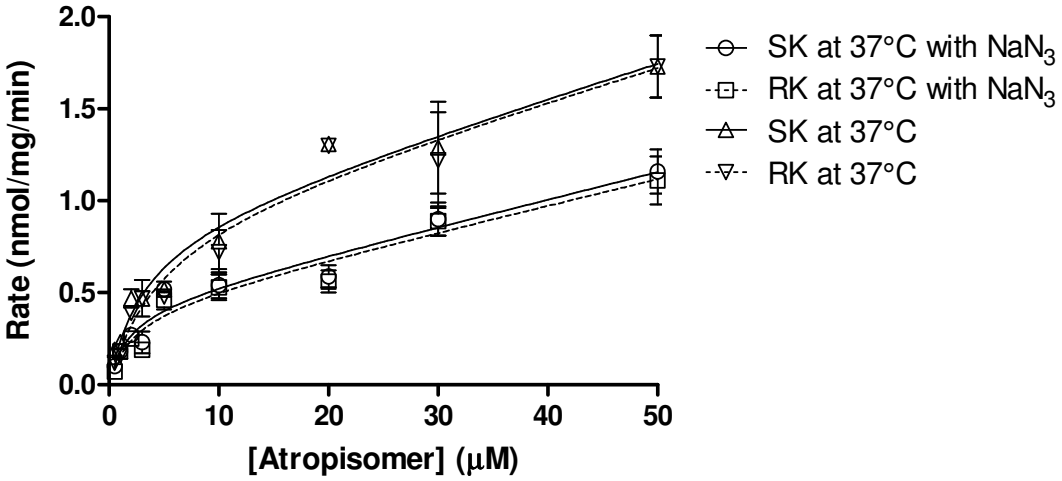

Figure 5.11 Comparison of initial rate of uptake of S-ketotifen (SK) and R-ketotifen (RK) atropisomers after loading racemic ketotifen (K) with and without 10 mM NaN_3 into RBE4 cell monolayers over 2 min at 37°C (data are means ± SD, *n* = 3).

Parameter estimates based on Equation 5.4 are given in Table 5.3, except at 4°C when only the passive component of Equation 5.4 was relevant.

Table 5.3 Parameter estimates based on Equation 5.4 for uptake of ketotifen (K) and norketotifen (N) atropisomers (loading racemate) by RBE4 cell monolayers at 4°C and 37°C and in the presence of NaN_3 (data are means ± SD, n = 3).

	37°C			4°C	37°C with 10 mM NaN_3		
	V_{max} (nmol/mg/min)	K_m (μM)	k (μl/mg/min) (Shared)	k (μl/mg/min)	V_{max} (nmol/mg/min)	K_m (μM)	k (μl/mg/min)
SK	0.91 ± 0.19	3.33 ± 1.60	17.8 ± 4.0	20.4 ± 2.2	0.45 ± 0.10	1.80 ± 1.11	14.4 ± 2.2
RK	0.91 ± 0.21	4.41 ± 2.18		20.6 ± 2.1	0.42 ± 0.10	2.04 ± 1.33	
SN	5.68 ± 1.70	11.2 ± 4.8	53.6 ± 22.8	110 ± 3	1.31 ± 0.15	3.14 ± 0.81	52.1 ± 29.0
RN	5.36 ± 1.90	13.9 ± 6.6		120 ± 3	1.10 ± 0.13	2.26 ± 0.68	

Corresponding data for uptake of N atropisomers are shown in Figures 5.12, 5.13 and 5.14.

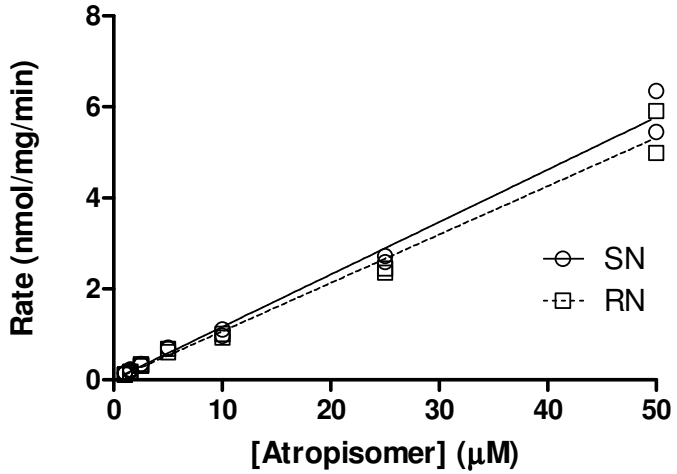

Figure 5.12 Initial rate of uptake of S-norketotifen (SN) and R-norketotifen (RN) after loading racemic norketotifen (N) into RBE4 cell monolayers over 2 min at 4°C (data are means ± SD, *n* = 3).

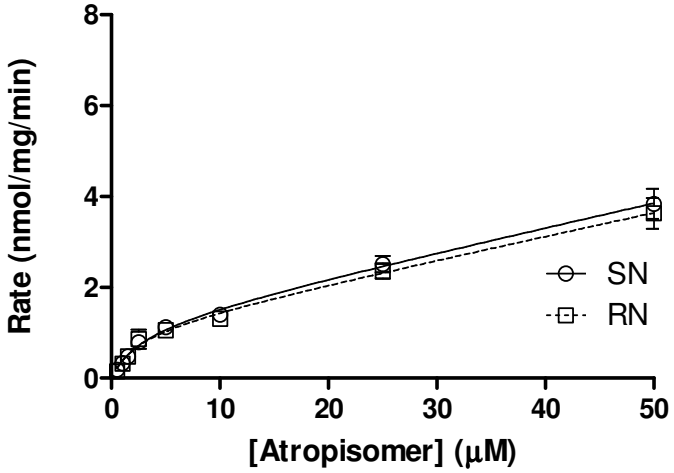

Figure 5.13 Initial rate of uptake of S-norketotifen (SN) and R-norketotifen (RN) after loading racemic norketotifen (N) and 10 mM NaN_3 into RBE4 cell monolayers over 2 min at 37°C (data are means ± SD, *n* = 3).

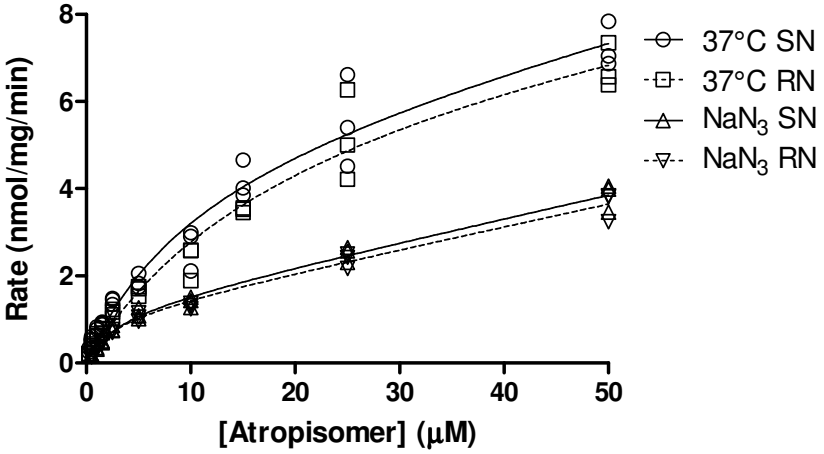

Figure 5.14 Comparison of initial rate of uptake of S-norketotifen (SN) and R-norketotifen (RN) after loading racemic norketotifen (N) with and without 10 mM NaN_3 into RBE4 cell monolayers over 2 min at 37°C (data are means ± SD, *n* = 3).

Uptake at 4°C and 37°C (with NaN_3) showed a reduced active transport for both K and N comparing with estimated parameters at 37°C. For passive diffusion, at 4°C k increased significantly for both K and N. This is possibly due to the effect of temperature on pKa, logD and other factors discussed before (Chapter 3). At 37°C (with NaN_3), for both K and N, k values were found similar to those at 37°C without NaN_3 (Table 5.3). This is because NaN_3 only depletes ATP to reduce active transport

instead of affecting other parameters, which alter passive diffusion. In addition, the uptake of K and N at 4°C were almost linear profiles (Figure 5.9 and 5.12). In contrast, uptake of K and N at 37°C (with NaN_3) were still non-linear, which suggested a reduced but still present active transport (Figure 5.10 and 5.13, Table 5.3).

5.4.4 Permeability of Caco-2 cell monolayers (loading racemates)

TEER value measured before and after the permeability study were all within the range of 300 – 400 Ω*cm^2. In addition, the P_{app} of [^{14}C]mannitol (< 10^{-6} cm/s) agreed with TEER result. Both results indicated the Caco-2 monolayers were intact all through the study. For RBE4 cells, on the other hand, the TEER value of monolayers has been reported to be approximately 100 Ω*cm^2 or even less (Faria et al, 2010). Moreover, P_{app} of sucrose through RBE4 cell monolayer has been reported to be 214 × 10^{-6} cm/s, which is much higher than that through *in vivo* rat BBB (less than 0.1 × 10^{-6} cm/s) (Gumbleton and Audus, 2001). These results indicated that compared with the "leaky" RBE4 cell monolayers, the Caco-2 monolayers are "tight and intact", thus providing a good barrier model to assess transcellular permeation.

P_{app} values for transport of K and N atropisomers across Caco-2 cell monolayers in the A to B and B to A directions are shown in Figure 5.15.

Results show there is no stereoselective transport of K or N atropisomers in either direction through Caco-2 cell monolayers after 2 h at 37°C. However, about twice as much of both K and N is transported from B to A than from A to B (Table 5.4). This may indicate an efflux mechanism involved in the transport of K and N through Caco-2 cell monolayers, which is not stereoselective.

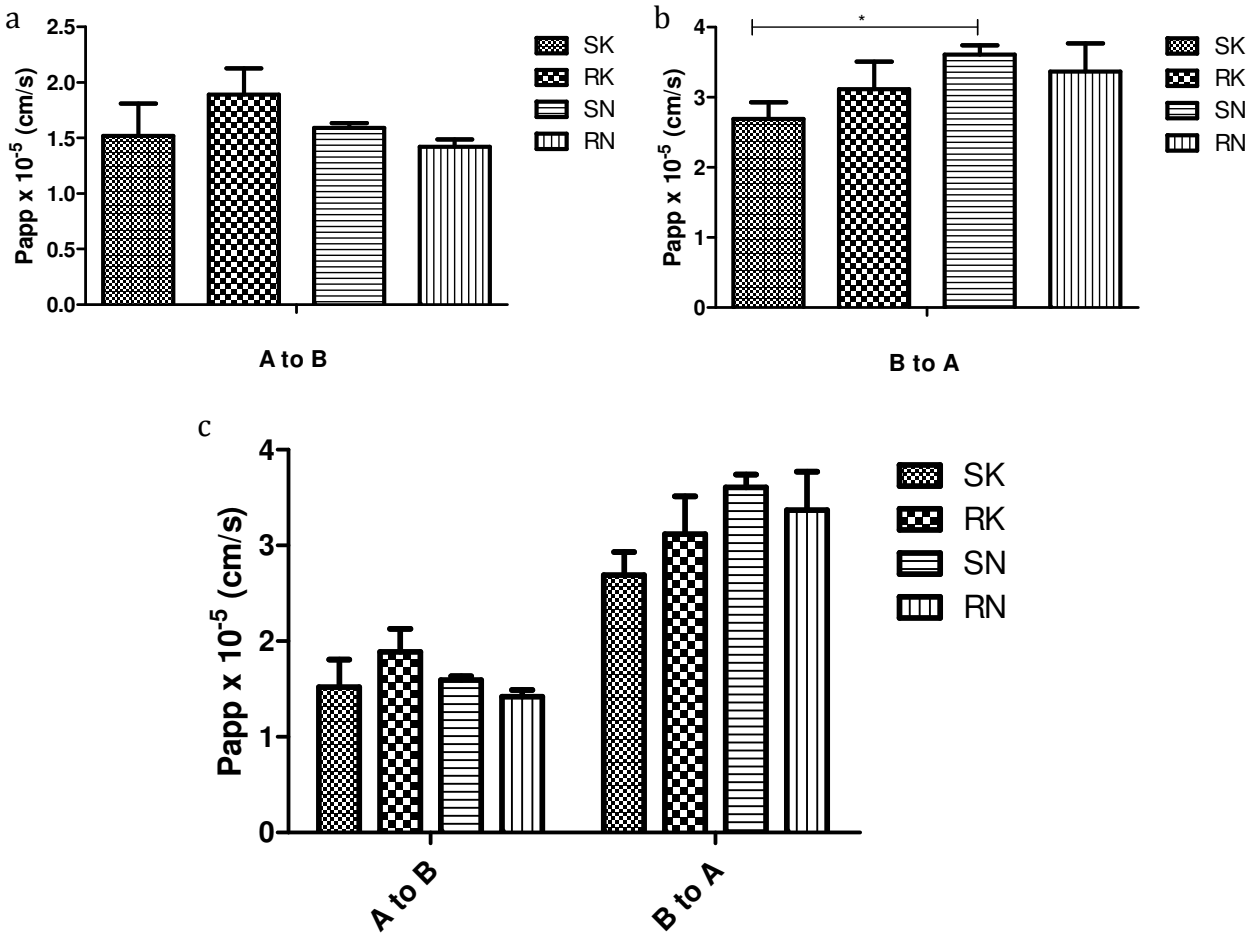

Figure 5.15 P_{app} values for transport of ketotifen (K) and norketotifen (N) atropisomers (loaded as racemates) across Caco-2 monolayers after 2 h at 37°C in the (a) apical to basolateral and (b) from basolateral to apical direction; (c) compares the two sets of data (data are means ± SD, *n* = 3, * P< 0.05)

Table 5.4 P_{app} values for transport of ketotifen (K) and norketotifen (N) atropisomers across Caco-2 cell monolayers after 2 h at 37°C (data are means ± SD, *n* = 3).

Compound	Direction	P_{app} (10^{-5} cm/s)	Efflux ratio
SK	A to B	1.52 ± 0.29	1.77
	B to A	2.69 ± 0.24	
RK	A to B	1.89 ± 0.24	1.65
	B to A	3.12 ± 0.39	
SN	A to B	1.59 ± 0.04	2.27
	B to A	3.61 ± 0.13	
RN	A to B	1.42 ± 0.07	2.37
	B to A	3.37 ± 0.40	

Mass balance for this study (Table 5.5) shows the recovery of K and N atropisomers from the donor and receptor sides and Caco-2 cell monolayers was > 72%.

Table 5.5 Mass balance for transport of K and N atropisomers across Caco-2 cell monolayers after 2 h at 37°C.

		Total (nmol)	Donor (nmol)	Receptor (nmol)	Cell (nmol)	Recovery (%)
A to B	SK	3.56	1.87	0.76	0.05	75.4
	RK	3.67	1.90	0.99	0.05	80.2
	SN	2.66	1.14	0.70	0.09	72.8
	RN	2.62	1.21	0.62	0.11	74.1
B to A	SK	9.69	5.68	1.24	0.08	72.3
	RK	10.03	5.90	1.50	0.11	74.9
	SN	7.77	4.49	1.45	0.22	79.3
	RN	7.87	4.27	1.35	0.22	74.3

Interestingly, despite the fact that the total recovery of K and N atropisomers is similar, the mass of K and N recovered from the Caco-2 cell monolayers was significantly different (Figure 5.16) in both the A to B and B to A directions, with the Caco-2 cells containing approximately twice as much N as K. This is consistent with the results from RBE4 cell uptake and log $D_{l/b}$ studies (Table 3.4). As discussed before (Section 3.5 and 5.4.3), it indicates the association of compounds with cell and liposome membranes. N associated more with Caco-2 membranes compared with K, therefore the recovered mass of N was more than K on Caco-2 cell monolayers. The difference was not affected by stereoselective binding to Caco-2 cell membranes because there was no significant difference between K atropisomers or N atropisomers (Table 5.5).

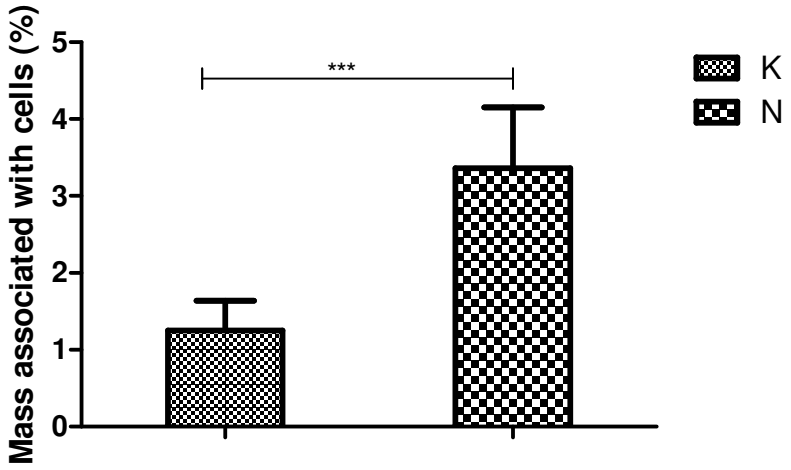

Figure 5.16 Mass percentage of ketotifen (K) and norketotifen (N) associated with Caco-2 cell monolayers after permeability study at 37°C for 2 h (data are means ± SD, *n* = 12, *** P < 0.0001).

5.5 Discussion

5.5.1 Effect of ATP depletion

The uptake of K and N at 37°C in the presence of 10 mM NaN_3 should occur predominantly by passive diffusion. Theoretically, 10 mM NaN_3 depletes ATP production to 30% by inhibiting mitochondrial oxidative phosphorylation (Kang et al, 2001; Togami et al, 2013). Although more efficient ATP depletion can be achieved using a combination of ATP depleters (Mandel et al, 1994; Wilson et al, 1990) this was not necessary in this study where the aim was to simply establish that active transport is involved.

5.5.2 Uptake and association

As discussed in Chapter 3, the difference between log $D_{o/b}$ and log $D_{l/b}$ could also be related to the interaction between K and N and liposomes. Both K and N at pH 7.4 are positively charged but K (pKa = 8.8) is less ionized than N (pKa = 10.3), such that negatively charged liposomes interact and bind more strongly to N than to K. The binding studies of K and N atropisomers to RBE4 cell membranes indicated binding of N to cell membranes was more than that of K (Figure 5.2). It was also consistent with cell experiments where for RBE4 cells there was more N associated with cells then K (Table 5.2 and 5.3). In addition, results from Caco-2 cell studies also indicate that more N is associated with Caco-2 cell monolayers during permeability experiments than that of K (Figure 5.16). The above results suggest that the higher "uptake" of N by RBE4 cells is due to association with cell membranes rather than uptake into cells.

5.5.3 Effect of temperature on RBE4 cell uptake

Active transports are reduced at 4°C but changing temperature can also affect passive distribution of ionic drugs into lipid bilayers, as discussed in Chapter 3.
In these uptake studies, among many factors changed by temperature, the association with membranes was the main factor (Table 5.3). This is because RBE4 cell uptake at 37°C with and without NaN_3 had similar passive diffusion coefficients for both K and N, whereas at 4°C, N had a much higher k than both K and N at 37°C and K at 4°C.

In addition, a reduction of temperature leads to a reduction of membrane fluidity, which would reduce passive diffusion across cell membranes.
Moreover, according to the Strokes-Einstein equation, a decrease in temperature decreases the diffusion coefficient of compounds due to decreased thermal motion; also, there is an increase in water viscosity with decreasing temperature. This means that at lower temperature, the diffusion constant is reduced for both K and N.
Besides all the above reasons, a reduction of temperature also may alter the binding profile of compounds to cell membranes. It is not possible, therefore, to simply conclude that a decrease in uptake at 4°C is due to elimination of active transport.

5.5.4 RBE4 uptake and Caco-2 monolayer permeability studies

RBE4 cell uptake and binding was not stereoselective for either K or N at 37°C (Tables 5.2). In addition, there was no stereoselective uptake (or association) of K or N atropisomers at 4 or 37°C with or without an ATP depleter (Tables 5.3).
For both K and N, the uptake (or association) was a combination of active transport and passive diffusion. This was suggested by the good fit ($R^2 \geq 0.96$) of the equation containing both active and passive components (Equation 5.4). It was also supported by results of the studies with ATP depleter, NaN_3, as uptake was reduced and more linear with NaN_3 (Figure 5.11 and 5.14).
In the Caco-2 cell permeability studies, with intact Caco-2 monolayers throughout experiments (based on TEER value and [^{14}C]mannitol result), there was no stereoselective transport of K or N atropisomers across Caco-2 cell monolayers after 2 h at 37°C. For both K and N, the B to A P_{app} was higher than the A to B $P_{app,}$ an indication of the presence of an efflux mechanism. However, there was no evidence of a stereoselective efflux mechanism for either K or N atropisomers, as the respective efflux ratios for SK and RK were 1.77 and 1.65, and for SN and RN were 2.27 and 2.37 (Table 5.4). Mass balance was similar for both K and N (Table 5.5) but N was found to associate with Caco-2 cell membranes to a greater extent than K (Figure 5.16). This is consistent with the RBE4 cell uptake result showing N is more associated with cell membranes than K.
As discussed before, RBE4 cells do not express occluding and only express very low level of claudin, thus they do not form restrictive paracellular barrier (TEER = 64 ± 5 Ω*cm^2) (Rist et al, 1997; Tsukita and Furuse, 2000; Veszelka et al, 2018), which is

critical for investigate permeability for small molecular compounds, such as K and N. Even co-culture with other cells, such as astrocytes, does not improve the paracellular barrier enough for permeability studies (Veszelka et al, 2018). As a result, to ensure the paracellular barrier, Caco-2 cells were used as a transcellualr permeability model in this thesis.

Although there are no reports of stereoselective transporters on RBE4 cells, there are many reports of stereoselective transport mechanisms on Caco-2 cells. These apply to P-gp (cetirizine, fexofenadine, ginsenoside Rh2, methadone) and MRP transporters (cetirizine, nerapamil) (Gu et al, 2010; He et al. 2010; Shen et al, 2007). The stereoselective transport of fexofenadine by P-gp has also been reported in human (Miura et al, 2007). As P-gp and some of the MRPs are also expressed by REB4 cells, it is likely that stereoselective transport also occurs in RBE4 cells. This supports the use of both RBE4 and Caco-2 cells as screening models.

However, as RBE4 and Caco-2 cells are from different origins (endothelial and epithelial cells), they do differ in transporter expressions.

Although RBE4 cells express both P-gp (Babakhanian et al, 2007) and BCRP (Lee et al, 2007), BCRP level has been reported to be very low (Veszelka et al, 2018). In addition, MRP 1, 3 and 5 have been found at RBE4 cell but at much lower level compared to the Caco-2 cells.

In Caco-2 cell monolayers, both BCRP and P-gp are expressed, at a much higher level compared to that in RBE4 cells (Veszelka et al, 2018). Moreover, an overexpression of P-gp at the Caco-2 cell monolayer has been reported (Lohmann et al, 2002). It was concluded these cells can be used to investigate if a compound is a substrate of efflux transporters (Rodrigues et al, 2009; Wilhelm and Krizbai, 2014).

As discussed, Caco-2 cell express a much higher level of efflux transporters compared to RBE4 cells. The efflux mechanism indicated by the Caco-2 cells could be overestimated compared to that in rat BBB.

In summary, using both cell lines as BBB models, there was no stereoselective transport of K or N across and no stereoselective association with cell membranes. The lower sedative effect of SN is therefore unlikely due to stereoselective transport across the BBB. However, there are more possibilities such as poor correlation between *in vitro* and *in vivo* studies and stereoselective binding to H_1 receptors in the CNS after crossing the BBB. It is important, therefore, to investigate the binding

of K and N atropisomers to CNS H_1 receptors (Chapter 6) and the B/P ratios *in vivo* (Chapter 7).

Chapter 6 *In vitro* studies of the binding of ketotifen and norketotifen atropisomers to CNS H_1 receptors in rat

6.1 Introduction

Histamine plays an important role in the CNS where it is involved in regulation of arousal, the sleep-wake cycle, memory and cognition. This is mainly through interaction with histamine H_1 receptors (Brown et al, 2001; Tashiro et al, 2005, 2008). Therefore when an antihistamine crosses the BBB and reaches the CNS, it may block CNS H_1 receptors and gives rise to sedative effects and cognitive deficits. Research has indicated that the severity of sedative effects produced by H_1 antagonists is correlated to their CNS H_1 receptor occupancy (Gupta et al, 2007; Tashiro et al, 2005, 2008; Yanai et al, 2011). This is illustrated in Figure 6.1. Antihistamines are classified as sedative, less sedative or non-sedative according to whether their H_1 receptor occupancy is 50 – 100%, 20 – 50% or 0 – 20%, respectively (Yanai and Tashiro, 2007). On this basis, K is clearly a highly sedative antihistamine.

Although CNS H_1 receptor occupancy of many antihistamines has been well studied and although many antihistamines are chiral, there is no information on whether H_1 receptor occupancy is stereoselective and, in particular, no information on whether H_1 receptor occupancy of K and N atropisomers is stereoselective. As discussed in Chapter 5, one hypothesis to explain the different sedative effects of K and N atropisomers is that they cross the BBB to a similar extent but bind to CNS H_1 receptors to different extent.

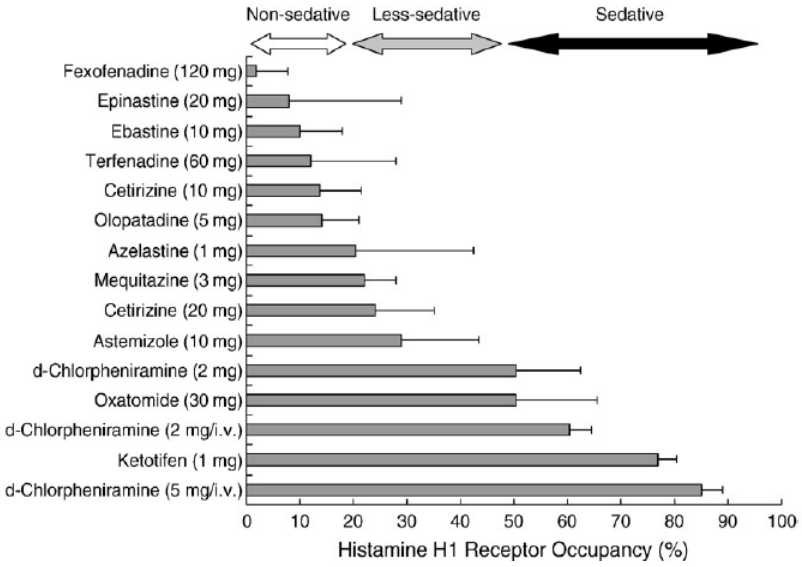

Figure 6.1 H_1 receptor occupancy by various antihistamines.

Yanai and Tashiro, 2007, reproduced with permission

Different methods have been used to determine the sedative effects of antihistamines. Some have involved statistical analysis of proportional impairment ratio (PIR) (McDonald et al, 2008; Shamsi and Hindmarch 2000) based on psychomotor performance tests and visual analogue scale (VAS) questionnaires (Izumi et al, 2008). Others have inferred sedative effects of antihistamines through determination of their relative H_1 receptor occupancy by techniques such as positron emission tomography (PET) (Tashiro et al, 2008; Yanai et al, 2011; Zhang et al, 2010) or binding of radiolabelled antihistamines to tissues rich in H_1 receptors. The latter have included rodent brain membranes *ex vivo* (Chang et al, 1979; Gupta et al, 2007; Malany et al, 2009) brain cells from cows (Yamashita et al, 1991), insects transfected by human genes (Appl et al, 2012) and rodent cells *in vitro* (Anthes et al, 2002; Moguilevsky et al, 1994).

Although PET is a non-invasive technique to determine binding of antihistamines (Yanai and Tashiro 2007), it requires special equipment for imaging and preparation. A traditional binding assay using brain tissue is a more convenient way to investigate the affinity of K and N atropisomers as it is easy to set up, well-validated and poses fewer ethical issues.

This Chapter reports the use of a traditional receptor occupancy assay as described by Chang et al, (1979) to investigate the affinity of antihistamines for H_1 receptors. It involved determining the extent of inhibition of [^{3}H] mepyramine binding to H_1

receptors in rat brain membranes. The ability to compete with mepyramine binding assesses the affinity of K and N atropisomers for brain H_1 receptors and is therefore an indirect measure of their relative sedative effects.

6.2 Materials

Male Wistar rats (age 6 weeks, 130-150 g) were purchased and housed in the animal facility of Otago University until required. [^{3}H] Mepyramine (pyridinyl 5-^{3}H, 250 µCi, 58.8 mCi/mmol in 0.5 ml ethanol:water (9:1)) and triprolidine hydrochloride (> 99 %) were purchased from Sigma (USA). Disodium hydrogen phosphate (anhydrous, 99%) was purchased from Asia Pacific Specialty Chemicals Ltd. Potassium dihydrogen phosphate (≥ 99.5 %) was purchased from BDH Laboratory Supplies (UK). Glass fibre filters (GF/B) were purchased from Whatman (Maidstone, England) and pipettes from Eppendorf® (Hamburg, Germany). OPTIPHASE 'HISAFE' 2 scintillation cocktail, miniature 6 ml Pony polyethylene scintillation vials, Tricarb® 2910TR Liquid Scintillation Analyzer and QuantaSmart™ software (version 4.00) were all purchased from PerkinElmer (Waltham, MA, USA).
All other materials were obtained as described in Sections 2.2, 4.2 and 5.2.

6.3 Methods

6.3.1 Preparation of rat brain membrane suspensions

Five rats were sacrificed by decapitation and three brains were removed for the H_1 receptor occupancy test. These brains were placed on ice and frozen at -80°C until required. The following method of sample preparation was based on Chang et al. (1979). Briefly, rat brains were weighed and homogenized in 30 volumes (w/v) ice-cold 50 mM phosphate buffer (prepared by diluting 30.16 ml 1 M sodium hydrogen orthophosphate and 19.84 ml 1 M potassium dihydrogen phosphate to 1 Liter and adjusting pH to 7.4) using a glass homogeniser tube with a manual Teflon pestle. Brain homogenate was centrifuged at 50,000 g for 10 min and the pellet resuspended in the same volume of ice-cold fresh phosphate buffer using the homogenizer. The suspension was centrifuged as described above and the washing procedure repeated 3 times. The final pellet was resuspended in the same volume of ice-cold fresh phosphate buffer. All suspensions from three rat brains were pooled

and mixed thoroughly to ensure a sufficient amount to carry out all inhibition studies. The pooled suspension was used within 24 h to reduce variability in results.

6.3.2 Determination of K_d of [^{3}H] mepyramine binding to H_1 receptors

In order to estimate inhibition constants (K_I) for K and N, the equilibrium dissociation constant (K_d) for specific binding of [^{3}H] mepyramine to H_1 receptors was first determined. To an aliquot of rat brain membrane suspension (0.45 ml containing 15 mg tissue), [^{3}H] mepyramine (final concentration 0.2 – 10 nM) was added to give a final volume of 0.5 ml. A parallel incubation was carried out containing triprolidine (final concentration 2 μM). Incubations were carried out in triplicate. Suspensions were thoroughly mixed and incubated at 25°C for 30 min after which 4 ml ice-cold fresh phosphate buffer was added. The suspensions were rapidly filtered through glass fibre filters under vacuum and filters washed with 3 × 4 ml ice-cold fresh phosphate buffer taking no more than 15 s in total to reduce the loss of [^{3}H] mepyramine. After washing, the filters were transferred to 6 ml Pony scintillation vials followed by 5 ml scintillation cocktail. Vials were vortexed for 30 s and radioactivity counted using the scintillation counter over 5 min.

6.3.3 Determination of K and N concentration ranges for K_I determination

A concentration range of 0.01 – 10000 nM of racemic K and N was investigated to determine the optimum range for accurate determination of K_I values. To an aliquot of rat brain membrane suspension (0.45 ml containing 15 mg tissue), [^{3}H] mepyramine (final concentration 2 nM) was added followed by a solution of racemic K or N to a final concentration in the range 0.01 – 10000 nM in a final volume of 0.5 ml. Subsequent steps were as described in Section 6.3.2. Incubations were carried out in duplicate.

6.3.4 Total binding (TB), non-specific binding (NB) and specific binding (SB) of K and N atropisomers to H_1 receptors

In order to determine TB of K and N atropisomers, incubations were carried out as previously described in the presence of individual K and N atropisomers at final concentrations in the range 0.01 – 2500 nM and 0.01 – 1000 nM respectively (based on the results of Section 6.3.3). [^{3}H] Mepyramine solution was added to each sample to give a final concentration of 2 nM in a final volume of 0.5 ml. A parallel incubation

was carried out in the presence of triprolidine (final concentration 2 μM) to measure NB and to allow calculation of SB of K and N atropisomers. Subsequent steps were as described in 6.3.2. Incubations were carried out in triplicate.

6.3.5 Data processing

6.3.5.1 K_d of [^{3}H] mepyramine binding

GraphPad Prism 5 was used to analyse data from Section 6.3.2. The K_d was calculated by fitting a "One site-total and non-specific binding" model (Figure 6.2) which is based on Equations 6.1 and 6.2:

$$\mathbf{SB = B_{max} \times X / (X + K_d)} \qquad \mathbf{6.1}$$

$$\mathbf{NB = NS \times X + Background} \qquad \mathbf{6.2}$$

where NS is the slope of the NB plot, B_{max} is the maximum number of receptor binding sites and X is the concentration of [^{3}H] mepyramine. Simulation is shown below (Figure 6.2):

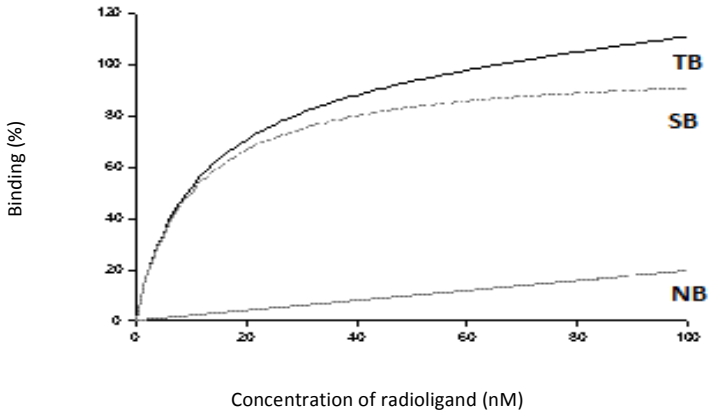

Figure 6.2 Simulation for the "One site-total and non-specific binding" model in GraphPad Prism 5 (TB, SB and NB are total, specific and non-specific binding respectively).

6.3.5.2 SB of K and N atropisomers

SB of [^{3}H] mepyramine to rat brain H_1 receptors in 15 mg brain tissue in the presence of K and N atropisomers was calculated using data from section 6.3.4 and Equation 6.3:

SB / 15 mg brain tissue (%) = (TB – NB) × 100/ B_0 **6.3**

where TB and NB are substituted as counts per min (CPM) for the respective binding of [^{3}H] mepyramine and B_0 is the CPM for binding in the absence of inhibitor.

6.3.5.3 Calculation of K_I of K and N atropisomers

The K_I values for K and N atropisomer inhibition of [^{3}H] mepyramine binding were determined using GraphPad Prism 5 using the model called "One site-fit K_I". By entering the concentration of radioligand (X) and its K_d as constants, the model estimated K_I as described in Equations 6.4 and 6.5.

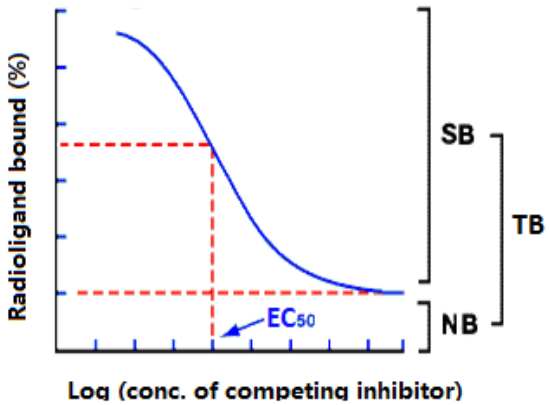

Figure 6.3 Simulation of the "One site-fit K_I" model in GraphPad Prism 5 (TB, SB and NB are total, specific and non-specific binding respectively).

Log EC_{50} = log $10^{\log K_I}$ × (1 + X / K_d) **6.4**

Y = NB + (TB – NB) / (1 + $10^{(\text{Log X} - \text{Log EC}_{50})}$) **6.5**

where EC_{50} is the concentration of inhibitor causing 50% inhibition, K_I is the inhibition constant of the inhibitor, K_d is in nM units and X is the concentration of [^{3}H] mepyramine in nM units, Y is binding in percentage unit.

This model assumes that the (a) binding is reversible and at equilibrium and (b) Hill coefficient is 1. It fits the K_I of the unlabelled ligand directly. After entering the concentration of radioligand and its K_d as constants, Prism directly fits the K_I of unlabelled ligand without reporting EC_{50}.

6.3.5.4 Statistical analysis:

Data were analysed by one-way ANOVA with post-hoc Bonferroni testing to compare selected data sets. Results are presented as means ± SD. Differences for which $p < 0.05$ were taken as significant.

6.4 Results

6.4.1 Determination of K_d of [^{3}H] mepyramine binding to H_1 receptors

Fitting of the data for TB and NB of [^{3}H] mepyramine in the absence and presence of triprolidine respectively is shown in Figure 6.4. The K_d of [^{3}H] mepyramine binding was estimated to be 7.8 ± 3.8 nM which is close to the published value of 9.4 ± 0.67 nM for binding of [^{3}H] mepyramine to Wistar rat brain cortex (Inagaki et al, 1989) but differs from the value of 4.0 ± 1.1 nM for binding to Sprague-Dawley rat brain membranes (Chang et al, 1979). The difference presumably reflects the different species of rat (Wistar male rats were used here).

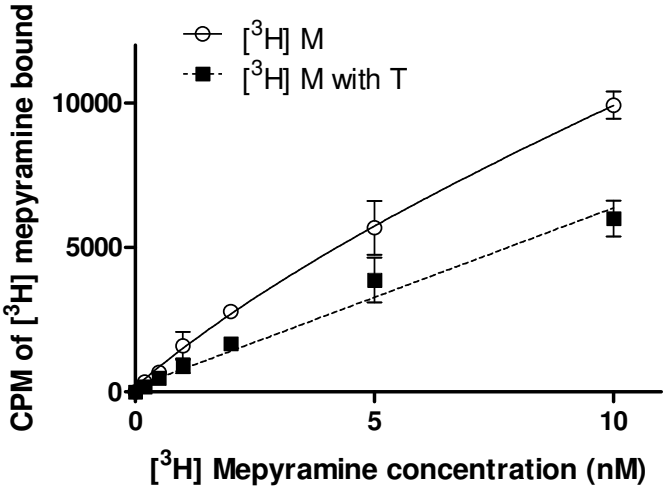

Figure 6.4 Total (open circles) and non-specific (closed squares) binding of [^{3}H] mepyramine ([^{3}H] M) to H_1 receptors in rat brain membrane suspensions. Nonspecific binding is determined in the presence of 2 μM triprolidine (T) (data are means ± SD, *n* = 3).

Given the high value of K_d, it could have been preferable to conduct experiments using an extended concentration range of [^{3}H] mepyramine. However, evidence shows that, in addition to the higher affinity sites, a lower affinity binding component becomes apparent when the [^{3}H] mepyramine concentration is higher than 10 nM (Hill and Young, 1980). As a result, the concentration range of 0 – 10 nM was appropriate for this study.

6.4.2 Determination of K and N concentration ranges for K_I determination

TB of [^{3}H] mepyramine to rat brain H_1 receptors in the presence of 0.01 – 10000 nM K and N racemates is shown in Figure 6.5. K inhibited [^{3}H] mepyramine binding to a greater extent than N but the inhibition curves levelled off at similar concentrations. There is some indication that binding of [^{3}H] mepyramine decreases further at high inhibitor concentration presumably because both SB and NB decrease at high concentrations of inhibitor. In fact, there is the potential to overestimate the affinity of an inhibitor if the upper limit of the concentration range is too high. This is why it is necessary to evaluate an optimum inhibitor concentration range before the actual inhibition study. Based on these results, the selected concentration ranges for K and N atropisomers were 0.01 – 2500 nM (-11 to -5.6 M in log scale) and 0.01 – 1000 nM (-11 to -6.0 M in log scale) respectively.

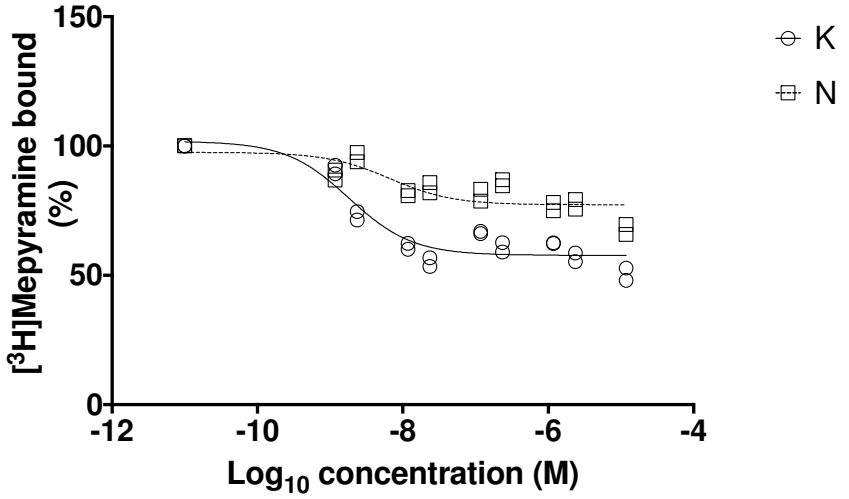

Figure 6.5 Total binding of 2 nM [^{3}H] mepyramine to rat brain membrane H_1 receptors in the presence of K and N racemates (data are presented in individual date point, n = 2).

6.4.3 TB of [^{3}H] mepyramine in the presence of K and N atropisomers

TB of [^{3}H] mepyramine in the presence of SK and RK is shown in Figure 6.6 a. There was a small but not significant difference between the TB of [^{3}H] mepyramine in the presence of SK and RK. This indicates the affinity of RK for rat brain membrane H_1 receptors is lower than that of SK, however, this difference is not significant.

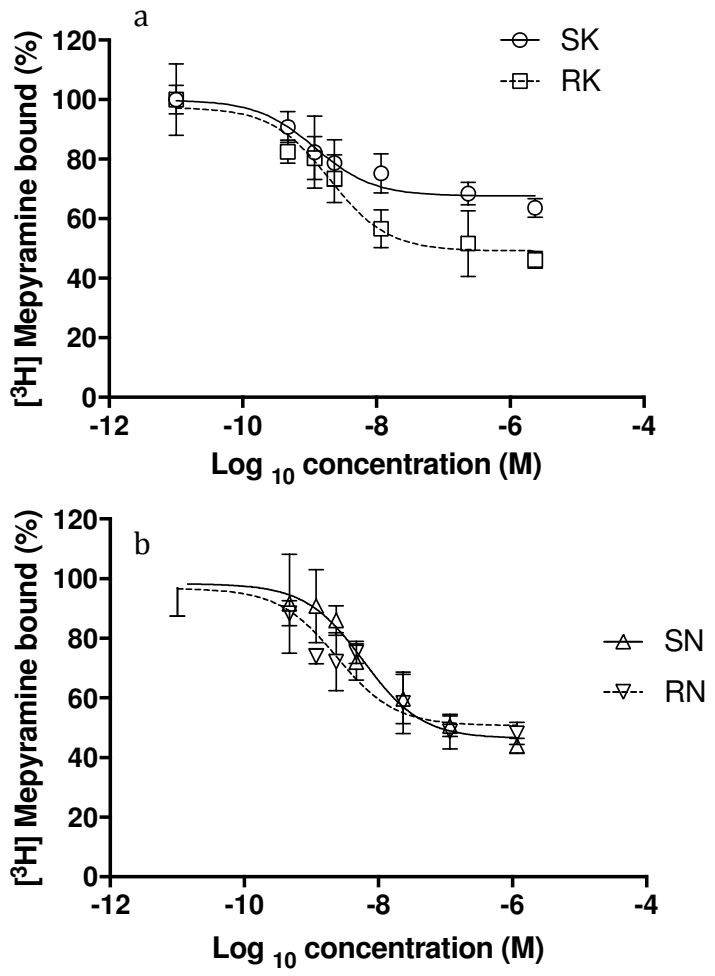

Figure 6.6 Calculated total binding of [^{3}H] mepyramine to rat brain membrane H_1 receptor in the presence of (a) K and (b) N atropisomers (data are means ± SD, *n* = 3).

Corresponding data for SN and RN is shown in Figure 6.6 b. In this case, the affinity of RN is lower than that of SN, but this difference was not significant probably because of the higher variability in the N data.

6.4.4 Determination of NB of [^{3}H] mepyramine in the presence of K and N atropisomers

There was concern that K and N could affect NB. Therefore, the effect of K and N on NB was determined by measuring binding of K and N in the presence of 2 μM triprolidine. The [^{3}H]mepyramine bound was approximately 50% of that in the absence of triprolidine as shown in Figure 6.7. This 50% NB presumably results from non-specific binding of K and N to brain tissue. The data show that the NB of [^{3}H]mepyramine was independent of K and N concentration indicating that K and N atropisomers do not change the NB of [^{3}H]mepyramine over the concentration range tested. However, the relatively high NB probably reduces the accuracy and precision of the measurements of SB since it is calculated by subtracting NB from TB.

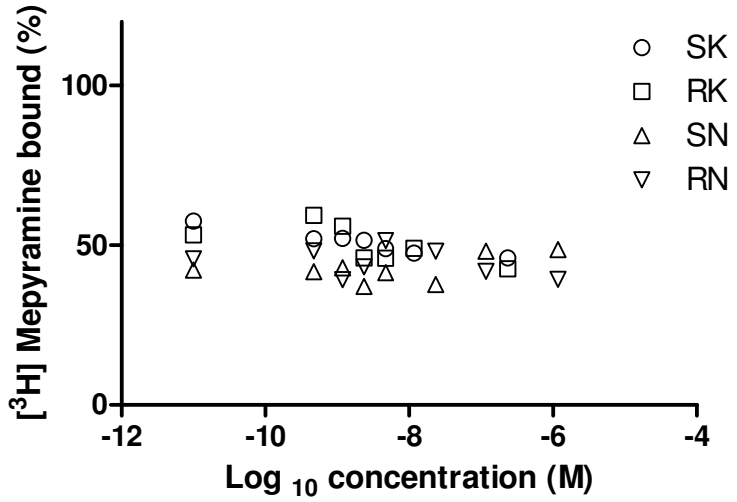

Figure 6.7 Non-specific binding of 2 nM [^{3}H] mepyramine to rat brain membrane in the presence of K and N atropisomers and 2 μM triprolidine (data are means ± SD, *n* = 3).

6.4.5 SB of [^{3}H] mepyramine to H_1 receptors in the presence of K and N atropisomers

SB of [^{3}H] mepyramine to rat brain membrane H_1 receptors in the presence of K and N atropisomers was calculated from the TB and NB results using Equation 6.3. The SB data were analysed using "One site-fit K_I" model in GraphPadPrism5 based on Equation 6.4 and 6.5. Parameters including logK_I and K_I were estimated by software by non-linear fitting. The results show a significant difference in the inhibition of SB of [^{3}H] mepyramine between SK and SN, between RK and SN, moreover between SN and RN (Figures 6.8 and 6.9, Table 6.1). Among the four atropisomers, SK was the

most potent inhibitor of SB of [^{3}H] mepyramine to rat brain membrane H_1 receptors while SN was the weakest.

Table 6.1 Estimated log K_I (M) and K_I (nM) for specific binding of [^{3}H] mepyramine to rat brain membrane H_1 receptors in the presence of S-ketotifen (SK), R-ketotifen (RK), S-norketotifen (SN) and R-norketotifen (RN) (data are means ± SD, *n* = 3).

	SK	RK	SN	RN
Log K_I (M)	-9.03 ± 0.16	-8.81 ± 0.16	-8.33 ± 0.18	-8.73 ± 0.17
K_I (nM)	1.03 ± 0.42	1.65 ± 0.58	5.10 ± 2.00	2.08 ± 0.75

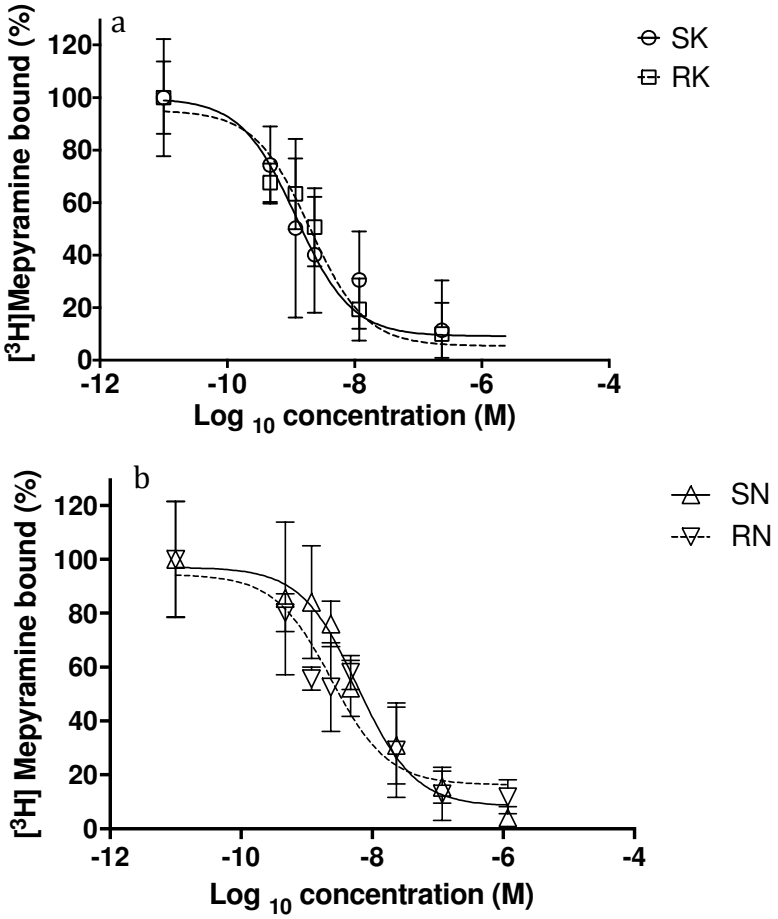

Figure 6.8 Calculated SB of [^{3}H] mepyramine to rat brain membrane H_1 receptor in the presence of (a) K and (b) N atropisomers (data are means ± SD, *n* = 3).

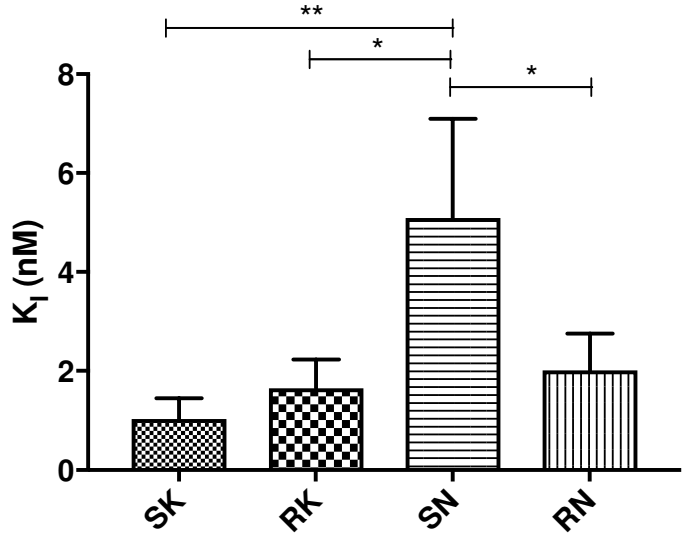

Figure 6.9 Comparison of the inhibition (K_I) of SB of [^{3}H] mepyramine to rat brain membrane H_1 receptors by K and N atropisomers (data are means ± SD, *n* = 3; * P< 0.05, ** P< 0.01).

6.5 Discussion

The H_1 receptor affinity in this work is determined by a classic method using cell membranes (Chang et al, 1979). It is based on competitive inhibition of a highly selective H_1 receptor substrate (mepyramine). While there are advantages to using purified H_1 receptors, it would significantly increase the cost of experiments significantly.

For curve fitting, the one-site model (Equations 6.4 and 6.5) is used. It assumes Hill coefficient is 1. However, it is possible that the value of Hill coefficient is not 1. In this work different Hill coefficient values were put into equation and the "goodness of fit" retested. The results indicate there was no improvement in R^2 using Hill coefficients other than 1. As a result, a Hill coefficient of 1 is appropriate to interpret our data.

Based on previous studies of cell membrane binding and functional assays (Appl et al. 2012; Bakker et al. 2007; Gallois-Bernos and Thurmond, 2012; Seifert et al. 2003), the log K_I of racemic K (in M) varies from -9.02 ± 0.01 to -10.4 ± 0.1, similar with the values of log K_I for K atropisomers found here (Table 6.1). The K_I value for K, taken as the average of the values for SK and RK (1.34 nM), is similar to a published K_I value for inhibition of [^{3}H]mepyramine binding by K to guinea pig H_1 receptors (1.26 nM) (Sharif et al. 1994).

K and N atropisomers showed similar profile on NB (approximately 50% for all atropisomers of K and N), which was independent of concentrations of K and N

atropisomers. For the atropisomers of K and N, the inhibition of SB of [^{3}H] mepyramine to rat brain membrane H_1 receptors suggests the affinity of SK was the highest while SN was the weakest (Tables 6.1, Figures 6.9) and there are some stereoselective bindings between SK and SN, RK and SN, more over, SN and RN. SK gives the most negative log K_I for SB whereas SN gives the least negative log K_I for SB (Tables 6.1). Although the differences are not great, they are larger than that between the enantiomers of fexofenadine (2.3 times greater for S-fexofenadine) (Kusuhara et al, 2013) and sufficient to conclude that binding to CNS H_1 receptors contributes to the lower sedative effect of SN. Although no significant difference was found between SK and RK, based on the current sample number (n = 3), the power calculated using Mini-tab (one way ANOVA, CI 95%) is 26%. This is not enough to detect a significant difference in the H_1 receptor affinity between SK and RK. However, the initial sample number was chosen as the literature indicates n = 3 is adequate (Anthes et al, 2002). By using the variation and mean value found in this work, in order to detect a significant difference with 80% power, n = 10 is required. As a result, in future studies comparing the H_1 receptor affinity of K atropisomers, at least 10 measurements would be required.

To investigate another possibility to explain the different sedative effects, which is the stereoselective transporter hypothesis, the total and free B/P ratios were determined using rat tail vein injection combined with RED technique in the next chapter (Chapter 7).

Chapter 7 Determination of total and free brain-to-plasma ratio of K and N atropisomers by injecting racemic K and N through rat tail vein

7.1 Introduction

The last two chapters were focused on the stereoselectivity of K and N *in vitro*. The uptake and permeability of K and N atropisomers in and through cell monolayers were investigated in Chapter 5. In Chapter 6, the binding of K and N atropisomers to H_1 receptors in rat brain homogenates was studied. This chapter describes the results of a study that investigated the stereoselective uptake of K and N into the brain of the live animal.

To investigate compound distribution in the live animal brain, several models can be used: *in situ* brain perfusion (Alata et al, 2014; Smith and Allen, 2003), *in vivo* carotid artery injection technique (brain uptake index, BUI) (Yamazaki, 1994a), microdialysis (Hammerlund-Udenaes, 2016; Gupta et al, 2006), PET (Honer et al, 2014; Tashiro et al, 2005) and rat tail vein injection method (Kato et al, 1997; Wohlfart et al, 2011; Zhou et al, 2016). Advantages and disadvantages of these techniques are discussed in the following sections.

7.1.1 *In situ* brain perfusion technique

In situ brain perfusion is performed by inserting a cannula into the heart or major arteries that lead to the brain (such as carotid artery) of an anaesthetized animal. A perfusate, such as a buffer, containing a compound of interest, is then pumped through the cannula, in such a way the brain circulation of a live animal is taken over for a certain period. After the perfusion, brain tissue is collected and analysed to access the BBB permeability of the compound of interest (Smith and Allen, 2003).

It is a widely used method because by modifying perfusate composition, the technique provides controllable conditions to investigate individual factors that affect the permeability of the BBB, which are difficult to achieve in *in vivo* conditions. Examples of conditions are adding certain ions to the perfusate to determine the effect of ions on the BBB permeability; adding albumin to the perfusate to

investigate the effect of binding to plasma proteins on the BBB permeability; adding transporter inhibitor or substrate to perfusate to study the effect of a certain transporter on the BBB permeability. It also minimizes drug metabolism by bypassing metabolizing organs (Alata et al, 2014; Hammerlund-Udenaes, 2014). However, there are limitations to using this technique. First, this method requires surgical procedures that are technically challenging to perform. In addition, it measures the initial rate of brain uptake. As a result, for a single time point experiment, when a compound equilibrates faster than the chosen time point, significant back flux from brain back to the perfusate occurs. Therefore, the result does not reflect the initial rate thus may not be accurate (Zhao et al, 2009). Moreover, unless combined with other methods such as ultrafiltration, this method by itself does not provide information on the unbound drug concentration in the brain (Di et al, 2008).

7.1.3 *In vivo* techniques

Microdialysis:

The microdialysis method is a well-established and widely used *in vivo* model. It plants a dialysis probe (s) in brain of a living animal by surgical procedures. There are two ways of implanting probe (s). A single probe only is implanted in the brain of conscious animals whereas for the dual probe method, probes are implanted in blood and brain but only in anaesthetized animals. The real-time unbound drug concentration can be measured by determining the drug concentration in the dialysate from the probe (s) (Erdo et al, 2017).

Although the microdialysis technique is time-, labour- and resource-demanding, it is still a "gold standard" to investigate the extent and rate of drug transport through the BBB. There are advantages of this technique. First, it presents the real-time profile of a compound in brain and/or blood over a short or relatively long period. Second, it measures free concentration in a specific brain region and/or blood where the probe is implanted (Hammerlund-Udenaes, 2016). However, it damages brain tissue including the BBB to a certain extent during surgery (Morgen et al, 1996). In addition, this method is not suitable for all compounds. For instance, lipophilic compounds, such as ketotifen, may non-specifically bind to the dialysis probe

membrane, which consequently leads to poor recovery (Di et al, 2008; Hammerlund-Udenaes, 2014), but this can be tested by appropriate *in vitro* studies.

PET

PET is a non-invasive imaging technique that measures both extent and rate of radiolabelled drug distribution in a living animal or human (Bauer et al, 2016; Gunn and Rabiner, 2017; Hammerlund-Udenaes, 2014). By injecting a compound of interest labelled with [^{11}C] or [^{18}F], drug distribution and concentration in tissue can be measured (Gunn and Rabiner, 2017). It has been used for various areas, such as determination of drug distribution, target engagement (receptor occupancy and transporter affinity), pharmacologic activity and biomarker development (Bauer et al, 2016; Gunn and Rabiner, 2017). Because of its non-invasive and quantitative nature, PET has been widely used to determine H_1 receptor occupancy and sedative effects of antihistamines (Tagawa et al, 2001; Yanai et al, 2011; Yanai et al, 2017) in both animals and humans. However, equipment for making radiolabelled drugs, determination of labelled drugs, and software and experience of data analysis and modelling are required. Consequently, PET is an extremely resource-demanding and expensive technique. In addition, PET cannot distinguish between free and bound drugs. As a result, it measures the concentration and distribution rate of both bound and free drugs instead of free drugs (Hammerlund-Udenaes, 2014).

Carotid artery injection:

In the carotid artery injection method a single injection of a drug together with a reference standard is administered through the carotid artery of an animal. The animal is then killed 5 to 15 seconds after the injection and brain is collected for analysis. BUI is calculated based on the relation of the brain uptake rates between the drug and the reference compound (Aschner and Gannon, 1994). Thus, it requires co-administration of a reference compound, and the use of this technique is limited by the permeability surface area product (PA, no less than 10 µl/min) value of the test compound (Pardridge, 1995). In addition, it is not applicable for compounds that do not readily cross the BBB, because a 5 – 15 s post-injection time is sometimes not long enough for compounds to accumulate in brain to be detectable (Hammerlund-Udenaes, 2014).

Rat tail vein injection:

The rat tail vein injection (intravenous injection) and carotid artery injection techniques are both easy to perform, relatively cheap, straightforward techniques, thus they are simple and useful tools to investigate drug uptake by brain. Unlike the carotid artery injection technique, the rat tail vein injection method does not require a reference compound to calculate the brain uptake rate of the compound of interest. The rat tail vein injection technique requires injection of drug solution through the rat tail vein. Blood and brain tissue are collected at a certain time point (from less than a minute to 60 min). It investigates the unidirectional uptake rate of compound into brain with the assumption that there is no elimination from brain during the experiment. (Hammerlund-Udenaes, 2014; Patlak et al, 1983; Smith, 2003). The longer post-injection time (compared to carotid artery injection method) results in enough drug accumulation in brain. However, it also leads to the greater risk of metabolism in the brain, in addition to increased risk of violation of the assumption that there is only a unidirectional transport occurring during the experiment. Therefore, an optimized time should be established to secure detection and reduce metabolism (Hammerlund-Udenaes, 2014). The method is widely used to measure the total B/P ratio that describes the distribution of a compound between brain and plasma (Kato et al, 1997; Wohlfart et al, 2011; Zhou et al, 2016). Another reason for choosing this technique is that research has been published using this method to investigate central effects of several antiallergy agents including K racemate (Kato et al, 1997). These researchers, however, only focused on the total concentrations of racemic K in brain tissue homogenate and plasma and the total B/P ratio.
Gupta's group suggested the importance of investigating free enantiomer concentrations in brain and plasma and consequently the free enantiomer B/P ratio (Gupta et al, 2006). According to their results, the total B/P ratio of enantiomers could be misleading. This occurs when there is stereoselective non-specific binding of enantiomers to plasma and/or brain tissue. Thus, total enantiomer concentrations and B/P ratios cannot be used to distinguish stereoselective uptake of enantiomers into the brain (Gupta et al, 2006). Therefore, it is more useful to determine free B/P ratio in addition to the total B/P ratio of K and N atropisomers to investigate if there is stereoselective transport on the BBB or a stereoselective binding to plasma protein and/or brain tissue. However, the rat tail vein injection method only provides total concentrations and total B/P ratio; as a result, RED was introduced as

a further sample treatment to determine the free compound in brain tissue and plasma collected from the rat tail vein injection experiment. Di et al suggested a similar experimental procedure to determine free B/P ratio using combined methods (Di et al, 2008).

In this chapter, after injecting racemic K or N solution through rat tail vein, the total and free brain and plasma concentrations of K and N atropisomers are quantified using the chiral HPLC assay (Chapter 4) and then the corresponding B/P ratios are calculated. The aim of the research in this chapter was to compare the total and free concentrations and B/P ratios of K and N atropisomers to investigate if there is stereoselective transport across the BBB and/or stereoselective binding to brain tissue and/or plasma proteins.

7.2 Materials

Wistar rats (15 males, 6 weeks, 130 – 150 g) were housed in the animal facility of Otago University. This study had ethics approval from the Animal Ethics Committee of University of Otago (ethics approval number: 32/2013). Saline solution (0.9%), an animal balance, decapitation cones, a rodent guillotine, scissors, forceps and other surgical appliances were provided by the Animal Welfare Office, University of Otago. Funnels (15 glass funnels) were purchased from the Glassblowing Unit, University of Otago. Syringes (0.3 ml BD Ultra-fine 0.3 ml 30 G insulin syringe) and BD Vacutainer® (K2 EDTA 7.2 mg, 4 ml) were purchased from BD (Auckland New Zealand).

All other materials were obtained and described in Section 2.2, 4.2 and 5.2.

7.3 Methods

7.3.1 Rat tail vein injection

Stock solutions of K and N racemic fumarates were prepared by dissolving 27.5 mg of K fumarate or 27.8 mg of N fumarate in 5 ml of 0.9% saline solution, which is equivalent to 4 mg/ml of K and N solutions. Volumes of K and N injection solutions were calculated individually based on body weight of rats (Equation 7.1). The injected dose was 3 mg/kg K or N in all non-control groups.

Injection volume (in ml) = 0.75 × body weight (in kg) **7.1**

Wistar rats were divided into three groups (five rats per group), and different injection solutions were administered through rat tail vein as follows: (1) the control group (drug-free saline as injection solution); (2) the K group (4 mg/ml K as injection solution); and (3) the N group (4 mg/ml N as injection solution).
Although N is a trace metabolite of K in human, it accounts for 62% metabolized K at 4 h in cultured rat hepatocytes (Le Bigot et al, 1987). As a result, it is possible that K can be metabolized into N in rats if the post-injection time is long enough. In addition, the concentration of K in both brain and plasma is reducing 2 min after the tail vein injection (Kato et al, 1997). To minimize the concentration of N from metabolized K and get a reasonable concentration of K and N in brain and plasma, 2 – 6 min is the best end-point range for this experiment (Kato et al, 1997). Considering the applicability to perform the technique in reality, the decapitation time was chosen at 5 min after the tail vein injection.
To perform the rat tail vein injection, a rat was wrapped in a towel leaving the rat tail out. The rat tail was left in a warm water bath for 5 min to make the tail vein more visible. An aliquot of K, N or saline solution was injected through the rat tail vein. The rat was transferred into a decapitation cone 4 min after injection and decapitated at 5 min post injection. Blood was collected from thoracic cavity into labelled BD Vacutainer tubes through a glass funnel. Tubes were inverted several times gently to mix the blood and the anticoagulant (EDTA) and then placed on ice. The rat head was dissected and the brain was collected in a Petri dish on ice for processing or stored at -80°C until required.
Blood samples were centrifuged at 2000 rpm for 10 min at 4°C. Plasma was separated from blood cells and then aliquot (0.5 ml) into labelled 1.7 ml centrifuge tubes. Rat plasma from the control group (a pool of five rats) was used as a blank matrix for the standard curve for the chiral HPLC assay (Chapter 4). An aliquot (0.5 ml) of plasma sample was subjected to chiral analysis to determine the total concentration of K or N in plasma, while another aliquot of plasma sample was used for RED assay (Section 7.3.2) to investigate the free K or N concentration in plasma. The unused plasma aliquots were stored at -80°C until required.
Rat brains from control group (three out of five brains) were kept for the CNS H_1 receptor binding study (Chapter 6). The other two brains from the control group were used as the blank matrix to prepare standard curves for the chiral HPLC assay.

The blank matrices of brain and brain samples in K and N groups were prepared the same way as stated below. Rat brains were weighed and homogenized in two volumes of Milli-Q water (w/v). The brain homogenate was divided into two aliquots, one of which was further diluted with Milli-Q water from 1 in 3 diluted to 1 in 10 diluted brain homogenate and the other aliquot was stored at -80°C. The 1 in 10 diluted brain homogenate was aliquot (0.5 ml) into labelled 1.7 ml centrifuge tubes. Aliquots (0.5 ml) of the 1 in 10 diluted brain homogenate samples were subjected to chiral analysis to determine the total concentration of K and N in brain while another aliquot was used for the RED assay (Section 7.3.2) to investigate the free K and N concentrations in brain. The unused aliquots of 1 in 10 diluted brain homogenate samples were stored at -80°C until required.

The total B/P ratio was calculated using Equation 7.2.

$$\textbf{Total B/P ratio } (B_T/P_T) = TC_{brain} \times 10 / TC_{plasma} \qquad 7.2$$

where the TC_{brain} and TC_{plasma} are total concentration of K or N atropisomers in brain homogenates (1 in 10 diluted) and plasma respectively.

7.3.2 RED assay

Plasma (0.5 ml) and brain homogenate (0.5 ml) samples were placed into the sample chamber (indicated by the coloured retainer ring) of the RED unit, and 0.75 ml of dialysis buffer (Ringer-HEPES buffer pH 7.4) solutions were placed into the buffer chamber. A higher volume of buffer was used to avoid sample volume change during the dialysis procedures. Units were covered and sealed with para film before incubating at 37°C in an orbital shaker at approximately 250 rpm for 4 h at which time K and N reached equilibrium in the RED units.

Aliquots (0.49 ml) of plasma and brain homogenate samples were removed from sample side while 0.5 ml of dialysis buffer solutions were removed from buffer side of RED units after incubation. Rat plasma, rat brain homogenate or dialysis buffer (0.49 ml) was mixed with 10 µl of internal standard (10 µg/ml metoprolol) to make a final concentration of 200 ng/ml metoprolol in 0.5 ml of sample.

These samples were subjected to the chiral HPLC assay to determine the free concentrations of K and N atropisomers in rat plasma and brain homogenate.

The free B/P ratio, which is independent of effects of binding of drug to brain tissue and plasma, was calculated using Equation 7.3.

Free B/P ratio (B_F/P_F) = $FC_{brain} \times 10 / FC_{plasma}$ **7.3**

where the FC_{brain} (1 in 10 diluted) and FC_{plasma} are free concentration of K or N atropisomers in brain homogenates and plasma respectively.

Another B/P ratio, which is independent of effect of drug plasma binding, was calculated as follows:

$B_T/P_F = TC_{brain} \times 10 / FC_{plasma}$ **7.4**

This B_T/P_F ratio is calculated using the total brain concentration ($TC_{brain,}$ 1 in 10 diluted) and the free plasma concentration (FC_{plasma}). By comparing the B_T/P_F, the B_F/P_F and the B_T/P_T ratios, a difference between B_T/P_F and the B_F/P_F is indicative of binding to brain tissue, and a difference between B_T/P_F and the B_T/P_T is indicative of binding to plasma protein.

Non-specific binding of K and N atropisomers to RED unit membrane was determined by filling the sample sides of the RED units with 0.5 ml buffer containing 10 μM K or N atropisomers and 0.5 ml of drug-free buffer was filled in the buffer side. Samples were analysed using the same procedures as those used to analyse plasma and brain homogenate samples. Buffer (0.49 ml) solutions from both sides were mixed with 10 μl of internal standard (10 μg/ml metoprolol) and subjected to the chiral HPLC assay to determine percentage of K or N atropisomers bound to RED membrane. Results showed the nonspecific binding of K and N atropisomers to the RED membranes were all at about the same level (10%) as recommended in the instructions for the assay (no more than 10% nonspecific binding). In addition, there was no evidence of stereoselective binding to the RED membranes for atropisomers of K or N.

7.3.3 Data processing and statistics

GraphPad Prism 5 was used to analyse data and calculate B/P ratios from Section 7.3.1 and 7.3.2. Data were analysed by one-way ANOVA with post hoc Bonferroni test to compare selected sets. Results are presented as means ± SD. Differences for which $p < 0.05$ were taken as significant.

7.4 Results and Discussion

7.4.1 Total and free of K and N atropisomer concentrations in rat brain homogenate

The total and free concentrations of K (Figure 7.1) atropisomers in rat brain homogenate showed there was no significant difference between SK and RK 5 min after injecting racemic K through rat tail vein. Similar results (Figure 7.2) indicated that there was no significant difference between SN and RN in rat brain homogenate.

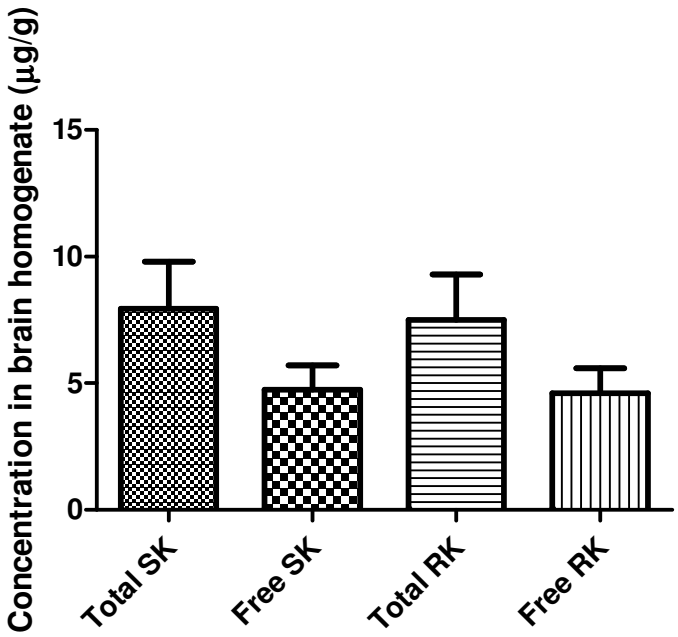

Figure 7.1 Total and free concentrations of ketotifen atropisomers (SK and RK) in rat brain homogenate 5 min after injecting 3mg/kg racemic ketotifen through rat tail vein (n = 3*, data are means ± SD).

* One rat was dead before the endpoint (possibly due to the stress from the procedures) and another one showed very low concentration of SK and RK in both brain and plasma, which may be because the K solution was not injected into tail vein). These two rats were excluded from the statistical analysis.

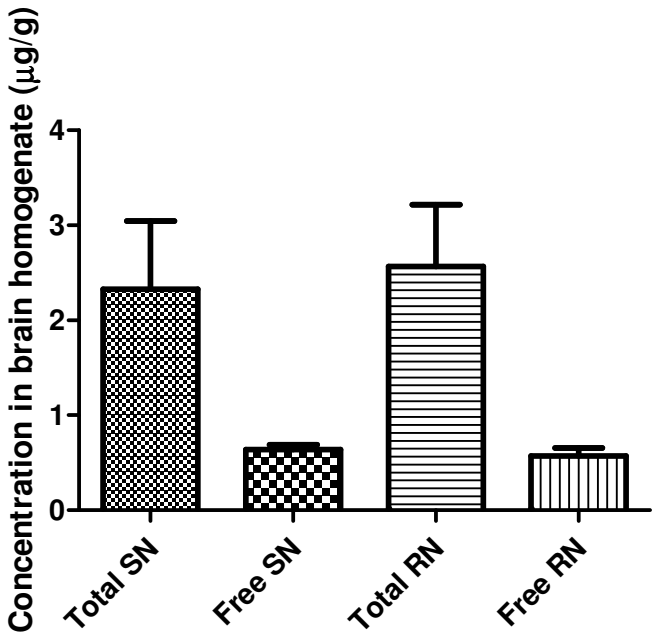

Figure 7.2 Total and free concentration of norketotifen atropisomers (SN and RN) in rat brain homogenate 5 min after injecting 3mg/kg racemic norketotifen through rat tail vein (*n* = 5, data are means ± SD).

The total concentration of K and N in brain homogenate, however, were approximately 2-fold and 3-fold of the free concentrations of K and N respectively. This suggests there was binding of K and N to brain tissues (Figure 7.1 and 7.2). This agrees with the results from RBE4 and Caco-2 cell studies, which indicated that N is more likely to associate with cell membranes (Chapter 5, Figures 5.2 and 5.16). It explains, to some extent, the higher binding fraction of N to brain tissues (Figures 7.1 and 7.2).

There are significant differences ($P < 0.0001$) between the free fractions of K (0.61 ± 0.03) and N (0.26 ± 0.07) in brain homogenate. Results also indicate, both total and free fraction of N, that N penetrates the brain much less than K (Figures 7.1 and 7.2). Consequentially, there is less free N than K available in the interstitial fluid (ISF), which would result in less interaction between N and H_1 receptors in the CNS. According to H_1 receptor occupancy results (Chapter 6), affinity of K and N atropisomers for the CNS H_1 receptors from the lowest to the highest are SN, RN, RK and SK. Therefore, lower free concentrations in the ISF in addition to lower affinity for the CNS H_1 receptors suggested less sedative effects caused by N (especially SN).

7.4.2 Total and free concentrations K and N atropisomers in rat plasma

The total and free concentrations of K (Figure 7.3) atropisomer in rat plasma showed no significant difference between SK and RK 5 min after injecting racemic K through rat tail vein. Similar results (Figure 7.4) indicated that in rat plasma there was no significant difference between SN and RN 5 min after injecting racemic N through rat tail vein. This suggests that there was no stereoselective binding of K or N atropisomers to plasma proteins. However, the bound fraction of N (90% bound) in rat plasma is more than that of K (75% bound) 5 min after the tail vein injection (Figures 7.3 and 7.4). As a result, the free concentrations of N atropisomers were slightly lower than those of K. The degree of binding of K to plasma protein agrees with reported results (Jewell, 2007; FDA drug approval package).

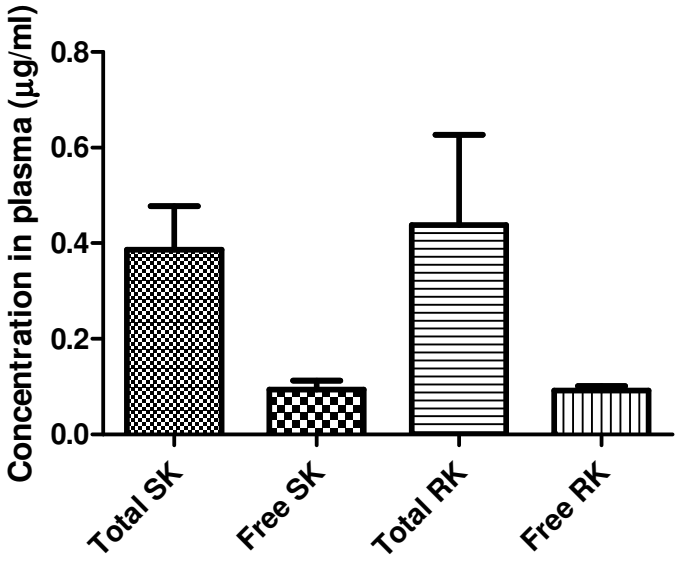

Figure 7.3 The concentration of ketotifen atropisomers (SK and RK) in rat plasma 5 min after injecting 3 mg/kg racemic ketotifen through rat tail vein (*n* = 3, data are means ± SD).

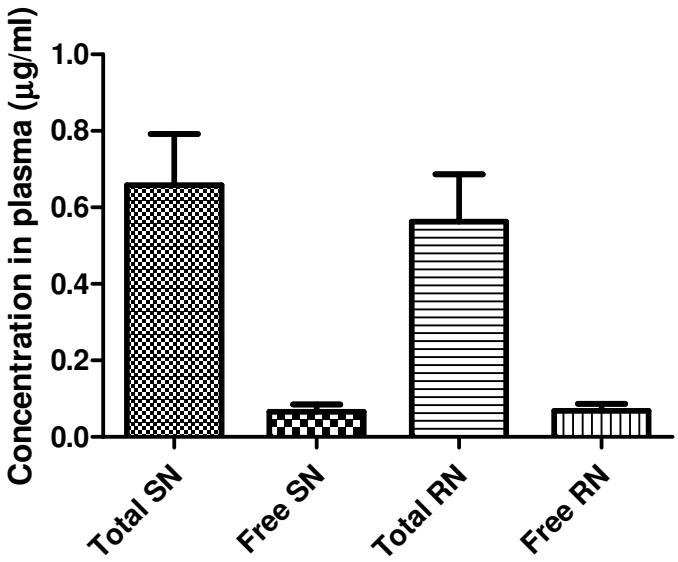

Figure 7.4 The concentration of norketotifen atropisomers (SN and RN) in rat plasma 5 min after injecting 3 mg/kg racemic norketotifen through rat tail vein (*n* = 5, data are mean ± SD).

In plasma, the free concentration of N is lower than that of K. This suggests less free N is available in the blood stream to cross the BBB in both passive and active mechanisms. This may also contribute, to the lower total concentration of N in rat brain (Figure 7.2), although it has been reported that transport of compounds through the BBB may not only depend on the free fraction but also the total concentration (Pardridge et al, 1983; Tanaka and Mizojiri, 1998).

In plasma, the total concentrations of N atropisomers were higher than those of K. It may be the result from N being less lipophilic than K, therefore, N accumulates less in tissues (and brain), and thus more is left in blood (Figures 7.3 and 7.4). Similar to the results from rat brain homogenate, the total plasma concentrations of K and N atropisomers were much higher than those of free plasma concentrations suggesting binding of K and N atropisomers to plasma proteins.

Different from the plasma results, in brain homogenate the concentrations of K atropisomers were higher than those of N. The difference between K and N concentrations in brain could be a result of the following possibilities. First, as discussed, after binding to plasma protein, there is less free N available in blood to cross the BBB. Second, K is more lipophilic than N, thus it passively penetrates the BBB more readily than N. Third, an active influx transporter was reported for lipophilic cationic antihistamines, which transports K though the rat brain

endothelial cell monolayers (Yamazaki, 1994b). Nevertheless, according to the structure of N, it is also a possible substrate of this cationic transporter. This was supported by the RBE4 cell uptake results (Tables 5.2 and 5.3). An active influx mechanism was found, which contributed to actively transport both K and N into brain. This is supported by the results for free concentrations of K and N in brain and plasma (Figures 7.1 to 7.4). The free concentrations of both K and N atropisomers in brain homogenate were higher than the free concentrations in plasma. This indicates an active influx mechanism at the BBB for both K and N, because if there is only a passive mechanism, no matter before or at the equilibrium stage, the free concentrations of K and N in brain would be less or equal to the free concentrations in plasma. Interestingly, the B/P ratios (both B_T/P_T and B_F/P_F) of K atropisomers were much higher than those of N (Figure 7.5). The assumption is that at equilibrium, without the effects of active transport, the free concentration in brain equals the free concentration in plasma. However, according to results (Figure 7.5), the ratio of free concentrations of K atropisomers in brain over those in plasma (free B/P ratios) was about 40, whereas the values of N atropisomers were only about 10. This suggests the following: (a) an active influx mechanism present at the BBB; (b) this active transporter transports K more than N from plasma to the brain.
In addition to the active transport mechanism and nonspecific binding, a trace of residual blood left in the brain capillaries may also contribute to the difference between total and free concentration of K and N to some extent. This is because K and N may bind to the plasma protein left in the brain, as there was no experimental procedure to remove blood remaining in the brain. However, it has been published that in male adult Wistar rats (250 g), the cerebral blood volume is 3.4 ± 0.4 ml/100g of brain, which equals 0.034 ml/g of brain (Shockley and LaManna, 1988). According to total concentrations in plasma, the effects of residue blood on free concentrations of K and N in brain homogenate were approximately 0.3 and 5.1% respectively. Therefore, the effect of residual blood in brain is negligible.

7.4.3 Comparison of different B/P ratios of K and N atropisomers

The relatively high total B/P ratio of K (18-20, Figures 7.5) is consistent with the result from Kato et al (Kato et al, 1997), who reported the total B/P ratio of K was approximately 26 at 6 min after tail vein injection of 3 mg/kg ketotifen in mice. The

total B/P ratio of K was approximately four times that of N; a similar trend was seen in the free B/P ratios of K and N (Figures 7.5 and 7.6). It suggests both total and free concentrations of K are four times that of N in the CNS versus peripheral. Moreover, H_1 receptor occupancy results (Figure 6.9 and Table 6.1) suggested the affinity of SN to the CNS H_1 receptor were lower than that of RN, SK and RK. The H_1 receptor inhibition constants of the four atropisomers from the lowest to the highest were SN (K_I = 5.10 ± 2.00 nM), RN (K_I = 2.08 ± 0.75 nM), RK (K_I = 1.65 ± 0.58 nM) and SK (K_I = 1.03 ± 0.42 nM) (Table 6.1). As a result, there may be at least four-times higher sedative effect of K compared to that of N because the sedative effect is related to the ability of compound to reach the CNS and interact with the H_1 receptors (Yanai et al. 2011). However, no significant stereoselectivity between SK and RK or SN and RN was found in both total and free B/P ratios (Figures 7.5 and 7.6).

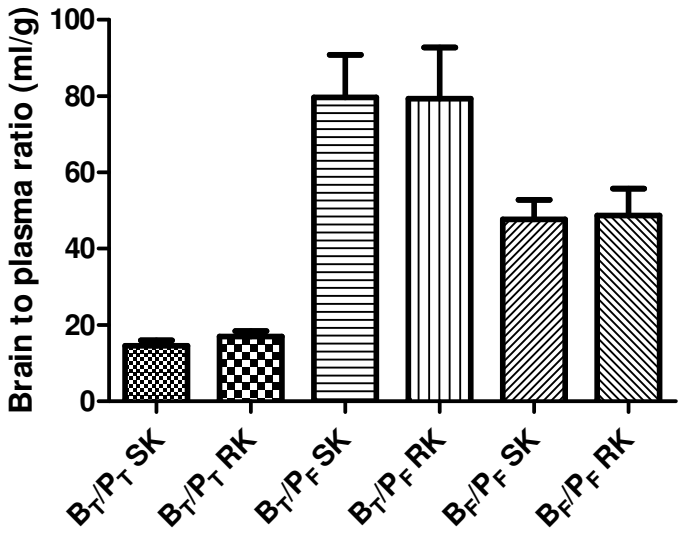

Figure 7.5 Different brain-to-plasma ratios of ketotifen atropisomers (SK and RK) 5 min after tail vein injection (*n* = 3, data are means ± SD).

Comparison between B_T/P_T, B_T/P_F and B_F/P_F ratios for K atropisomers showed there was no significant stereoselective transport between SK and RK through the BBB (Figure 7.5). In addition, there was no stereoselective binding of SK and RK to plasma protein and/or brain tissue.

The highest B_T/P_F ratios were a result of (a) the effect of binding of K to plasma proteins (reduces P_F) and (b) the active mechanism transports K from plasma to

brain which increases the B_F (also B_T). As a result, there is a further increase of the B_T/P_F ratio of K.

Similar to K, there was no stereoselective transport of N atropisomers when they cross the BBB. In addition, there was no stereoselective binding of N atropisomers to plasma proteins and/or brain tissues. The B_T/P_T, B_T/P_F and B_F/P_F ratios of N atropisomers (Figure 7.6) showed a similar trend as those of K atropisomers.

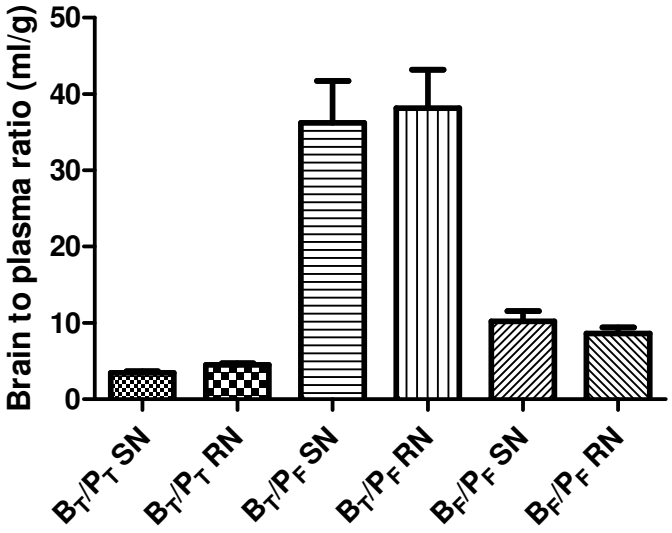

Figure 7.6 The brain-to-plasma ratios of norketotifen atropisomers (SN and RN) 5 min after tail vein injection (n = 5, data are means ± SD).

There is no stereoselective transport of K or N atropisomers across the BBB or stereoselective binding to plasma proteins and/or brain tissues 5 min after injecting racemic K or N through rat tail vein. Although both K and N partition into brain, the free B_F/P_F ratio of K is 4 times that of N. Moreover, affinity of K atropisomers for the CNS H_1 receptors are higher than that of N atropisomers (especially SN). These suggest K is four times more likely to get into brain and lead to a greater sedative effect compared to N.

As a much lower sedative effect was observed (Aberg A. K. G, Patent US9439895 B2) for SN than RN, SK and RK, at this stage, we can conclude only that N atropisomers penetrate the BBB in a similar manner but to a lesser extent than K. The difference between SN and RN may be because of their stereoselective affinity to CNS H_1 receptors (Chapter 6, Table 6.1).

7.4.4 Equation used to calculate concentrations of K and N atropisomers in undiluted brain homogenate samples

Brain homogenate samples (1 in 10 diluted) were used to determine the free and total concentrations of K and N atropisomers in the CNS. To calculate the undiluted concentrations, the dilution factor "10" was used in Equations 7.2 to 7.4. This, however, may not be appropriate as diluting brain homogenate samples could affect the equilibrium between binding sites and K or N atropisomers.

To determine the concentrations of K and N atropisomers in undiluted brain homogenate, it is appropriate to use the dilution factor directly when drug concentration ($[D_T]$) $\gg$ binding sites ($[BS_T]$). In contrary, when $[D_T] \ll [BS_T]$ and $[D_T] = [BS_T]$, it may be not accurate to simply use the dilution factor as the actual factor between concentration of the diluted and undiluted samples could vary. This is because dilution does not affect binding equilibrium much when binding sites were saturated with a much higher drug concentration.

In this work, although Equations 7.2 to 7.4 could be affected by inappropriate dilution factor, in the worst scenario as long as the $B_F/P_F > 10$, an active influx transport was indicated. That is, by simply multiplying the dilution factor to calculate the undiluted concentration may lead to an over estimated B_F/P_F when $[D_T] \leq [BS_T]$, but it did not affect the final conclusion that there was an active influx mechanism involved in transport K and N into the CNS. Moreover, many other researchers have used the same way to back calculate for undiluted concentration (Bao et al, 2019; Friden et al, 2011; Li et al, 2011; Maurer et al, 2005; Melander et al, 2016; Wan et al, 2007). Therefore, in this work, dilution factor "10" was used to back calculate K and N atropisomer concentrations in 1 in 10 diluted brain homogenate.

7.5 Conclusion

Based on the results, there was no stereoselective transport of K or N atropisomers through the BBB. Although K and N bound to plasma and brain tissue to different extents, there was no indication of stereoselective binding. An active influx transport mechanism, though not stereoselective, is probably present at the BBB for both K and N, which transports more K than N into brain. However, there was four times less N than K in brain homogenate, which indicates less N penetrates the BBB. Moreover, the CNS H_1 receptor occupancy results (Chapter 6) suggested the affinities

for the H_1 receptor from the lowest to the highest were SN, RN, RK and SK. Therefore, the lower sedative effect observed for SN compared with RN may be a result of stereoselective affinity to CNS H_1 receptors. On the other hand, the lower sedative effect of SN compared to SK and RK may be due to (a) the lower B_F of SN than K atropisomers and (b) the lower stereoselective affinity of SN for the H_1 receptor, compared with the K atropisomers.

Chapter 8 Discussion

K (Figure 1.1), a chiral compound, is a first-generation antihistamine with antiinflammatory properties. The antiinflammatory potency attributes to the inhibition of histamine release from mast cells and reduction of mast cell activity by stabilizing their membranes (Dimkovic et al, 1992; Zhang et al, 2016). It was suggested that the stabilization effect on mast cells is antihistaminic independent, but may be attributed to inhibition of platelet-activating factor (PAF) (Grant et al, 1990).

Clinically, K is used, as the racemate, by both oral and ocular routes. Because of the antihistaminic and antiinflammatory potency of K, it is widely used as an antiallergic and antianaphylactic agent in both adults and children (Hsu et al, 2016; Kabra et al, 2000; Sokol et al, 2013). Oral K has been used in patients with allergic rhinitis, allergic conjunctivitis, atopic dermatitis, urticaria, asthma, mastocytosis, and food allergy in some countries including Canada, Europe, and Mexico (Sokol et al, 2013). However, only the ocular administration has been approved for patients with allergic conjunctivitis in the United States, which is due to the CNS side effects, especially the sedative effect.

N is an active metabolite of K (by the oxidative N-demethylation metabolic pathway) (Le Bigot et al, 1987). It is similar to K, not only in its structure but also in antihistaminic and antiinflammatory potency, which makes N a potential compound to treat allergic and anaphylactic conditions, such as pruritus (Aberg et al, 2015). In addition, N is a chiral compound, having S- and R-atropisomers. Moreover, the S-atropisomer of N was reported to show much less sedative effect compared to RN and K (Chapter 1, Section 1.1). This indicated SN could be a useful and potent antihistaminic as well as antiinflammatory agent with a much less sedative side effect compared to K. Therefore, it is important to understand how the sedative effect is induced by antihistamines and why SN is lacking of sedative effect.

As discussed (Section1.1), in the CNS, histamine is involved in regulation of sleep and wakefulness (Table 1.1), thus sedative side effect occurs when antihistamine binds

to the CNS H_1 receptor. In order to explain why SN lacks the sedative side effect, the following hypotheses have been posited and tested in this thesis:

1. Stereoselective transporter hypothesis:
At the BBB, there is a stereoselective transporter involved in transporting K and N atropisomers. This transporter functions (a) as an influx transporter, which selectively transports less SN than RN, SK and RK into brain or (b) as an efflux transporter, which selectively pumps more SN than RN, SK and RK out of brain. As a result, there is less SN in the CNS available to bind to the H_1 receptor, thus less sedative effect.
2. Stereoselective specific binding hypothesis:
In the CNS, SN has lower affinity for the H_1 receptor compared to RN, SK and RK. As a result, there is less SN bound to the H_1 receptor than RN, SK and RK. Consequently, SN causes less sedative effect.
3. Stereoselective non-specific binding hypothesis:
There are non-specific bindings of SN, RN, SK and/or RK to plasma proteins and/or brain tissue. The stereoselective non-specific bindings result in more SN binding to plasma proteins and/or brain tissues compared to RN, SK and RK. Consequently there is less SN available in the plasma and/or in the CNS than RN, SK and RK thus less sedative effect.
The lack of sedative effect from SN could be a result of one or combination of the above hypotheses, which are discussed in the following sections.

8.1 Stereoselective transporter hypothesis

Many research groups have reported stereoselective transporters, such as the P-gp, MCT and GULT-1 (Bickel et al, 2001; Chang et al, 2015; McAllister et al, 2001), which were also found at the BBB. Among these, P-gp has been found to be involved in transporting some of the second-generation antihistamines (cetirizine and fexofenadine) (Table 8.1) (Miura et al, 2007; Miura and Uno, 2010) and other drugs (citalopram, ivermectin, loperamide, mefloquine, pioglitazone and tacrolimus) (Chang et al, 2015; Choong et al, 2010; Miura et al, 2007; Miura and Uno, 2010). However, to date, there was no stereoselective influx or efflux transporters reported in transporting K or N atropisomers. As a result, the stereoselective transporter,

which may contribute to transport of K and N atropisomers across the BBB, was investigated in this thesis.

Table 8.1 Stereoselective transporters and antihistamines

Antihistamines	Transporter	Enantiomer/atropisomers preference	Literature
Fexofenadine	P-gp	Efflux S-enantiomer more than R-enantiomer	Akamine and Miura, 2018; Miura et al, 2007; Miura and Uno, 2010
	OATP2B1	Uptake more R-enantiomer than S-enantiomer	Akamine et al, 2014; Akamine and Miura, 2018
Cetirizine	p-gp	Efflux more R-enantiomer than S-enantiomer	He et al 2010
	MRPs	Efflux more R-enantiomer than S-enantiomer	

8.1.1 Stereoselective influx transporter hypothesis

The stereoselective influx transporter hypothesis was mainly based on an unidentified influx transporter, which has been reported to actively transport cationic first-generation antihistamines (including K) into RBE cell monolayer (Ishiguro et al, 2004; Suzuki et al, 2010). Similar to the reported influx mechanism, an influx transporter was found in our RBE4 cells studies (Chapter 5, Section 5.4.3), which indicates an active mechanism was involved in uptake of both K and N into RBE4 cell monolayers.

In addition to the influx transporter at the REB4 cell monolayers, the *in vivo* work suggested a similar influx mechanism existing in rat BBB. The B_F/P_F of K (over 40) and N (approximately 10) further suggested the existence of an active influx mechanism is involved in transporting K and N to rat brain via the BBB (Figure 7.5 and 7.6).

As transporter-substrate interactions occur in chiral environments, the transporter found at the RBE4 cell monolayer and the active mechanism indicated in the B_F/P_F results, could be a potential candidate, which participates in stereoselective transport of K and N atropisomers through the BBB.

However, despite the active influx transporter found both *in vitro* and *in vivo*, according to current results, none of these active influx mechanisms showed

significant stereoselectivity on transporting K or N atropisomers across the BBB. Although K and N atropisomers were transported by an active influx mechanism into the REB4 cell monolayers and across the rat BBB, the mechanism was not stereoselective. As a conclusion, the stereoselective active influx transporter hypothesis is not supported.

8.1.2 Stereoselective efflux transporter hypothesis

Another hypothesis based on stereoselective transporter is the stereoselective efflux transporter hypothesis. That is, at the BBB, a stereoselective efflux transporter selectively pumps more SN out of brain and consequentially leads to less sedative effects compared to RN, SK and RK.

As discussed (Section 1.6.1), there are three main efflux transporters expressed at the BBB (P-gp, BCRP and MRPs). Although MRP 1, 2 and 4 were confirmed to be located on the luminal membrane of the human BBB (Dallas et al, 2006), only MRP4 is expressed in quantifiable levels at the human and rodent BBB (Agarwal et al, 2012; Kalvass et al, 2013; Shawahna et al, 2011). Therefore, in this thesis, only MRP4, p-gp and BCRP were discussed as potential candidates of stereoselective efflux transporter involved in transporting K and N atropisomers.

Among these three efflux transporters, BCRP is expressed 1.6-fold higher than p-gp whereas MRP4 is 10 times less abundant than p-gp (Shawahna et al, 2011). In addition to the lower expression at the BBB, MRP4 is an organic anion transporter, which is unlikely to be involved in transporting K or N, as both are cationic compounds. As a result, only BCRP and p-gp were considered the possible stereoselective efflux transporters for K and N atropisomers.

Although RBE4 cells express both P-gp (Babakhanian et al, 2007) and BCRP (Lee et al, 2007), RBE4 cells do not form complete tight junctions thus do not generate the necessary restrictive paracellular barrier properties (Tsukita and Furuse, 2000). As a result, to investigate these potential stereoselective efflux transporters, Caco-2 cell monolayers were used. As both BCRP and P-gp are expressed in Caco-2 cell monolayers, it was concluded these cells could be used to investigate if a compound is a substrate of efflux transporters (Rodrigues et al, 2009; Wilhelm and Krizbai, 2014).

P_{app} results from the Caco-2 cell monolayer permeability study (Table 5.4) showed the P_{app} ratios of K and N from B to A side over the A to B side were approximately 1.6 and 2.2 respectively (Table 5.4). This indicated some extent of contribution of an efflux transport mechanism, though it is unclear which transporter, BCRP and/or p-gp, was involved.

However, the efflux mechanism found at the Caco-2 cell monolayers was not stereoselective for either K or N atropisomers (Table 5.4). This suggested, neither BCRP nor p-gp was involved in stereoselectively transporting K or N atropisomers through the Caco-2 cell monolayers. As a result, the stereoselective efflux transporter hypothesis is not supported.

As a conclusion, there were influx (RBE4 cell monolayer and rat B_F/P_F ratios) and efflux (Caco-2 cell monolayer) mechanisms involved in transporting K and N atropisomers. However, none of these mechanisms was stereoselective for K and N atropisomers. Therefore, both of the stereoselective influx and efflux hypotheses are not supported; so this research does not support stereoselective transport across the BBB as the explanation for the different sedative effects caused by SN, RN, SK and RK. As a result, the next hypothesis, stereoselective specific binding to the CNS H_1 receptor, was tested. Before discussing these H_1 receptor results, some limitations with the above results are discussed.

8.1.3 Discrepancy in transporter results

As discussed in the above sections, results from Caco-2 experiments showed that for both K and N, the P_{app} of B to A direction was higher than that of A to B direction (Table 5.4). The P_{app} ratios of B to A over the A to B directions were approximately 1.6 and 2.2 for K and N respectively. This indicated an efflux mechanism involved in transporting K and N at the Caco-2 cell monolayers.

In contrast, the *in vivo* results suggested a different story. The B_F/P_F ratios of K and N were approximately 40 and 10 respectively (Figures 7.5 and 7.6), which showed a 40 (for K) and 10 (for N) times higher B_F than P_F. The difference between B_F and P_F indicated an influx mechanism participated in transporting K and N across the rat BBB. This is because assuming there was only a passive mechanism, the free brain concentrations of K and N would always be less or equal to the free plasma concentrations (Hu and Li, 2011). If there was an efflux mechanism, the free brain

concentration would be less than the free plasma concentration of K and N as efflux transporter pumps K and N back from brain to plasma. Therefore, the *in vivo* B_F/P_F ratios (Figures 7.5 and 7.6) indicated an influx mechanism involved in transporting K and N at the rat BBB.

According to above results, there was a discrepancy between efflux or influx mechanism between the *in vitro* Caco-2 cell monolayer results and the *in vivo* rat free B/P ratios.

This discrepancy could be a result of the following possibilities, which were mainly caused by using the Caco-2 cell monolayers as the model to study the BBB permeability.

One possibility is that there are over expressed efflux transporters on the Caco-2 cell line. To investigate the BBB permeability, Lohmann's and coworkers compared the Caco-2 cell monolayer with a BBB cell model, the primary cultured porcine brain capillary endothelial cells (PBCEC). Their results suggested that for the screened compounds, Caco-2 cell monolayers have a good correlation with the PBCEC for predicting the BBB permeability. However, Caco-2 cell monolayers did show a more restricted permeability for the P-gp substrate (cyclosporin A), which may have indicated an overexpression of P-gp at the Caco-2 cell monolayer (Lohmann et al, 2002).

Another possibility is that according to real-time PCR results, MRP2 is expressed (approximately 10 fold) more than P-gp on Caco-2 cells (Rodrigues et al, 2009). In addition, MRP3 was also expressed on Caco-2 cells (Sun and Pang, 2008). Both MRP2 and MRP3 are not found on the luminal membrane of the human BBB (Dallas et al, 2006). Although MRP 1, 3 and 5 have been found in RBE4 cells, they are at much lower levels compared to that of Caco-2 cells. Therefore, these transporters may cause the efflux mechanism indicated by Caco-2 cells.

Besides these two possibilities, Caco-2 cells may not express the influx transporter, which is involved in transporting K and N at the BBB. These hypotheses could be tested by inhibitor studies, which were not carried out in this thesis. Moreover, Caco-2 cell work was carried out over a 2 h period whereas the B/P ratio *in vivo* was performed at only one time point of 5 min. As a result, this short time, the equilibrium of the efflux mechanism may not be reached. Therefore, at a later time point, the efflux mechanism may be showing a greater influence.

8.2 Stereoselective specific binding hypothesis

Beside the stereoselective transporter hypothesis, which was found not to contribute to the less sedative effect caused by SN (Section 8.1), stereoselective binding to the CNS H_1 receptor is the next hypothesis to explain the observed different degrees of sedative effects caused by SN, RN, SK and RK.

Stereoselective specific binding of compounds to CNS receptors, such as the muscarinic receptor, α2-noradrenergic receptor, D_1 and D_2-dopamine receptors, has been reported by different research groups (Table 1.11) (Farde et al, 1988; Messer, et al, 1992; Waelbroeck et al, 1990).

Moreover, some second-generation antihistamines have been found having stereoselective affinity to H_1 receptors. R-cetirizine has higher affinity to H_1 receptors than the racemic cetirizine and the S-cetirizine (Gillard et al, 2002). Whereas for fexofenadine, the S-enantiomer is a more potent H_1 receptor antagonist compared to the R-enantiomer (Kusuhara et al, 2013).

Similar results were found from our H_1 receptor occupancy experiment (Table 6.1), which support the stereoselective binding of K and N atropisomers to the CNS H_1 receptor hypothesis.

Results indicated significantly different affinities (K_I) between SN (5.10 ± 2.00 nM) and SK (1.03 ± 0.42 nM), SN and RN (2.08 ± 0.75 nM) and SN and RK (1.65 ± 0.58 nM), though the difference between SK and RK were not significant (Table 6.1 and Figure 6.9). The K_I of SN was approximately 2.5 times of RN, 5 times that of SK and 3 times that of RK. As a higher K_I indicates a lower affinity of compounds for the receptor, this suggested SN has the least affinity to H_1 receptors in rat brain homogenate for K and N atropisomers.

However, this difference between SN and SK was significant but not substantial comparing to the reported K_I for R-cetirizine, S-cetirizine, which were 3 and 100 nM respectively (Gillard et al, 2002). According to Gillard's group, the K_I of S-cetirizine was 33 times of the R-cetirizine, while base on our result, K_I of SN was only 2.5 times of RN, 5 times of SK and 3 times of RK. On the other hand, Kusuhara's group has reported the K_I for R-fexofenadine and S-fexofenadine was 30 and 13 nM respectively, which difference (2.3 times difference) was similar to our result (Kusuhara et al, 2013).

Therefore, this stereoselective binding could be a factor, which contributes to the different sedative effects caused by SN (0 out of 10), RN (3 out of 10) and K (10 out of 10) (Table 1.6).

Although this hypothesis was supported by the H_1 receptor occupancy results, there was another hypothesis, the stereoselective non-specific binding hypothesis, may also participate in the different sedative effects caused by K and N atropisomers.

8.3 Stereoselective non-specific binding hypothesis

The stereoselective specific binding could be a factor that contributing to the lower sedative effect caused by SN compared to RN, SK and RK (as discussed in Section 8.2). As non-specific binding also happens in chiral environments, it raised another hypothesis: stereoselective non-specific binding. Other research groups have reported stereoselective binding of compounds to plasma proteins (Martinez-Gomez et al, 2007; Shen et al, 2013).

Moreover, it has been reported that stereoselective plasma protein binding takes place for the second-generation antihistamine cetirizine. R-cetirizine (85% bound) stereoselectively binds to plasma protein more than that of the S-enantiomer (50% bound) (Gupta et al, 2006).

In this thesis, it was posited that stereoselective non-specific binding occurs such that: (a) more SN is bound to plasma proteins than RN, SK and RN thus less free SN is available in the plasma compared to RN, SK and RK and/or (b) more SN is bound to brain tissues than RN, SK and RK thus less free SN is available in the ISF for binding to the CNS H_1 receptor.

Results from the *in vivo* experiments (Figures 7.3 and 7.4) suggested, for both total and free plasma concentrations, there was no significant difference between concentrations of SK and RK or between SN and RN. As a result, there was no evidence for stereoselective non-specific binding of K or N atropisomers to plasma proteins.

Similarly, there was no significant difference between concentrations of SK and RK or between SN and RN (Figures 7.1 and 7.2) in both total and free concentrations in brain homogenate. Therefore, there was no evidence for stereoselective non-specific binding of K or N atropisomers to brain tissue.

However, the original data suggesting SN caused less sedative effects than RN and K was obtained from mice (Table 1.6), while our *in vivo* experiment was performed in rats. There may be a factor of species, which contributed to the plasma protein binding result.

It has been reported that sometimes the stereoselective binding to plasma protein can be species dependent. Differences were observed between human, bovine, dog (Fitos et al, 2002, Pistolozzi and Bertucci, 2008), and, between rat and rabbit (Zhu and Zhang, 2008). Nevertheless, no clear evidence indicated species difference between rat and mouse. Thus the plasma protein binding results obtained from rats could be a reasonable indicator for the plasma protein binding profiles in mice.

In addition to the non-specific binding of K and N atropisomers to plasma protein, the non-specific binding of K and N atropisomers to brain tissues was also investigated. The total and free brain homogenate concentrations of K atropisomers indicated there was no stereoselective non-specific binding of SK or RK to rat brain tissues. Similar results were found for SN and RN that according to B_T and B_F of N atropisomers, there was no stereoselective non-specific binding of SN or RN to rat brain tissues.

REB4 cell experiments agreed with this as there was no stereoselective non-specific binding of K or N atropisomers to REB4 cell monolayers (Figure 5.2), which suggested there was no stereoselective non-specific binding of K or N atropisomers to the rat BBB.

As a conclusion, there was no evidence for non-specific binding of SN, RN, SK or RK to rat plasma proteins or brain tissues.

Although there was no evidence of stereoselective non-specific binding of K or N atropisomers, on the other hand, there was different plasma protein binding between racemic K and N. N binds to plasma protein (approximately 90%) to a higher extent than that of K (approximately 75%) (Section 7.4.2). Besides the influx mechanism (Section 8.1.1), which leads to an approximately 4 times higher B_F/P_F of K compared to that of N (Figures 7.5 and 7.6), the higher plasma protein binding of N may contribute to the less free brain homogenate concentration of N than K (Figures 7.1 and 7.2).

8.4 Other possible hypothesis

8.4.1 Stereoselective metabolism at the BBB

The three main hypotheses were discussed in above sections (Section 8.1 – 8.3), but there is another possible hypothesis, the stereoselective metabolism at the BBB. The hypothesis is that at the BBB, enzymes stereoselectively break down more SN than RN, SK and RK when they cross the BBB. As a result, SN cannot reach the CNS or reaches the CNS in a very limited amount, thus much less sedative effect occurs. To posit the stereoselective metabolism hypothesis, it is important to understand the metabolism of N.

It has been reported that N is metabolised into (a) reduced norketotifen (reduced N) through ketoreduction and (b) N-sulfate norketotifen (N-sulfate N) by sulfation (Figure 8.1) (Le Bigot et al, 1987).

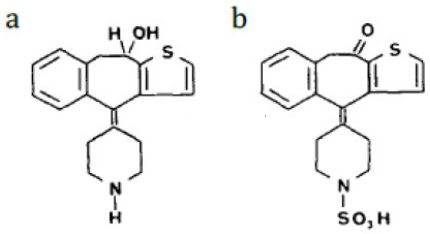

Figure 8.1 Structures of (a) reduced norketotifen and (b) N-sulfate norketotifen.

For these two metabolites of N, N-sulfate N, however, was not found in either human or in rat from 4 h up to 4 days incubation with hepatocytes, while reduced N was not reported in the paper (Le Bigot et al, 1987). This may be caused by (a) the limitation of LOD of the analytical method in the 1980s, (b) oxidative N-demethylation is not a main route of K metabolism in human hepatocytes thus only a trace of N was found in human hepatocytes culture, and (c) in rats, although oxidative N-demethylation is a main metabolic route of K (62% of K turns to N in 4h), N-sulfate and ketoreduction are not main metabolic routes, thus the N-sulfate and ketoreduction metabolites of N could be very limited (Le Bigot et al, 1987). As a result of above reasons, there may be a further metabolic route of N that was not indicated in the results presented by Le Bigot's group. Nonetheless, this possible metabolic route of N is not, at least not at the rat BBB, proven to be significant for the following reasons.

First, although many enzymes were found in and near the BBB (De Lange, 2012, Shawahna et al, 2011), there is no clear evidence to suggest enzyme participation in metabolism of N either in or near the BBB.

Ghosh's group reviewed enzymes expressed in human brain tissue and/or the BBB. It has been confirmed that CYP1A1, CYP1B1, epoxide hydrolase and UGTs were found (Ghosh et al, 2011), in which UGT2B10, UGT1A3 and UGT1A4 are involved in K metabolism (Kato et al, 2013; Mey et al, 1999; Weiner et al, 2006). Although UGT1A3 and 1A4, especially UGT1A4, have been reported to participate in stereoselective metabolism of K by N-glucuronidation, which is restricted to primates, owing to species difference (Mey et al, 1999). Moreover, for N, N-glucuronidation is not a reported metabolic route in human or rat. Therefore, in both peripheral and the CNS, N-glucuronidation is unlikely to be involved in stereoselective metabolism of N.

In addition, Shawahna's group suggested that only CYP1B1 and CYP2U1 were quantifiable CYPs at the BBB. It has been reported that only several main phase II enzymes were quantifiable at the BBB, which include glutathione S-transferase (GST) (GSTP1, GSTM3, GSTO1 and GSTM2) and catechol-O-methyltransferase (COMT) (Shawahna et al, 2011). However, none of them is involved in known metabolic pathways of N.

In summary, according to the reported enzymes at or near the BBB and the metabolic routes of N, there is no evidence in literatures suggesting metabolism, let alone stereoselective metabolism, of N at the BBB.

This is supported by the *in vivo* work in this thesis, which found no significant difference between SN and RN in either the B_T or the B_F in rat brain (Figure 7.2). However, these results may not be enough to fully support that there is no stereoselective metabolism of N at the rat BBB. This will be discussed in the following section (Section 8.5).

As a conclusion, the stereoselective metabolism hypothesis was supported by neither literatures nor our *in vivo* results. Thus, the posited metabolic barrier may not be involved, at least not involved significantly, in the sedative difference between SN and RN.

8.4.2 Other GPCR receptors and ion channels

As the sedative effects are caused by various reasons, in addition to hypotheses discussed above, it is also possible that the different sedative effects resulted from other GPCR receptors and/or ion channels instead of the H_1 receptors.

Although K and N are H_1 receptor "inverse agonists", they are not highly selective only for the H_1 receptor. K has been reported to show affinity for several other receptors such as H_2 receptors (858-fold lower affinity than for H_1 receptors), H_3 receptors (1752-fold lower affinity than for H_1 receptors) (Sharif et al, 1994) and muscarinic receptors (Mahdy and Webster, 2014, Simons and Simons, 2011). However, muscarinic receptors do not lead to sedation after interacting with K. Blockage of H_3 receptors results in extended wakefulness rather than sedation (as discussed in Section 1.2). GPCR receptors (5-HT_2 antagonism and α1 and α2-adrenergic antagonism) may also be relevant to the sleep-wakefulness cycle (Krystal et al, 2013), but there is no evidence of affinity of K or N is more selective for these receptors than the H_1 receptors (Gallois-Bernos and Thurmond, 2012; Takashima et al, 1992).

There are two main ion channels involved in sedative effects, (a) calcium activated potassium channel (alcohol induced sedation) and (b) γ-aminobutyric acid type A (GABAA) gated chloride channel (intravenous anaesthetics induced sedation) (Sandstorm and Nash, 2004). Similarly, there is no evidence to indicate correlation between K and sedation due to affects on ion channels.

As a result, it is unlikely that other GPCR receptors or ion channels are participated in the different sedative effects caused by K and N atropisomers.

8.5 limitations of this thesis and further work

As discussed at the end of last section (Section 8.4), the *in vivo* experiment showed no stereoselective metabolism of K or N atropisomers in rat brain. This was possibly due to the design of the *in vivo* work. It was designed to investigate the stereoselective transport of K and N atropisomers across the BBB. Therefore, it was terminated at 5 min to minimize the effects from possible metabolism of K and N. It was adequate to meet the designed purposes but it also has the following limitations:

First, the 5 min terminating point of the *in vivo* experiments could be not long enough to show a possible stereoselective metabolism of K and N, in neither peripheral nor CNS.

Therefore, in future it would be interesting to investigate the metabolism of N. as the available paper was for research done in 1987 (Le Bigot et al, 1987), when the analytical assay had poor sensitivity compared with today's quantification technologies. Also, to investigate if there is any stereoselective metabolism of N in peripheral and in the CNS would be useful, as these stereoselective metabolisms could be contributing to the less sedative effect caused by SN.

Second, there was only one time point in the *in vivo* study, which was adequate to show there was no stereoselective influx mechanism (that is the predominant mechanism) of K or N atropisomers across the BBB. However, the single time point was not enough to review the kinetic of elimination of K or N. At 5 min, interactions of K and N with the efflux transporter or enzyme may not reach equilibrium. As a result, there could be potential a stereoselective mechanism of K or N which was not determined in this thesis.

Therefore, the *in vivo* elimination kinetics of N may be another possible future work to look at. This is because the elimination kinetics maybe a better indicator on the possible stereoselective efflux and/or metabolism of N atropisomers.

Third, as discussed in Section 8.2, the less sedative effect caused by SN may be attributed to the lowest affinity of SN for the CNS H_1 receptors than that of RN, SK and RK; however, the antihistaminic effect also comes from binding of K and N to the H_1 receptor in peripheral. As a result, in the CNS a lower affinity for the H_1 receptor contributes to a less sedative effect, whereas in the peripheral a lower affinity for the H_1 receptor leads to a lower antihistaminic therapeutic effect.

Therefore, it is a rational question to ask if the stereoselective binding of SN only occurs to the CNS H_1 receptor, by which it results in a less sedative side effect while maintaining the antihistaminic potency. On the other hand, if the stereoselective binding of SN also occurs to the peripheral H_1 receptor, it will result in a less antihistaminic potency compared with racemic K and N.

It has been reported in an *in vitro* study that for 18 tested antihistamines (including four sets of stereoisomers), there was no difference between the affinities to the cerebellum and lung H_1 receptors in guinea pig. However, the density of the H_1

receptor in the cerebellum tissue was six times higher than that of lung tissue (Ter Laak et al, 1993). Although Ter Laak's group has not tested K or N and it was not clear if it was species dependent, it is a rational assumption that similar results could be observed for K and N atropisomers in mice and rats. As a result, it may be interesting to investigate in future if this stereoselective binding of SN to the H_1 receptor occurs only in the CNS or also in peripheral H_1 receptors in different species.

In addition to above limitations, receptor affinity (K_I) values provide limited information on pharmacological actions, as compounds with similar K_I values may have different second messengers, thus different pharmacological actions. Therefore, even K and N have been reported as "inverse agonist"for the H_1 receptor, it is still interesting to investigate pharmacological actions of K and N atropisomers in future studies.

8.6 Conclusion

In conclusion, according to results from the B/P ratios and H_1 receptor binding studies, the less sedative effect caused by SN compared to RN, SK and RK was due to a lower uptake of N than K into the brain and reduced binding of SN to CNS H_1 receptors.

References:

ABBOTT, N. (2005) Dynamics of CNS barriers: Evolution, differentiation, and modulation. *Cell. Mol. Neurobiol.* 25**,** 5–23.

ABBOTT, N. J., PATABENDIGE, A. A. K., DOLMAN, D. E. M., YUSOF, S. R. & BEGLEY, D. J. (2010) Structure and function of the blood-brain barrier. *Neurobiol. Dis*. 37, 13–25.

ABBOTT, N. J., RONNBACK, L. & HANSSON, E. (2006) Astrocytes-endothelial interactions at the blood-brain barrier. *Nature Rev. Neurosci*. 7, 41–53.

ABERG, G. A. K., ARULNESAN, N., BOLGER, G. T., CIOFALO, V. B. & PUCAJ, K. (2015) Characterization and validation of a canine pruritic model. *Drug Dev. Res*. 76, 246–250.

ABERG, G. A. K. & JOHNSON, K. (2014) Medicinal treatment of dermal diseases in companion animals. United States Patent No. US8778971B2.

ABERG, G. A. K. & CIOFALO, V. B. (2015) Medicinal treatment of dermal diseases in companion animals. European Patent No. EP2911510A1.

ADKINSON, N. F. JR., BOCHNER, B. S., BURKS, A, W., BUSSE, W. W., HOLGATE, S. T., LEMANSKE, R. F. JR. & O'HEHIR, R. E. (2013) Middleton's Allergy: Principle and Practice. 8th edition. Elesvier Saunders, Philadelphia.

AGARWAL, S., UCHIDA, Y., MITTAPALLI, R. K., SANE, R., TERASAKI, T. & ELMGUIST, W. F. (2012) Quantitative proteomics of transporter expression in brain capillary endothelial cells isolated from P-glycoprotein (P-gp), breast cancer resistance protein (Bcrp), and P-gp/Bcrp knockout mice. *Drug Metab. Dispos.* 40, 1164–1169.

AGUNDEZ, J. A. G., JIMENEZ-JIMENEZ, F. J., ALONSO-NAVARRO, H. & GARCIA-MARTIN, E. (2014) Drug and xenobiotic biotransformation in the blood-brain barrier: A neglected issue. *Front. Cell Neurosci.* 8, 335.

AHMAD, A., TAKEUCHI, K., OZAKI, T., UNNO, K., MOHAMMAD, S., AKECHI, H., MORIOKA, E., HONDA, K. & IKEDA, M. (2016) Possible treatment of circadian sleep disorders using daily ketotifen administration. *Sleep Biol. Rhythms*. 14, 117–120.

AKAMINE, Y. (2015) Determinants of the stereoselective pharmacokinetics of fexofenadine. *Yakugaku Zasshi*. 135, 473–481.

AKAMINE, Y. & MIURA, M. (2018) An update in the clinical pharmacokinetics of fexofenadine enantiomers. *Expert Opin. Drug Metab. Toxicol.* 14, 429–434.

AKAMINE, Y., MIURA, M., KOMORI, H., SAITO, S., KUSUHARA, H., TAMAI, I., IEIRI, I., UNO, T. & YASUI-FURUKORI, N. (2014) Effects of one-time apple juice ingestion on the fexofenadine enantiomers. *Eur. I. Clin. Pharmacol*. 70, 1087–1095.

ALATA, W., PARIS-ROBIDAS, S., EMOND V., BOURASSET, F. & CALON, F. (2014) Brain uptake of a fluorescent vector targeting the transferrin receptor: A novel application of in situ brain perfusion. *Mol. Pharm*. 11, 243–253.

ALESSANDRO, G., GIUSEPPE, M., VINCENZO, C. & SERENA, O. (2014) Recent advances in chiral separation of amino acids using capillary electromigration techniques. *J. Chromatogr*. *A*. 1363, 41–50.

ANDERSON, B. D. (1996) Prodrugs for improved CNS delivery. *Adv. Drug Deliv. Rev*. 19, 171–202.

ANDERSON, P. H., GRONVALD, F. C., HOHLWEG, R., HANSEN, L. B., GUDDAL, E., BRAESTRUP, C. & NIELSEN, E. B. (1992) NNC-112, NNC-687 and NNC-756, new selective and highly potent dopamine D_1 receptor antagonists. *Eur. J. Pharmacol.* 219, 45–52.

ANTHES, J. C., GILCHREST, H., RICHARD, C., ECKEL, S., HESK, D., WEST, R. E. JR., WILLIAMS, S. M., GREENFEDER, S., BILLAH, M., KREUTNER, W. & EGAN, R. E. (2002) Biochemical characterization of desloratadine, a potent antagonist of the human histamine H_1 receptor. *Eur. J. Pharmacol.* 449**,** 229–37.

APPL, H., HOLZAMMER, T., DOVE, S., HAEN, E., STRABER, A. & SEIFERT, R. (2012) Interactions of recombinant human histamine H_1, H_2, H_3 and H_4 receptors with 34 antidepressants and antipsychotics. *Naunyn-Schmiedeberg's Arch. Pharmacol.* 385, 145–170.

ARMSTRONG, D. W., WARD, T. J., ARMSTRONG, R. D. & BEESLEY, T. E. (1986) Separation of drug stereoisomers by the formation of beta-cyclodextrin inclusion complexes. *Science* 232**,** 1132–1135.

ARNDT, P., VOLK, C., GORBOULEV, V., BUDIMAN, T., POPP, C., ULZHEIMER-TEUBER, I., AKHOUNDOVA, A., KOPPATZ, S., BAMBERG, E., NAGEL, G. & KOEPSELL, H. (2001) Interaction of cations, anions, and weak base quinine with rat renal cation

transporter rOCT2 compared with rOCT1. Am. J. Physiol. Renal Physiol. 281, 454–468.

ASCHNER, M. & GANNON, M. (1994) Manganese (Mn) transport across the rat blood-brain barrier: Saturable and transferrin-dependent transport mechanisms. *Brain Res. Bull*. 33, 345–349.

BABAKHANIAN, K., BENDAYAN, M. & BENDAYAN, R. (2007) Localization of P-glycoprotein at the nuclear envelope of rat brain cells. *Biochem. Biophys. Res. Commun.* 361**,** 301–306.

BABU, E., TAKEDA, M., NARIKAWA, S., KOBAYASHI, S., ENOMOTO, A., TOJO, A., CHA, S. H., SEKINE, T., SAKTHISEKARAN, D & ENDOU, H. (2002) Role of human organic anion transporter 4 in the transport of ochratoxin A. *Biochim. Biophys. Acta* 1590, 64–75.

BAHAR, F. G., OHURA, K., OGIHARA, T. & IMAI, T. (2012) Species difference of esterase expression and hydrolase activity in plasma. J. Pharm. Sci. 101, 3979–3988.

BAKKER, R. A., NICHOLAS, M. W., SMITH, T. T., BURSTEIN, E. S., HACKSELL, U., TIMMERMAN, H., LEURS, R., BRANN, M. R. & WEINER, D. M. (2007) *In vitro* pharmacology of clinically used central nervous system-active drugs as inverse H1 receptor agonists. *J. Pharmacol. Exp. Ther*. 322, 172–179.

BALABANOV, R. & DORE-DUFFY. P. (1998) Role of the CNS microvascular pericyte in the blood-brain barrier. *J. Neurosci. Res*. 53, 637–644.

BALBUENA, P., LI, W. & EHRICH, M. (2011) Assessments of tight junction proteins occludin, claudin 5 and scaffold proteins ZO1 and ZO2 in endothelial cells of the rat blood-brain barrier: Cellular responses to neurotoxicants malathion and lead acetate. *Neurotoxicology* 32**,** 58–67.

BALBUENA, P., LI, W., MAGNIN-BISSEL, G., MELDRUM, J. B. & EHRICH, M. (2010) Comparison of two blood-brain barrier *in vitro* systems: Cytotoxicity and transfer assessments of malathion/oxon and lead acetate. *Toxicol. Sci.* 114**,** 260–271.

BALTES, E., COUPEZ, R., GIEZEK, H., VOSS, G., MEYERHOFF, D. & BENEDETTI, M. S. (2001) Absorption and disposition of levocetirizine, the eutomer of cetirizine, administered alone or as cetirizine to healthy volunteers. *Fundam. Clin. Pharmacol*. 15, 269–277.

BAO, X., WU, J., SANAI, N. & LI, J. (2019) Determination of total and unbound ribociclib in human plasma and brain tumor tissues using liquid chromatography coupled with tandem mass spectrometry. *J. Pharm. Biomed. Anal*. 166, 197–204.

BAUER, B., HARTZ, A. M. S., FRICKER, G. & MILLER, D. S. (2005) Modulation of P-glycoprotein transport function at the blood–brain barrier. *Exp. Biol. Med*. 230, 118–127.

BAUER, M., ROMERMANN, K., KARCH, R., WULKERSDORFER, B., STANEK, J., PHILIPPE, C., MAIER-SALAMON, A., HASLACHER, H., JUNGBAUER, C., WADSAK, W., JAGER, W., LOSCHER, W., HACKER, M., ZEITLINGER, M. & LANGER, O. (2016) Pilot PET study to assess the functional interplay between ABCB1 and ABCG2 at the human blood-brain barrier. *Clin. Pharmacol. Ther*. 100, 131–141.

BEGLEY, D. J., LECHARDEUR, D., CHEN, Z. D., ROLLINSON, C., BARDOUL, M., ROUX, F., SCHERMAN, D. & ABBOTT, N. J. (1996) Functional expression of P-glycoprotein in an immortalised cell line of rat brain endothelial cells, RBE4. *J. Neurochem.* 67**,** 988–95.

BEIBEI, C., MAN, H., CHENG, Z. & BIN, H. (2014) Chiral separation of selenoamino acods in biological samples. *J. Chromatogr. A.* 1363, 62–70.

BENEDETTI, M. S., WHOMESLEY, R., POGGESI, T., CAWELLO, W., MATHY, F-X., DELPORTE, M-L., PAPELEU, P. & WATELET, J-B. (2009) Drug metabolism and pharmacokinetics. *Drug Metab. Rev*. 41, 344–390.

BICKEL, E., YOSHIKAWA, T. & PARDRIDGE, W. M. (2001) Delivery of peptides and proteins through the blood-brain barrier. *Adv. Drug. Deliv. Rev*. 46, 247–279.

Bioanalytical method validation. Guidance for industry (2001). U.S. Department of Health and Human Services. Food and Drug Administration.

BLASCHKE, G. & TERHECHTE, A. (1995) Investigation of the stereoselective metabolism of the chiral H_1-antihistaminic drug terfenadine by high-performance liquid chromatography. *J. Chromatogr. A*. 694, 219–225.

BONGERS, G., BAKKER, R. A. & LEURS, R. (2007) Molecular aspects of the histamine H_3 receptor. *Biochem. Pharmacol*. 73, 1195–1204.

BREYER-PFAFF, U. & NILL, K. (2000) High-affinity stereoselective reduction of the enantiomers of ketotifen and of ketonic nortriptyline metabolites by aldo-keto reductases from human liver. *Biochem. Pharmacol.* 59**,** 249–260.

BRINGMANN, G., PRICE MORTIMER, A. J., KELLER, P. A., GRESSER, M. J., GARNER, J. & BREUNING, M. (2005) Atroposelective synthesis of axially chiral biaryl compounds. *Angew. Chem. Int. Ed*. 44, 5384–5427.

BROWN, R. E., STEVENS, D. R. & HAAS, H. L. (2001) The physiology of brain histamine. *Prog. Neurobiol.* 63, 637–672.

BUSCH, A. E., KARBACH, U., MISKA, D., GORBOULEV, V., AKHOUNDOCA, A., VOLK, C., ARNDT, P., ULZHEIMER, J. C., SONDERS, M. S., BAUMANN, C., WALDEGGER, S., LANG, F. & KOEPSELL, H. (1998) Human neurons express the polyspecific cation transporter hOCT2, which translocates monoamine neurotransmitters, amantadine, and memantine. *Mol. Pharmacol.* 54, 342–352.

CALHAU, C., MARTEL, F., PINHEIRO-SILVA, S., PINHEIRO, H., SOARES-DA-SILVA, P., HIPOLITO-REIS, C. & AZEVEDO, I. (2002) Modulation of insulin transport in rat brain microvessel endothelial cells by an ecto-phosphatase activity. *J. Cell. Biochem.* 84**,** 389–400.

CAMPO, V. L., BERNARDES, L. S. & CARVALHO, I. (2009) Stereoselectivity in drug metabolism: Molecular mechanisms and analytical methods. *Curr. Drug Metab*. 10, 188–205.

CARSON, S., LEE, N. & THAKURTA, S. (2010) Drug class review: Newer antihistamines. Oregon Health Science University, Oregon.

CESTELLI, A., CATANIA, C., DAGOSTINO, S., DI LIEGRO, I., LICATA, L., SCHIERA, G., PITARRESI, G. L., SAVETTIERI, G., DE CARO, V., GIANDALIA, G. & GIANNOLA, L. I. (2001) Functional feature of a novel model of blood brain barrier: Studies on permeation of test compounds. *J. Control. Release* 76**,** 139–147.

CHANG, K. L., PEE, H. N. & HO, P. C. (2015) Influence of drug transporters and stereoselectivity on the brain penetration of pioglitazone as a potential medicine against Alzheimer's disease. *Sci. Rep*. 5, 1–7.

CHANG, R. S. L., TRAN, V. T. & SNYDER, S. H. (1979) Heterogeneity of histamine H_1-receptors: Species variations in [^{3}H] mepyramine binding of brain membranes. *J. Neurochem.* 132, 1653–1663.

CHANKVETADZE, B., BURJANADZE, N., PINTORE, G., BERGENTHAL, D., BERGANDER, K., MAHLENBROCK, C., BREITKREUZ, J. R. & BLASCHKE, G. (2000) Separation of brompheniramine enantiomers by capillary electrophoresis and study of chiral recognition mechanisms of cyclodextrins using NMR-spectroscopy, UV

spectrometry, electrospray ionization mass spectrometry and X-ray crystallography. *J. Chromatogr. A.* 875**,** 471–484.

CHEN, Z. S., LEE, K. & KRUH, G. D. (2001) Transport of cyclic nucleotides and estradiol 17-β-D-glucuronide by multidrug resistance protein 4: Resistance to 6-mercaptopurine and 6-thioguanine. *J. Biol. Chem.* 276, 33747–33754.

CHOONG, E., DOBRINAS, M., CARRUPT, P-A. & CHIN, B. (2010) The permeability P-glycoprotein: A focus on enantioselectivity and brain distribution. *Expert. Opin. Drug Metab. Toxicol*. 6, 953–965.

CIARIMBOLI, G., GAUTRON, S. & SCHLATTER, E. (2016) Organic Cation Transporters Integration of Physiology, Pathology and Pharmacology, Spriger International Publishing. Switzerland.

CIHLAR, T. & HO, E. S. (2000) Fluorescence-based assay for the interaction of small molecules with the human renal organic anion transporter 1. *Anal. Biochem*. 283, 49–55.

CLAUDE, P. (1978) Morphological factors influencing transepithelial permeability: A model for the resistance of the zonula occludens. *J. Memebr. Biol*. 10, 219–232.

COORAY, H. C., BLACKMORE, C. G., MASKELL, L. & BARRAND, M. A. (2002) Localisation of breast cancer resistance protein in microvessel endothelium of human brain. *Neuroreport. 13*, 2059–2063.

DALLAS, S., MILLER, D. S. & BENDAYAN, R. (2006) Multidrug resistance-associated proteins: Expression and function in the central nervous system. *Pharmacol. Rev*. 58, 140–161.

DAUCHY, S., DUTHEIL, F., WEAVER, R. J., CHASSOUX, F., DAUMAS-DUPORT, C., COURAUD, P-O., SCHERRMANN, J-M., DE WAZIERS, I. & DECLECES, X. (2008) ABC transporters, cytochromes P450 and their main transcription factors: Expression at the human blood-brain barrier. *J. Neurochem*. 107, 1518–1528.

DAVSON, H. & SEGAL, M. B (1995) Physiology of the CSF and blood-brain barriers. 1st ed, CRC Press, Florida.

DEBAULT, L. E. & CANCILLA, P. A. (1980) ϒ-Glutamyl transpeptidase in isolated brain endothelial cells: Induction by glial cells *in vitro*. *Science* 207, 653–655.

DE BOER, A. G. & GAILLARD, P. J. (2007) Drug targeting to the brain. *Ann. Rev. Pharmacol. Toxicol*. 47, 323–55.

DEELEY, R. G., WESTLAKE, C. & COLE, S. P. C. (2006) Transmembrane transport of endo- and xenobiotics by mammalian ATP-binding cassette multidrug resistance proteins. *Physiol. Rev. 86*, 849–899.

DE LANGE, E. C. M. (2012) The physiological characteristics and transcyrosis mechanisms of the blood-brain barrier (BBB). *Curr. Pharm. Biotechnol*. 13, 1–9.

DI, L., KERNS, E. H. & CATER, G. T. (2008) Strategies to assess blood-brain barrier penetration. *Expert Opin. Drug Discov*. 3, 677–687.

DIMKOVIC, N., DJUKANOVIC, L., RADMILOVIC, A., BOJIC, P. & JULOSKI, T. (1992) Uremic pruritus and skin mast cells. *Nephron* 61, 5–9.

EASSON, L. H. & STEDMAN, E. (1933) Studies on the relationship between chemical constitution and physiological action. Molecular dissymmetry and physiological activity. *Biochem. J*. 27, 1257–1266.

ECKER, G. F. & CHIBA, P. (2009) Transporters as drug carriers: Structure, function, substrates. John Wiley & Sons, Germany.

ELENA, S. L., MARIA, L. M. & ANTONIO, L. C. (2016) Improving the sensitivity in chiral capillary electrophoresis. *Electrophoresis* 37, 19–34.

ENOMOTO, A., KIMURA, H., CHAIROUNGDUA, A., SHIGETA, Y., JUTABHA, P., CHA, S. H., HOSOYAMADA, M., TAKEDA, M., SEKINE, T., IGARASHI, T., MATSUO, H., KIKUCHI, Y., ODA, T., ICHIDA, K., HOSOYA, T., SHIMOKATA, K., NIWA, T., KANAI, Y. & ENDOU, H. (2002a) Molecular identification of a renal urate anion exchanger that regulates blood urate levels. *Nature* 417, 447–452.

ENOMOTO, A., WEMPE, M. F., TSUCHIDA, H., SHIN, H. J., CHA, S. H., ANZAI, N., GOTO, A., SAKAMOTO, A., NIWA, T., KANAI, Y., ANDERS, M. W. & ENDOU, H. (2002b) Molecular identification of a novel carnitine transporter specific to human testis. Insights into the mechanism of carnitine recognition. *J. Biol. Chem.* 277, 36262–36271.

ERDO, F., NAGY, I., TOTH, B., BUI, A., MOLNAR, E., TIMAR, A., MAGNAN, R. & KRAJCSI, P. (2017) Abcb1a (P-glycoprotein) limits brain exposure of the anticancer drug candidate seliciclib *in vivo* in adult mice. *Brain Res. Bull*. 132, 232–236.

ERIC. L. & CAROLINE, W. (2015) The many faces of packed column supercritical fluid chromatography: A critical review. *J. Chromatogr. A*. 1382, 2–46.

ERICA, S. S., LAIZE, Z., CARLOS, A. K., BERENICE DE SILVA, J., ROSENDO, A. Y. & EDITE, F. H. (2011) Estimating the octanol/water partition coefficient for

aliphatic organic compounds using semi-empirical electrotopological index. *Int. J. Mol. Sci.* 12, 7250–7264.

EYAL, S., HSIAO, P. & UNADKAT, J. D. (2009) Drug interactions at the blood-brain barrier: Fact or fantasy? *Pharmacol. Ther*. 123, 80–104.

FARDE, L., PAULI, S., HALL, H., ERIKSSON, L., HALLDIN, C., HOGBERG, T., NILSSON, L., SJOGREN, L. & STONE-ELANDER, S. (1988) Stereoselective binding of ^{11}C-raclopride in living human brain–a search for extrastriatal central D2-dopamine receptors by PET. *Psychopharmacology (Berl.)* 94, 471–478.

FARIA, A., PESTANA, D., TEIXEIRA, D., AZEVEDO, J., DE FREITAS, V., MATEUS, N & CALHAU, C. (2010) Flavonoid transport across RBE4 cells: A blood-brain barrier model. *Cell Mol. Biol. Lett*. 15, 234241.

FAUSTINO-ROCHA, A. I., FERREIA, R., GAMA, A., OLIVERIA, P. A. & GINJA, M. (2017) Antihistamines as promising drugs in cancer therapy. *Life Sci*. 172, 27–41.

FDA Drug Approval Package, Pharmacological Review (s). Zaditor (ketotifen fumarate) ophthalmic solution. Ciba Vision. Application number: 21-066. Approval date: 07 February 1999.

FERGUSON, P. D., GOODALL, D. M. & LORAN, J. S. (1996) Systematic approach to the treatment of enantiomeric separations in capillary electrophoresis and liquid chromatography III. A binding constant-retention factor relationship and effects of acetonitrile on the chiral separation of tioconazole. *J. Chromatogr. A.* 475, 25–35.

FERREIRA, R., SANTOS, T., GONCALVES, J., BALTAZAR, G., FERREIRA, L., AGASSE, F. & BERNARDINO, L. (2012) Histamine modulates microglia function. *J Neuroinflammation*. 9.

FISHER, H., GOTTSCHLICH, R. & SEELIG, A. (1998) Blood-brain barrier permeation: Molecular parameters governing passive diffusion. *J. Membrane Biol*. 165, 201–211.

FITOS, I., VISY, I. & SIMONYI, M. (2002) Species-dependency in chiral-drug recognition of serum albumin studied by chromatographic methods. *J. Biochem. Bioph. Meth.* 54, 71–84.

FRIDEN, M., BERGSTROM, F., WAN, H., REHNGREN, M., AHLIN, G., HAMMARLUND-UDENAES, M. & BREDBERG, U. (2011) Measurement of unbound drug exposure in

brain: Modeling of pH partitioning explains diverging results between the brain slice and brain homogenate methods. *Drug Metab. Dispos.* 39, 353–362

FRIEDRICH, A., PRASAD, P. D., FREYER, D., GANAPATHY, V. & BRUST, P. (2003) Molecular cloning and functional characterization of the OCTN2 transporter at the RBE4 cells, an *in vitro* model of the blood-brain barrier. *Brain Res.* 968**,** 69–79.

FUJITA, T., IWASA, J. & HANSCA. C. (1964) A new substituent constant, π, derived from partition coefficients. *J. Am. Chem. Soc*. 86, 5175–5180.

GALAON, T. & DAVID, V. (2012) The influence of mobile phase pH on the retention and selectivity of related basic compounds in reversed-phase liquid chromatography. *Rev. Roum. Chim.* 57**,** 131–140.

GALIC, S., SCHNEIDER, H-P., BROER, A., DEITMER, J. W. & BROER, S. (2003) The loop between helix 4 and helix 5 in the monocarboxylate transporter MCT1 is important for substrate selection and protein stability. *Biochem. J*. 376, 413–422.

GALLOIS-BERNOS, A. C. & THURMOND, R. L. (2012) Alcaftadine, a new antihistamine with combined antagonist activity at histamine H_1, H_2 and H_4 receptors. *J. Receptor Ligand Channel Res*. 5, 9–20.

GERALD, G. & MARTIN, G. S. (2000) Recent progress in chiral separation principles in capillary electrophoresis. *Electrophoresis* 21, 4112–4135.

GERSTNER, E. R. & FINE, R. L. (2007) Increased permeability of the blood-brain barrier to chemotherapy in metastatic brain tumors: Establishing a treatment paradigm. *J. Clin. Oncol*. 25, 2306–3212.

GHOSH, C., PUVENNA, V., GONZALEZ-MARTINEZ, J., JANIGRO, D. & MARCHI, N. (2011) Blood-brain barrier P450 enzymes and multidrug transporters in drug resistance: A synergistic role in neurological diseases. *Curr. Drug Metab.* 12, 742–749.

GIACOMINI, K. M., HUANG, S-M., TWEEDIE, D. J., BENETM L. Z., BROUWER, K. L. R., CHU, X., DAHLIN, A., EVERS, R., FISHER, V., HILLGREN, K. M., HOFFMASTER, K. A., ISHIKAWA, T., KEPPLER, D., KIM, R. B., LEE, C. A., NIEMI, M., POLLI, J. W., SUGIYAMA, Y., SWAAN, P. W., WARE, J. A., WRIGHT, S. H., WAHTEE, S., ZAMEK-GLISZCYNSKI, M. J. & ZHANG, L. (2010) Membrane transporters in drug development. *Nature Rev. Drug Discov*. 9, 215–236.

GILLARD, M., VAN DER PERREN, C., MOGUILEVSKY, N., MASSINGHAM, R. & CHATELAIN, P. (2002) Binding characteristics of cetirizine and levocetirizine to

human H1 histamine receptors: Comtribution of Lys^{191} and Thr^{194}. *Mol. Pharmacol.* 61, 391–399.

GONZALEZ-MARISCAL, L., LECHUGA, S. & GARAY, E. (2007) Role of tight junctions in cell proliferation and cancer. *Prog. Histochem. Cytochem.* 42, 1–57.

GRANT, S. M., GOA, K. L., FITTON, A., & SORKIN, E. M. (1990). Ketotifen. A review of its pharmacodynamic and pharmacokinetic properties, and therapeutic use in asthma and allergic disorders. *Drugs* 40, 412–448.

GUMBLETON, M. & AUDUS, K. (2001) Progress and limitations in the use of *in vitro* cell cultures to serve as a permeability screen for the blood-brain barrier. *J. Pharm. Sci.* 90, 1681-1698.

GUNN, R. N. & RABINER, E. A. (2017) Imaging in central nervous system drug discovery. *Semin. Nucl. Med*. 47, 89–98.

GUPTA, A., CHATELAIN, P., MASSINGHAM, R., JONSSON, E. & HAMMARLUND-UDENAES, M. (2006) Brain distribution of certirizine enantiomers: Comparison of three different tissue-to-plasma partition coefficients: K_p, $K_{p,u}$, and $K_{p,uu}$. *Drug Metab. Dispos*. 34, 318–323.

GUPTA, A., GILLAD, M., CHRISTOPHE, B., CHATELAIN, P., MASSINGHAM, R. & HAMMARLUND-UDENAES, M. (2007) Peripheral and central H_1 receptor occupancy by levocetirizine, a non-sedative antihistamine; a time course study in the guinea pig. *Br. J. Pharmacol*. 151, 1129–1136.

GUSTAVO, N-A., RICARDO, M-G., ANA-MARICELA, G-G., GUADALUPE-ELIDE, M-F. & JOSE-ANTONIO, A-M. (2016) The histamine H_3 receptor: Structure, pharmacology and function. *Mol. Pharmacol*. 90, 649–673.

HAAS, A. L., SERGEEVA, O. A. & SELBBACH, O. (2008) Histamine in the nervous system. *Physiol. Rev*. 88, 1183–1241.

HAGENBUCH, B. & MEIER, P. J. (2004) Organic anion transporting polypeptides of the OATP/SLC21 family: Phylogenetic classification as OATP/SLCO superfamily, new nomenclature and molecular/ functional properties. *Pflugers Arch.* 447, 653–665.

HAGOS, Y., BAHN, A., VORMFELDE, S. V., BROCKMOLLER, J. & BURCKHARDT, G. (2007) Torasemide transport by organic anion transporters contributes to hyperuricemia. *J. Am. Soc. Nephrol*. 18, 3101–3109.

HAMMARLUND-UDENAES, M. (2014) *In vivo* approaches to assessing the blood-brain barrier. *Top Med. Chem*. 10, 21–48.

HAMMARLUND-UDENAES, M. (2016) Intracerebral microdialysis in blood-brain barrier drug research with focus on nanodelivery. *Drug Discov. Today Technol*. 20, 13–18.

HASANNEJAD, H., TAKEDA, M., TAKI, K., SHIN, H. J., BABU, E., JUTABHA, P., KHAMDANG, S., ALEBOYEH, M., ONOZATO, M. L., TOJO, A., ENOMOTO, A., ANZAI, N., NARIKAWA, S., HUANG, X. L., NIWA, T & ENDOU, H. (2004) Interactions of human organic anion transporters with diuretics. *J. Pharmacol. Exp. Ther.* 308, 1021–1029.

HASEGAWA, M., KUSUHARA, H., SUGIYAMA, D., ITO, K., UEDA, S., ENDOU, H. & SUGIYAMA, Y. (2002) Functional involvement of rat organic anion transporter 3 (rOat3; Slc22a8) in the renal uptake of organic anions. *J. Pharmacol. Exp. Ther*. 300, 746–753.

HASSAN, Y. ABOUL-ENEIN, I. A. (2003). Chiral separation by liquid chromatography and related technologies. 1st ed, Marcel Dekker Inc., New York.

HE, Y., LIU, Y. & ZENG, S. (2010) Stereoselective and multiple carrier-mediated transport of cetirizine across Caco-2 monolayers with potential drug interaction. *Chirality* 22, 684–692.

HEDIGER, M. A., ROMERO, M. F., PENG, J. B., ROLFS, A., TAKANAGA, H. & BRUFORD, E. A. (2004) The ABCs of solute carriers: Physiological, pathological and therapeutic implications of human membrane transport proteins. *Pflugers. Arch., EJP.* 447, 465–468.

HILL, S. J., GANELLIN, C. R., TIMMERMAN, H., SCHWARTZ, J. C., SHANKLEY, N. P., YOUNG, J. M., SCHUNACK, W., LEVI, R. & HAAS, H. L. (1997) International Union of Pharmacology. XIII. Classification of histamine receptors. *Pharmacol. Rev*. 49, 253–278.

HILL, S. J. & YOUNG, J, M. (1980) Histamine H_1 receptors in the brain of the guinea-pig and the rat: Differences in ligand binding properties and reginal distribution. *Br. J. Pharmac*. 68, 687–696.

HONER, M., GOBBI, L., MARTATELLO, L. & COMLEY, R. A. (2014) Radioligand development for molecular imaging of the central nervous system with positron emission tomography. *Drug Discov. Today*. 19, 1936–1944.

HSU. D. Z., CHU, P. Y., CHEN, S. J. & LIU, M. Y. (2016) Mast cell stabilizer ketotifen inhibits gouty inflammation in rats. *Am. J. Ther*. 23, 1009–1015.

HU, M. & LI, X. (2011) Oral bioavailability. Basic principles, advanced concepts, and applications. John Wiley & Sons, Inc, New Jersey.

HUGHES, C. S., VADEN, S. L., MANAUGH, C. A., PRICE, G. S. & HUDSON, L. C. (1998) Modulation of doxorubicin concentration by cyclosporine A in brain and testicular barrier tissues expressing P-glycoprotein in rats. *J. Neurooncol*. 37, 45–54.

INAGAKI, N., FUKUI, H., TAGUCHI, Y., WANG, N. P., YAMATODANI, A. & WADA, H. (1989) Charaterization of histamine H_1-receptors on astrocytes in primary culture: [^{3}H] mepyramine binding studies. *Eur. J. Pharmacol.* 173, 43–51.

ISHIGURO, N., NOZAWA, T., TSUJIHATA, A., SAITO, A., KISHIMOTO, W., YOKOYAMA, K., YOTSUMOTO, T., SAKAI, K., IGARASHI, T. & TAMAI, I. (2004) Influx and efflux transport of H_1-antagonist epinastine across the blood-brain barrier. *Drug Metab. Dispos.* 32**,** 519–524.

IZUMI, N., MIZUGUCHI, H., UMEHARA, H., OGINO, H. & FUKUI, H. (2008) Evaluation of efficacy and sedative profiles of H_1 antihistamines by large-scale surveillance using the Visual Analogue Scale (VAS). *Allergol. Int.* 57, 257–263.

JEWELL, R. (2007) Ketotifen. *xPharm: The Comprehensive Pharmacology Reference*. 1–5.

JIANG, X., ANDJELKOVIC, A. V., ZHU, L., YANG, T., BENNET, M. L. V., CHEN, J., KEEP, R. F. & SHI. Y. (2018) Blood-brain barrier dysfunction and recovery after ischemic strock. Prog. Neurobiol. 163, 144–171.

JOO, F. & KARNUSHINA, I. (1973) A procedure for the isolation of capillaries from rat brain. *Cytobios.* 8**,** 41–48.

JUN. S., TOMOYUKI, I. & YOSHIO, O. (2014) Synthesis and application of immobilized polysaccharide-based chiral stationary phases for enantioseparation by high-performance liquid chromatography. *J. Chromatogr. A*. 1363, 51–61.

KABRA, S. K., PANDEY, R. M., SINGH, R. & SETH, V. (2000) Ketotifen for asthma in children aged 5 to 15 years: A randomized placebo-controlled trial. *Ann. Allergy Asthma Immunol*. 85, 46–52.

KALIMO, H. (2005) Pathology and genetics: Cerebrovascular diseases. 5th ed. Neuropath. Press, Basel.

KALIVAS, P. W. (1982) Histamine-induced arousal in the conscious and pentobarbital-pretreated rat. *J. Pharm. Exp. Ther*. 222, 37–42.

KALVASS, J. C., POLLO, J. W., BOURDET, D. L., FENG, B., HUANG, S-M., LIU, X., SIMTH, Q. R., ZHANG, L. K. & ZAMEK-GLISZCZYNSKI, M. J. (2013) Why clinical modulation of efflux transporter at the human blood-brain barrier is unlikely: The ITC evidence-based position. *Clin. Pharmacol. Ther*. 94, 80–94.

KANDEL, E. R., SCHWARTZ, J. H. & JESSEL, T. M. (2000) Principles of Neural Science, 4th Ed. McGraw-Hill, New York.

KANG, J., HEART, E. & SUNG, C. K. (2001) Effects of cellular ATP depletion on glucose transport and insulin signaling in 3T3-L1 adipocytes. *Am. J. Physiol. Endocrinol. Metabo.* 280**,** 428–435.

KATO, M., NISHIDA, A., AGA, Y., KITA, J., KUDO, Y., NARITA, H. & ENDO, T. (1997) Pharmacokinetic and pharmacodynamic evaluation of central effect of the novel antiallergic agent betotastine besilate. *Drug Res.* 47, 1116–1124.

KATO, Y., IZUKAWA, T., ODA, S., FUKAMI, T., FINEL, M., YOKOI, T. & NAKAJIMA, M. (2013) Human UDP- glucuronosyltransferase (UGT) 2B10 in drug N-glucuronidation: substrate screening and comparison with UGT1A3 and UGT1A4. *Drug Metab. Dispos*. 4, 11389–1397.

KERDPIN, O., MACKENZIE, P. I., BOWALGAHA, K., FINEL, M. & MINERS, J. O. (2009) Influence of N-terminal domain histidine and proline residues on the substrate selectivities of human UDP-glucuronosyltransferase 1A1, 1A6, 1A9, 2B7 and 2B10. *Drug Metab. Dispos.* 37, 1948–1955.

KHAMDANG, S., TAKEDA, M., SHIMODA, M., NOSHIRO, R., NARIKAWA, S., HUANG, X. L., ENOMOTO, A., PIYACHATURAWAT, P & ENDOU, H. (2004) Interactions of human- and rat-organic anion transporters with pravastatin and cimetidine. *J. Pharmacol. Sci*. 94, 197–202.

KLEIN, C. D. P., TOBETEH, G. F., LAQUNA, A. V., HOLZGRABE, U. & MOHR, K. (2001) Lipophilicity and membrane interactions of cationic-amphiphilic compounds: Syntheses and structure-property relationships. *Eur. J. Pharm. Sci.* 14, 167–175.

KOEPSELL, H. (2013) The SLC22 family with transporters of organic cations, anions and zwitterions. *Mol. Aspects Med*. 34, 413–435.

KOEPSELL, H. & ENDOU, H. (2004) The SLC22 drug transporter family. *Pflugers Arch.* 447, 666–676.

KOEPSELL, H., LIPS, K. S. & VOLK, C. (2007) Polyspecific organic cation transporters: structure, function, physiological roles and biopharmaceutical implications. *Pharm. Res*. 24, 1227–1251.

KONIG, J., NULLER, F. & FROMM, M. F. (2013) Transporters and drug-drug interactions: Important determinants of drug disposition and effects. *Pharmacol. Rev*. 65, 944–966.

KRYSTAL, A. D., RICHELSON, E. & ROTH, T. (2013) Review of the histamine system and the clinical effects of H_1 antagonists: Basis for a new model for understanding the effects of insomnia medications. *Sleep Med. Rev*. 17, 263–272.

KUSUHARA, H., MIURA, M., YASUI-FURUKORI, N., YOSHIDA, K., AKAMINE, Y., YOKOCHI, M., FUKIZAWA, S., IKEJIRI, K., KANAMITSU, K., UNO, T. & SUGITAMA, Y. (2013) Effect of coadministration of single and multiple doses of rifampicin on the pharmacokinetics of fexofenadine enantiomers in healthy subjects. *Drug Metab. Dispos.* 41, 206–213.

KUSUHARA, H., SEKINE, T., UTSUNOMIYA-TATE, N., TSUDA, M., KOJIMA, R., CHA, S. H., SUGIYAMA, Y., KANAI, Y. & ENDOU, H. (1999) Molecular cloning and characterization of a new multispecific organic anion transporter from rat brain. *J. Biol. Chem*. 274, 13675–13680.

KUSUHARA, H. & SUGIYAMA, Y. (2005) Active efflux across the blood-brain barrier: Role of the solute carrier family. *Neurotherapeutics* 2, 73–85.

KVETA, K., TEREZA, S., JIRI, V. & EVA, T. (2014) Suppercritical fluid chromatography as a tool for enantioselective separation: A review. *Anal. Chim. Acta* 821, 1–33.

LAI, L. & TAN, T. M. (2002) Role of glutathione in the multidrug resistance protein 4 (MRP4/ABCC4)-mediated efflux of cAMP and resistance to purine analogues. *Biochem. J.* 361, 497–503.

LAI, Y. (2013) Transporters in Drug Discovery and Development. Detailed Concepts and Best Practice. Woodhead Publishing. Cambridge, UK.

LAMMERHOFER, M. (2010) Chiral recognition by enantioselective liquid chromatography: Mechanisms and modern chiral stationary phases. *J. Chromatogr. A.* 1217**,** 814–56.

LE BIGOT, J. F., BEGUE, J. M., KIECHEL, J. R. & GUILLOUZO, A. (1987). Species differences in metabolism of ketotifen in rat, rabbit and man: Demonstration of similar pathways *in vivo* and in cultured hepatocytes. *Life Sci*. 40, 883–890.

LE BIGOT, J. F., CRESTEIL, T., KIECHEL, J. R. & BEAUNE, P. (1983) Metabolism of ketotifen by human liver microsomes. *In vitro* characterization of a tertiary amine glucuronidation. *Drug Metab. Dispos.* 11**,** 585–589.

LEE, G., BABAKHANIAN, K., RAMASWAMY, M., PRAT, A., WOSIK, K. & BENDAYAN, R. (2007) Expression of the ATP-binding cassette membrane transporter, ABCG2, in human and rodent brain microvessel endothelial and glial cell culture systems. *Pharm. Res.* 24**,** 1262–74.

LEGGAS, M., ADACHI, M., SCHEFFER, G. L., SUN, D., WIELINGA, P., DU, G., MERCER, K. E., ZHUANG, Y., PANETTA, J. C., JOHNSTON, B., SCHEPER, R. J., STWART, C. F. & SCHUETZ, J. D. (2004). MRP4 confers resistance to topotecan and protects the brain from chemotherapy. *Mol. Cell. Biol.* 24, 7612–7621.

LEURS, R., BAKKER, R. A., TIMMERMAN, H. & DE ESCH, I. J. (2005) The histamine H_3 receptors: From gene cloning to H_3 receptor drugs. *Nat. Rev. Drug Discov*. 4, 107–118.

LEURS, R., VISCHER, H. F., WIJTMANS, M. & DE ESCH, I, J. P. (2011) En route to new blockbuster anti-histamines: Surveying the offspring of the expanding histamine receptor family. *Trends. Pharmacol. Sci.* 32, 250–257.

LI, D., FOURNEL-GIGLEUX, S., BARRE, L., MULLIERT, G., NETTER, P., MAGDALOU, J. & OUZZINE, M. (2007). Identification of aspartic acid and histidine residues mediating the reaction mechanism and the substrate specificity of the human UDP- glucuronosyltransferases 1A. *J. Biol. Chem.* 282, 36514–36524.

LI, D., UMLAND, J. P., CHANG, G., HUANG, Y., LIN, Z., SCOTT, D. O., TROUTMAN, M. D. & LISTON, T. E. (2011) Species independence in brain tissue binding using brain homogenates. *Drug Metabo. Dispos*. 30, 1270–1277.

LIN, J. S., SAKAI, K. & JOUVET, M. (1994) Hypothalamo-preoptic histaminergic projections in sleep-wake control in the cat. *Eur. J. Pharmacol*. 6, 618–625.

LING, P., NGO, K., NGUYEN, S., THURMOND, R. L., EDWARDS, J. P., KARLSSON, L. & FUNG-LEUNG, W-P. (2004) Histamine H_4 receptor mediates eosinophil chemotaxis with cell shape change and adhesion molecule upregulation. *Br. J. Pharmacol*. 142, 167–171.

LINNET, K. & EJSING, T. B. (2008) A review on the impact of P-glycoprotein on the penetration of drugs into the brain. Focus on psychotropic drugs. *Eur. Neuropsychopharmacol.* 18, 157–169.

LO, E. H., SINGHAL, A. B., TORCHILIN, V. P. & ABBOTT, N. J. (2001) Drug delivery to damaged brain. *Brain Res. Rev*. 38, 140–148.

LOE, D. W., DEELEY, R. G. & COLE, S. P. C. (1996). Biology of the multidrug resistance-associated protein, MRP. *Eur. J. Cancer* 32, 945–957.

LOHMANN, S., HUWEL, S. & GALLA, H. J. (2002) Predicting blood-brain barrier permeability of drugs: Evaluation of different *in vitro* assays. *J. Drug Target*. 10, 263–276.

LOPEZ-NIETO, C. E., YOU, G., BUSH, K. T., BARROS, E. J., BEIER, D. R. & NIGAM, S. K. (1997) Molecular cloning and characterization of NKT, a gene product related to the organic cation transporter family that is almost exclusively expressed in the kidney. *J. Biol. Chem*. 272, 6471–6478.

LU, H. (2007). Stereoselectivity in drug metabolism. *Expert. Opin. Drug Metab. Toxicol. 3*, 149–158.

LUO, T. & LEUNG, L. S. (2009) Basal forebrain histaminergic transmission modulate electroencephalographic activity and emergence from isoflurane anaesthesia. *Anaesthesia 111,* 725–733*.*

LUTKA, A. & GOLDA, B. (2006) The effect of pH on cyclodextrin complexation of trifluoperazine. *Acta Pol. Pharm*. 63, 3–8.

MAHDY, A. M. & WEBSTER, N. R. (2014) Histamine and antihistamines. *Anaesth. Intens. Care Med*. 15, 250–255.

MAKRIDES, V., BAUER, R., WEBER, W., WESTER, H-J., DISHER, S., HINZ, R., HUGGEL, K., OPFERMANN, T., HERZAU, M., GANAPATHY, V., VERRRY, F. & BRUST, P. (2007) Preferred transport of O-(2-[^{18}F]fluoroethyl)-D-tyrosine (D-FET) into the porcine brain. *Brain Res.* 1147, 25–33.

MALANY, S., HERNANDEZ, L. M., SMITH, W. F., CROWE, P. D. & HOARE, S. R. J. (2009) Analytical method for simultaneously measuring *ex vivo* drug receptor occupancy and dissociation rate: Application to (R)-dimethindene occupancy of histamine H_1 receptors. *J. Recept. Sig. Transd*. 29, 84–93.

MALGORZATA, D. & ALINA, R. (2014) Application of TLC, HPLC and GC methods to the study of amino acida and peptide enantiomers: A review. *Biomed. Chromatogr.* 28, 84–101.

MANDEL, L. J., DOCTOR, R. B. & BACALLAO, R. (1994) ATP depletion: A novel method to study junctional properties in epithelial tissues. II. Internalization of Na+,K(+)-ATPase and E-cadherin. *J. Cell Sci.* 107**,** 3315–3324.

MANN, R. & ANDREWS, E. (2007) Pharmacovigilance*. 2nd ed*. John Wiley & Sons, Chichester.

MARTINEZ-GOMEZ, M. A., VILLANUEVA-CAMANAS, R. M., SAGRADO, S. & MEDINA-HERNANDEZ, M. J. (2007) Evaluation of enantioselective binding of antihistamines to human serum albumin by ACE. *Electrophoresis* 28, 2635–2643.

MATSUSHIMA, S., MEADA, K., KONDO, C., HIRANO, M., SASAKI, M., SUZULI, H. & SUGIYAMA, Y. (2005) Identification of the hepatic efflux transporters of orgainc anions using double-transfected Madin-Darby canine kidney II cells expressing human organic anion-transporting polypeptide 1B1 (OATP1B1)/multidrug resistance-associated protein 2, OATP1B1/multidrug resistance 1, and OATP1B1/breast cancer resistance protein. *J. Pharmacol. Exp. Ther*. 314, 1059–1067.

MAURER, T. S., DEBARTOLO, D. B., TESS, D. A. & SCOTT, D. O. (2005) Relationship between exposure and nonspecific binding of thirth-three central nervous system drugs in mice. *Drug Metab. Dispos.* 33, 175–181.

MCALLISTER, A. S., KRIZANAC-BENGEZ, L., MACCHIA, F., NAFTALI, R. J., PEDLEY, K. C., MAYBERG, M. R., MARRONI, M., LEAMAN, S., STANNESS, K. A. & JANIGRO, D. (2001) Mechanisms of glucose transporter at the blood-brain barrier: An *in vitro* study. *Brain Res*. 409, 20–30.

MCDONALD, K., TRICK, L. & BOYLE, J. (2008) Sedation and antihistamines: An update. Review of inter-drug differences using proportional impairment ratios. *Hum. Psychopharmacol*. 23, 555–570.

MELANDER, E., ERIKSSON, C., JANSSON, B., GORANSSON, U. & HAMMARLUND-UDENAES, M. (2016) Improved method for quantitative analysis of the cyclotide kalata B1 in plasma and brain homogenate. *Pept. Sci*. 106: 910–916.

MESSER, W. S. JR., NGUR, D. O., ABUH, Y. F., DOKAS, L. A., TING, S. M., HACKSELL, U., NILSSON, B. M., DUNBAR, P. G. & HOSS, W. (1992) Stereoselective binding and activity of oxotremorine analogs at muscarinic receptors in rat brain. *Chirality* 4, 463–468.

MEY, U., WACHSMUTH, H. & BREYER-PFAFF, U. (1999) Conjugation of the enantiomers of ketotifen to four isomeric quaternary ammonium glucuronides in humans *in vivo* and in liver microsomes. *Drug Metab. Dispos.* 27**,** 1281–1292.

MICHAEL, S., MARKUS, F. & VOLKER, S. (1994) Enantiomer separation by capillary SFC and GC on chiral-nickel: Observation of unusual peak broadening phenomena. *Anal. Chem.* 66, 2893–2897.

MIDZYANOVSKAYA, I. S., BIRIOUKOVA, L. M., SHATSKOVA, A. B., VAN LUIJTELAAR, G. & TUOMISTO, L. M. (2016) H_1 histamine receptor densities are increased in brain regions of rats with genetically generalized epilepsies. *Epilepsy. Res*. 127, 135–140.

MILNER, E., SOUSA, J., PYBUS, B., AUSCHWITZ, J., CARIDHA, D., GARDNER, S., GRAUER, K., HARRIS, E., HICKMAN, M., KOZAR, M. P., LEE, P., LEED, S., LI, Q., MELENDEZ, V., MOON, J., NGUNDAM, F., O'NEIL, M., PARRIOTT, S., POTTER, B., SCIOTTI, R., TANGTEUNG, A. & DOW, G. S. (2012) Ketotifen is an antimalarial prodrug of norketotifen with blood schizonticidal and liver-stage efficacy. *Eur. J. Drug Metab. Pharmacokinet*. 37, 17–22.

MIURA, M. & UNO, T. (2010) Clinical pharmacokinetics of fexofenadine enantiomers. *Expert Opin. Drug Metab. Toxicol*. 6, 69–74.

MIURA, M., UNO, T., TATEISHI, T. & SUZUKI, T. (2007) Pharmacokinetics of fexofenadine enantiomers in healthy subjects. *Chirality* 19, 223–227.

MOGUILEVSKY, N., VARSOLONA, F., NOYER, M., GILLARD, M., GUILLAUME, J. P., GARCIA, L., SZPIRER, C., SZPIRER, G. & BOLLEN, A. (1994) Stable expression of human H_1 histamine receptor cDNA in Chinese hamster ovary cells. *Eur. J. Biochem*. 224, 489–495.

MONNIER, M., SAUER, R. & HATT, A. M. (1970) The activation effect of histamine on the central nervous system*. Int. Rev. Neurobiol.* 12, 265–305.

MONTI, J. M. (1993) Involvement of histamine in the control of the waking state. *Life Sci.* 53, 1331–1338.

MONTI, J. M., JANTOS, H., LESCHKE, C., ELZ, S. & SCHUNACK, W. (1994) The selective histamine H_1-receptor agonist 2-(3-trifluoromethylphenyl) histamine increases waking in rat. *Eur. Neuropsychopharmacol*. 4, 459–462.

MONTI, J. M., ORELLANA, C., BOUSSARD, M., JANTOS, H. & OLIVERA, S. (1990) Sleep variables are unaltered by zolantidine in rats: Are histamine H_2-receptors not involved in sleep regulation? *Brain Res. Bull*. 25, 229–231.

MONTI, J. M., PELLEJERO, T. & JANTOS, H. (1986) Effects if H_1- and H_2- hisamine receptor agonists and antagonists on sleep and wakefulness in rats. *J. Neural. Transm*. 66, 1–11.

MORGEN, M. E., SINGHAL, D. & ANDERSON, B. D. (1996) Quantitative assessment of blood-brain barrier damage during microdialysis. *J. Pharm. Exp. Ther*. 277, 1167–1176.

MULLER-GARTNER, H. W., WILSON, A. A., DANNALS, R. F., WAGNER JR., H. N. & FROST, J. J. (1992) Imaging muscarinic cholinergic receptors in human brain *in vivo* with SPECT, [^{123}I]4-iododexetimide, and [^{123}I]4-iodolevetimide. *J. Cereb. Blood Flow Metab.* 12, 562–570.

NAIK, P. & CUCULLO, L. (2012) *In vitro* blood–brain barrier models: Current and perspective technologies. *J. Pharm. Sci.* 101**,** 1337–1354.

NAKAGAWA, S., DELI, M.A., KAWAHUCHI, H., SHIMIZUDANI, T., SHIMONO, T., KITTEL, A., TANAKA, K. & NIWA, M. (2009) A new blood-brain barrier model using primary rat brain endothelial cells, pericyte and astrocytes. *Neurochem. Int*. 54, 253–263.

NIES, A. T., KOEPSELL, H., DAMME, K. & SCHWAB, M. (2011) Organic cation transporters (OCTs, MATEs), *in vitro* and *in vivo* evidence for the importance in drug therapy. *Handb. Exp. Pharmacol*. 201, 105–167.

NNANE, I. P., DAMANI, L. A. & HUTT, A. J. (1998) Development and validation of stability indicating high-performance liquid chromatographic assays for ketotifen in aqueous and silicon oil formulations. *Chromatographia* 48**,** 797–802.

OLA, A. S., AIDA, A. E., AMR, M. B. & HASSAN Y. A. (2010) A validated HPLC method for separation and determination of epinastine hydrochloride enantiomers. *J. Liq. Chromatogr. Relat. Technol.* 33, 413–422.

ONODERA, K., YAMATODANI, A., WATANABE, T. & WADA, H. (1994) Neuropharmacology of the histaminergic neuron system in the brain and its relationship with behavioral disorders. *Prog. Neurobiol*. 42, 685–702.

ORCHIN, M., MACOMBER, R. S., PINHAS, A. R. & WILSON, R. M. (2005) The vocabulary and concepts of organic chemistry. 2nd ed. John Wiley & Sons, New Jersey.

OSTROWSKI, N. L., BURKE JR, T. R., RICE, K. C., PERT, A. & PERT, C. B. (1987) The pattern of [^{3}H]cyclofoxy retention in rat brain after *in vivo* injection corresponds to the *in vitro* opiate receptor distribution. *Brain Res.* 402, 275–286.

PALACIOS, J. M., WAMSLEY, J. K. & KUHAR, M. J. (1981) The distribution of histamine H_1-receptors in the rat brain: An autoradiographic study. *Neuroscience* 6, 15–37.

PANDEY, P. K., SHARMA, A. K. & GUPTA, U. (2016) Blood brain barrier: An overview on strategies in drug delivery, realistic *in vitro* modeling and *in vivo* live tracking. *Tissue Barriers*. 4, 1.

PARDRIDGE, W. M. (1993) Brain drug delivery and blood-brain barrier transport. *Drug Deliv*. 83–101.

PARDRIDGE, W. M. (1995) Transport of small molecules through the blood-brain barrier: Biology and methodology. *Adv. Drug Deliv. Rev*. 5, 5–36.

PARDRIDGE, W. M. (2002) Drug and gene delivery to the brain: The vascular route. *Neuron* 36, 555–558.

PARDRIDGE, W. M. (2005) The blood-brain barrier: Bottleneck in brain drug development. *Neuro. Rx.* 2, 3–14.

PARDRIDGE, W. M. (2016) CSF, blood-brain barrier, and brain drug delivery. *Expert Opin. Drug Deliv*. 13, 963–975.

PARDRIDGE, W. M., SAKIYAMA, R. & FIERER, G. (1983) Transport od propranolol and lidocaine through the rat blood-brain barrier. Primary role of globulin-bound drug. *J. Clin. Invest. 71*, 900908.

PATLAK, C. S., BLASBERG, R. G. & FENSTERMACHER, J. D. (1983) Graphical evaluation of blood-to-brain transfer constants from multiple-time uptake data. *J. Cereb. Blood Flow Metab*. 3, 1–7.

PERRIN, D. D., DEMPSEY, B. & SERJEANT, E. P. (1981) pKa Prediction for organic Acids and bases, 1st ed, Chapman & Hall.

PIONTEC, J., WINKLER, L., WOLBURG, H., MULLER, S. L., ZULEGER, N., PIEHL, C., WIESNER, B., KRAUSE, G. & BLASING, I. E. (2008) Formation of tight junctions: Determination of homophilic interaction between classic claudins. *FASEB. J*. 22, 146–158.

PISTOLOZZI, M. & BERTUCCI, C. (2008) Species-dependent stereoselective drug binding to albumin: A circular dichroism study. *Chirality* 20, 552–558.

PLEMPER VAN BALEN, G., MARCA MARTINET, C., CARON, G., BOUCHARD, G., REIST, M., CARRUPT, P-A., FRUTTERO, R., GASCO, A. & TESTA, B. (2004) Liposome/water lipophilicity: Methods, information content, and pharmaceutical applications. *Med. Res. Rev.* 24, 299–324.

POTSCHKA, H., FEDROWITZ, M. & LASCHER, W. (2003) Multidrug resistance protein MRP2 contributes to blood-brain barrier function and restricts antiepileptic drug activity. *J. Pharm. Exp. Ther.* 306, 124–131.

PRELOG, V. & HELMCHEN, G. (1982) Basic principles of the CIP-system and proposal for a revision. *Angew. Chem. Int. Ed. Engl*. 21, 567–583.

RAMESH, V., THAKKAR, M. M., STRECKER, R. E., BASHEER, R. & MCCARLEY, R. W. (2004) Wakefulness-inducing effects of histamine in the basal forebrain of freely moving rats. *Behav. Brain Res*. 152, 271–278.

REDZIC, Z. & SEGAL, M. (2004) The structure of the choroid plexus and the physiology of the choroid plexus epithelium. *Adv. Drug Deliv. Rev*. 56, 1695–1716.

REESE, T. S. & KARNOVSKY, M. J. (1967) Fine structural localization of a blood-brain barrier to exogenous peroxidase. *J. Cell Biol*. 34, 207–217.

REGINA, A., KOMAN, A., PICIOTTI, M., EL HAFNY, B., CENTER, M. S., BERGMANN, R., COURAUD, P. O. & ROUX, F. (1998) Mrp1 multidrug resistance-associated protein and P-glycoprotein expression in rat brain microvessel endothelial cells. *J. Neurochem.* 71**,** 705–715.

REGINA, A., MORCHOISNE, S., BORSON, N. D., MCCALL, A. L., DREWES, L. R. & ROUX, F. (2001) Factor(s) released by glucose-deprived astrocytes enhance glucose transporter expression and activity in rat brain endothelial cells. *Biochim. Biophys. Acta* 26**,** 233–242.

REGINA, A., ROUX, F. & REVEST, P. A. (1997) Glucose transport in immortalized rat brain capillary endothelial cells *in vitro*: Transport activity and GLUT1 expression. *Biochim. Biophys. Acta* 17**,** 1–2.

REICHEL, A., ABBOTT, N. J. & BEGLEY, D. J. (2002) Evaluation of the RBE4 cell line to explore carrier-mediated drug delivery to the CNS via the L-system amino acid transporter at the blood-brain barrier. *J. Drug Target.* 10**,** 277–283.

REID, G., WIELINGA, P., ZELCER, N., DE HAAS, M., VAN DEEMTER, L., WIJINHOLDS, J., BALARINI, J. & BORST, P. (2003) Characterization of the transport of nucleoside

analog drugs by the human multidrug resistance proteins MRP4 and MRP5. *Mol. Pharmacol.* 63, 1094–1103**.**

REVEL, F., GOTTOWIK, J., GATTI, S., WETTSTEIN, J, G. &MOREAU, J-L. (2009) Rodent models of insomnia: A review of experimental procedures that induce sleep disturbances. *Neurosci. Biobehav. Rev*. 33, 874–899.

RIST, R. J., ROMERO, I. A., CHAN, M. W. K., COURAUD, P-O., ROUX, F. O. & ABBOTT, N. J. (1997) F-Actin cytoskeleton and sucrose permeability of immortalised rat brain microvascular endothelial cell monolayers: Effects of cyclic AMP and astrocytic factors. *Brain Res.* 768**,** 10–18.

RODRIGUES, A. C., CURI, R., GENVIGIR, F. D. V., HIRATA, M. H. & HIRATA, R. D. C. (2009) The expression of efflux and uptake transporters are regulated by stains in Caco-2 and HepG2 cells. *Acta Pharmacol. Sin.* 30, 956–964.

ROJAS-ZAMORANO, J. A., ESQUEDA-LEON, E., JIMENEZ-ANGUIANO, A., CINTRA-MCGLONE, L., MENDOZA MELENDEZ, M. A. & VELAZQUEZ MOCTEZUMA, J. (2009) The H_1 histamine receptor blocker, chlopheniramine, completely prevent the increase in REM sleep induced by immobilization distress in rats. *Pharmacol. Biochem. Behav*. 91, 291–294.

ROUX, F. & COURAUD, P-O. (2005) Rat brain endothelial cell lines for the study of blood- brain barrier permeability and transport functions. *Cell. Mol. Neurobiol.* 25**,** 41–57.

ROUX, F., DURIEU-TRAUTMANN, O., CHAVEROT, N., CLAIRE, M., MAILLY, P., BOURRE, J. M., STROSBERG, A. D. & COURAUD, P. O. (1994) Regulation of gamma-glutamyl transpeptidase and alkaline phosphatase activities in immortalized rat brain microvessel endothelial cells. *J. Cell Physiol,* 159**,** 101–113.

SAKUGAWA, T., MIURA, M., HOKAMA, N., SUZUKI, T., TATEISHI, T. & UNO, T. (2009) Enantioselective disposition of fexofenadine with the P-glycoprotein inhibitor. *Br. J. Clin. Pharmacol*. 67, 535–540.

SALVATORE, F. (2009) Chiral separation by CE employing CDs. *Electrophoresis* 30, S203–210.

SANDSTORM, D. J. & NASH, H. (2004) Drug target: Turning the channel (on) for sedation. Curr. Biol. 9, 185–186.

SASTRY, B. S. R. & PHILLIS, J. W. (1976) Depression of rat cerebral cortical neurones by H_1 and H_2 histamine receptor agonists. *Eur. J. Pharmacol*. 38, 269–273.

SCHINKEL, A. H. (1999) P-glycoprotein, a gatekeeper in the blood-brain barrier. *Adv. Drug Deliv. Rev*. 36, 179–194.

SCHLAGETER, K., MOLNAR, P., LAPIN, G. & GROOTHUIS, D. (1999) Microvessel organization and structure in experimental brain tumors: Microvessel populations with distinctive structural and functional properties. *Microvasc. Res*. 58, 312–328.

SCHUETZ, J. D., CONNELLY, M. C., SUN, D., PAIBIR, S. G., FLYNN, P. M., SRINIVAS, R. V., KUMAR, A. & FRIDLAND, A. (1999) MRP4: A previously unidentified factor in resistance to nucleoside-based antiviral drugs. *Nat. Med.* 5, 1048–1051.

SCHURIG. V. (1994) Enantiomer separation by gas chromatography on chiral stationary phases. *J. Chromatogr. A*. 666, 111–129.

SEKINE, T., WATANABE, N., HOSOYAMADA, M., KANAI, Y. & ENDOU, H. (1997) Expression cloning and characterization of a novel multispecific organic anion transporter. *J. Biol. Chem*. 272, 18526–18529.

SEIFERT, R., WENZEL-SEIFERT, K., BURCKSTUMMER, T., PERTZ, H. H., SCHUNACK, W., DOVE, S., BUSCHAUER, A. & ELZ, S. (2003) Multiple differences in agonist and antagonist pharmacology between human and guinea pig histamine H1 receptor. *J. Pharmacol. Exp. Ther*. 305, 1104–1115.

SHAMSI, Z. & HINDMARCH, I. (2000) Sedation and antihistamines: A review of inter-drug differences using proportional impairment ratios. *Hum. Psychopharmacol.* 15, S3–30.

SHARIF, N. A., SU, S. X. & YANNI, J. M. (1994) Emedastine: A potent, high affinity histamine H_1-receptor-selective antagonist for ocular use: Receptor binding and second messenger study. *J. Ocul. Pharmacol.* 10, 653–664.

SHAWAHNA, R., UCHIDA, Y., DECLEVED, X., OHTSUKI, S., YOUSIF, S., DAUCHY, S., JACOB, A., CHASSOUX, F., DAUMAS-DUPORT, C., COURAUS, P-O., TERASAKI, T. & SCHERRMANN, J-M. (2011) Transcriptomic and quantitative proteomic analysis of transporters and drug metabolizing enzymes in fresh isolated human brain microvessels. *Mol. Pharmaceutics* 8, 1332–1341.

SHEN, S., HE, Y. & ZENG, S. (2007) Stereoselective regulation of MDR1 expression in Caco-2 cells by cetirizine enantiomers. *Chirality* 19, 485–490.

SHEN, Q., WANF, L., ZHOU, H., JIANG, H., YU, L. & ZENG, S. (2013) Stereoselective binding of chiral drugs to plasma proteins. *Acta Pharmacol. Sin.* 34, 998–1006.

SHIGEMOTO, Y., FUJII, Y., SHINOMIYA, K. & KAMEI, C. (2004a) Participation of histaminergic H_1 and noradrenergic α_1 receptors in orexin A-induced wakefulness in rats. *Brain Res*. 1023, 121–125.

SHIGEMOTO, Y., SHINOMIYA, K., MIO, M., AZUMA, N. & KAMEI, C. (2004b) Effects of second-generation histamine H_1 receptor antagonists on the sleep-wakefulness cycle in rats. *Eur. J. Pharmacol*. 494, 161–165.

SHIMAMURA, T., SHIROISHI, M., WEYAND, S., TSUJIMOTO, H., WINTER, G., KATRITCH, V., ABAGYAN, R., CHEREZOV, V., LIU, W., HAN, G. W., KOBAYASHI, T., STEVENS, R. C. & IWATA, S. (2011) Structure of the human histamine H_1 receptor complex with doxepin. *Nature* 475, 65–70.

SHIMIZU, F., SANO, Y., BAEDA, T., ABE, M. A., NAKAYAMA, H., TAKAHASHI, R., UEDA, M., OHTSUKI, S., TERASAKI, T., OBINATA, M. & KANDA, T. (2008) Peripheral nerve pericytes originating from the blood-nerve barrier expresses tight junctional molecules and transporters as barrier-forming cells. *J. Cell Physiol*. 217, 388–399.

SHOCKLEY, R. P. AND LAMANNA, J. C. (1988) Determination of rat cerebral cortical blood volume changes by capillary mean transit time analysis during hypoxia, hypercapnia and hyperventilation. *Brain Res.* 454, 170–178.

SIAN, E. E. & BARBARA, K. H. (2014) Application of chiral chromatography coupled with mass spectrometry in the analysis of chiral pharmaceuticals in the environment. *Trends Anal. Chem*. 1, 34–51.

SIMONS, R. F. & SIMONS, J. K. (2008) H_1-antihistamines. *World Allergy Organ. J*. 145–155.

SIMONS, R. F. & SIMONS, J. K. (2011) Histamine and H_1-antihistamines: Celebrating a century of progress. *J. Allergy Clin. Immunol*. 6, 1139–1150.

SMITH, D. F. & JAKOBSEN, S. (2007) Stereoselective neuroimaging *in vivo*. *Eur. Neuropsychopharmacol*. 17, 507–522.

SMITH, D. F., MARTHI, K., MUNK, O. L., CUMMING, P., HANSEN, S. B. & JAKOBSEN, S. (2006) PET neuroimaging of [^{11}C]mirtazapine enantiomers in pigs. *Eur. Neuropsychopharmacol*. 16, 350–357.

SMITH, S. W. (2009) Chiral toxicology: It's the same thing only different. *Toxicol. Sci*. 110, 4–30.

SMITH, Q. R. (2003) A Review of blood-brain transport techniques. *Methods Mol. Med*. 89, 193–208.

SIMTH, Q. R. & ALLEN, D. (2003) In situ brain perfusion technique.*Methods Mol. Med*. 89, 209–218.

SOKOL, K. C., AMAR, N. K., STARKEY, J. & GRANT, J. A. (2013) Ketotifen in the management of chronic urticaria: Resurrection of an old drug. *Ann. Allergy Asthma Immunol*. 111, 433–436.

SOLOMONS, G., FYHLE, C. & SNYDER, S. (2012) Organic chemistry. 11th ed John Wiley & Sons. USA.

STALCUP, A. M., CHANG, S-C. & ARMSTRONG, D. W. (1991) Effect of the configuration of the substituents of derivatized β-cyclodextrin bonded phases on enantioselectivity in normal-phase liquid chromatography. *J. Chromatogr. A.* 540**,** 113–128.

STEWART, J. C. M. (1980) Colorimetric determination of phospholipids with ammonium ferrothiocyanate. *Anal. Biochem*. 104, 10–14.

STOJKOVIC, N., CEKIC, S., RISTOV, M., RISTIC, M., DUKIC, D., BINIC, M& VIRIJEVIC, D. (2015) Histamine and antihistamines. *Acta*. *Fac. Med. Naiss*. 32, 7–22.

SUN, H. & PANG, K. S. (2008) Permeability, transporter, and metabolism of solutes in Caco-2 cell monolayers: A theoretical study. *Drug Metab. Dispos.* 36, 102–123.

SUZUKI, T., OHMURO, A., MIYATA, M., FURUISHI, T., HIDAKA, S., KUGAWA, F., FUKAMI, T. & TOMONO, K. (2010) Involvement of an influx transporter in the blood–brain barrier transport of naloxone. *Biopharm. Drug Dispos.* 31**,** 243–252.

SWEET, D. H., NILLER, D. S., PRITCHARD, J. B., FUJIWARA, Y., BERIER, D. R. & NIHAM, S. K. (2002) Impaired organic anion transport in kidney and choroid plexus of organic anion transporter 3 (Oat3 (Slc22a8)) knockout mice. *J. Biol. Chem.* 277, 26934–26943.

SZABOLCS, F., JULIE, S., JEAN-LUC, V. & DAVY, G. (2014) Current and future trends in UHPLC. *Trends Anal. Chem.* 63, 2–13.

TAGAWA, M., KANO, M., OKAMURA, N., HIGUVHI, M., MATSUDA, M., MIZUKI, Y., ARAI, H., IWATA, R., FUJII, T., KOMEMUSHI, S., IDO, T., ITOH, M., SASAKI, H., WATANABE, T. & YANAI, K. (2001) Neuroimaging of histamine H_1-receptor occupancy in human brain by positron emission tomography (PET): A comparative study of ebastine, a second-generation antihistamine, and (+)-chlorpheniramine, a classical antihistamine. *Br. J. Clin. Phamacol*. 52, 501–509.

TAKASHIMA, T., TAMURA, G., YAMAUCHI, T. & MIYAMOTO, T. & SHIDA, T. (1992) Clinical study of WAL 801 CL (epinastine) on adult bronchial asthma-multicenter double blind controlled study versus ketotifen fumarate. *J. Clin. Ther. Med.* 8, 169–197.

TAKEDA, M., KHAMDANG, S., NARIKAWA, S., KIMURA, H., HOSOYAMADA, M., CHA, S. H., SEKINE, T. & ENDOU, H. (2002) Characterization of methotrexate transport and its drug interactions with human organic anion transporters. *J. Pharmacol. Exp. Ther*. 302, 666–671.

TAMAI, I. (2013) Pharmacological and pathophysiological roles of carnitine/organic cation transporters (OCTNs: SLC22A4, SLC22A5 and Slc22a 21). *Biopharm. Drug Dispos.* 34, 29–44.

TAMAI, I. & TSUJI, A. (2000) Transporter-mediated permeation of drugs across the blood-brain barrier. *J. Pharma*. *Sci.* 89, 1371–1388.

TANAKA, H. & MIZOJIRI, K. (1998) Drug-protein bindinf and blood-brain barrier permeability. *J. Pharmacol. Exp. Ther*. 288, 912□918.

TASAKA, K., CHUNG, Y. H., SAWADA, K. & MIO, M. (1988) Excitatory effect of histamine on the arousal system and its inhibition by H_1 blockers. *Brain Res. Bull*. 22, 271–275.

TASHIRO, M., DUAN, X., KATO, M., MIYAKE, M., WATANUKI, S., ISHIKAWA, Y., FUNAKI, Y., IWATA, R., ITOH, M. & YANAI, K. (2008) Brain histamine H_1 receptor occupancy of orally administered antihistamines, bepotastine and diphenhydramine, measured by PET with ^{11}C-doxepin. *Br. J. Clin. Pharmacol*. 65, 811–821.

TASHIRO, M., MOCHIZUKI, H., IWABUCHI, K., SAKURADA, Y., ITOH, M., WATANABE, T. & YANAI, K. (2002) Roles of histamine regulation of arousal and cognition: Functional neuroimaging of histamine H_1 receptors in human brain. *Life Sci*. 72, 409–414.

TASHIRO, M., MOCHIZULI, H., SAKURADA, Y., ISHII, K., ODA, K., KIMURA, Y., SASAKI, T., ISHWATA, K. & YANAI, K. (2005) Brain histamine H_1 receptor occupancy of orally administered antihistamines measured by positron emission tomography with ^{11}C-doxepin in a placebo-controlled crossover study design in healthy subjects: A comparison of olopatadine and ketotifen. *Br. J. Clin. Pharmacol*. 61, 16–26.

TATEISHI, T., MIURA, M., SUZUKI, T. & UNO, T. (2008) The different effects of itraconazole on the pharmacokinetics of fexofenadine enantiomers. *Br. J. Clin. Pharmacol*. 65, 693–700.

TAO-CHENG, J-H., NAGY, Z. & BRIGHTMAN, M. W. (1987) Tight junctions of brain endothelium *in vitro* are enhanced by astroglia. *J. Neurosci*. 7, 3293–3299.

TER LAAK, A. M., DONNE-OP DER KELDER, G. M., BAST, A. & TIMMERMAN, H. (1993) Is there a difference in the affinity of histamine H_1 receptor antagonists for CNS and peripheral receptors? An *in vitro* study. *Eur. J. Pharmacol*. 232, 199–205.

TESTA, B., VISTOLI, G. & PEDRETTI, A. (2016) Mechanisms and pharmaceutical consequences of processes of stereoisomerisztion – A didactic excursion. *Eur. J. Pharm. Sci.* 88, 101–123.

THAKKAR, M. M. (2011) Histamine in the regulation of wakefulness. *Sleep Med. Rev*. 15, 65–74.

TOGAMI, K., TOSAKI, Y., CHONO, S., MORIMOTO, K., HAYASAKA, M. & TADA, H. (2013) Enantioselective uptake of fexofenadine by Caco-2 cells as model intestinal epithelial cells. *J. Pharm. Pharmacol.* 65**,** 22–29.

TOKUNAGA, S., TAKEDA, Y., SHINOMIYA, K., HIRASE, M. & KAMEI, C. (2007) Effects of some H_1-antagonists on the sleep-wake cycle in sleep-disturbed rats. *J. Pharmacol. Sci*. 103, 201–206.

TSUKITA, S. & FURUSE, M. (2000) Pores in the wall: Claudins constitute tight junction strands containing aqueous pores. *J. Cell Biol.* 149**,** 13–16.

UNNO, K., OZAKI, T., MOHAMMAD, S., TSUNO, S., IKEDA-SAGARA, M., HONDA, K. & IKEDA, M. (2012) First and second generation H_1 histamine receptor antagonists produce different sleep-inducing profiles in rats. *Eur. J. Phamacol*. 683, 179–185.

URTTI, A. (2011) Proton pump inhibitors inhibit metformin uptake by organic cation transporters (OCTs). PLoS. One. 6, e22163, 1–11.

VARMA, M. V. S., ASHOKRAJ, Y., DEY, C. S. & PANCHAGNULA, R. (2003) P-glycoprotein inhibitors and their screening: A perspective from bioavailability enhancement. *Pharmacol. Res.* 48, 347–359.

VESZELKA, S. TOTH, A., WALTER, F. R., TOTH, A. E., GROF, I., MESZAROS, M., BOCSIL, A., HELLINGER, E., VASTAG, M., RAKHELY, G. & DELI, M. A. (2018) Comparison of a rat primary cell-based blood-brain barrier model with peithelial and brain

endothelial cell lines: Gene expression and drug transport. *Front. Mol. Neurosci.* 11, 1–20.

VIZUETE, M. L., TRAIFFORT, T., BOUTHENET, M. L., RUAT, M., SOUIL, E., TARDIVEL-LACOMBE, J. & SCHWARTZ, J. C. (1997) Detailed mapping of the histamine H_2 receptor and its gene transcripts in guinea-pig brain. *Neuroscience* 80, 321–343.

VOLK, C. (2014) OCTs, OATs and OCTNs: Structure and function of the polyspecific organic ion transporters of the SLC22 family. *Wiley interdiscip. Rev. Membr. Transp. Signal* 3, 1–13.

WAELBROECK, M., CAMUS, J., TASTENOY, M., LAMBRECHT, G., MUTSCHLER, E., TACKE, R. & CHRISTOPHE, J. (1990) Stereoselevtivity of procyclidine binding to muscarinic receptor subtypes M_1, M_2 and M_4. *Eur. J. Pharmacol. Mol. Pharmacol.* 189, 135–142.

WAN, H., REHNGREN, M., GIORDANETTO, F., BERGSTROM, F. & TUNEK, A. (2007) High-throughput screening of drug-brain tissue binding and in silico prediction for assessment of central nervous system drug delivery. *J. Med. Chem*. 50, 4606-4615.

WANG, M., HAN, J., DOMENICO, J., SHIN, Y. S., JIA, Y. & GELFAND, E. W. (2016) Combined blockade of the histamine H_1 and H_4 receptor suppresses peanut-induced intestinal anaphylaxis by regulating dendritic cell function. *Allergy* 71, 1561–1574.

WANG, Y-Q., TAKATA, Y., LI, R., ZHANG, A., ZHANG, M-Q., URADE, Y., QU, W-M. & HUANG, Z-L. (2015) Doxepin and diphenhydramine increased non-rapid eye movement sleep through blockade of histamine H_1 receptors. *Pharmacol. Biochem. Behav.*129, 56–64.

WAUQUIER, A., VAN DEN BROECK, W. A. E., AWOUTERS, E. & JANSSEN, P. A. J. (1981) A comparison between astemizole and other antihistamines on sleep-wakefulness cycles in dogs. *Neuropharmacol.* 20, 853–859.

WEINER, H., PLAPP, B., LINDAHL, R. & MASER, E. (2006) Enzymology and molecular biology of carbonyl metabolism-12. Purdue University Press. Indiana.

WELLER, K. & MAURER, M. (2009) Desloratadine inhibits human skin mast cell activation and histamine release. *J. Invest. Dermatol*. 129, 2723–2726.

WIELINGA, P. R., VAN DER HEIJDEN, I., REID, G., BEIJNEN, J. H., WIJNHOLDS, J. & BORST, P. (2003) Characterization of the MRP4- and MRP5-mediated transport of cyclic nucleotides from intact cells. *J. Biol. Chem.* 278, 17664–17671.

WILHELM, I. & KRIZBAI, I. A. (2014) *In vitro* models of the blood-brain barrier for the study of drug delivery to the brain. *Mol. Pham.* 11, 1949–1963.

WILHELM, I., NYUL-TOTH, A., SUCIU, M., HERMENEAN, A. & KRIZBAI, I. A. (2016) Heterogeneity of the blood-brain barrier. *Tissue Barriers*. 4, 1–8.

WILSON, J., WINTER, M. & SHASBY, D. (1990) Oxidants, ATP depletion, and endothelial permeability to macromolecules. *Blood* 76**,** 2578–2582.

WINDASS, A. S., LOWES, S., WANG, Y. & BROWN, C. D. A. (2007) The contribution of organic anion transporters OAT1 and OAT3 to the renal uptake of rosuvastatin. *J. Pharmacol. Exp. Ther*. 322, 1221–1227.

WOHLFART, S., KHALANSKY, A. S., GELPERINA, S., BEGLEY, D. & KREUTER, J. (2011) Kinetics of transport of doxorubicin bound to nanoparticles across the blood-brain barrier*. J. Control. Release* 154, 103–107.

WOLBURG, H., NOELL, S., MACK, A., WOLBURG-BUCHHOLZ, K. & FALLIER-BECKER, P. (2009) Brain endothelial cells and the glio-vascular complex. *Cell Tissue. Res*. 335, 75–96.

WOLFGANG, L. S. & HEIDRUM, P. (2005). Blood-brain barrier active efflux transporters: ATP-binding cassette gene family. *J. Am. Soc. Exp. Neuro. Ther. 2*, 86–98.

WU, Z., RAZZAK, M., TUCKER, I. G. & MEDLICOTT, N. J. (2004) Physicochemical characterization of ricobendazole: I. solubility, lipophilicity, and ionization characteristics. *J. Pharm. Sci.* 94, 983–993.

WU, Z., YU, Y., WU, Y., PATCH, C., SZABO, A. & HUANG, X. F. (2013) Reduction of histamine H_1 receptor binding induced by high-fat diet can be prevented by DHA and dietary fiber in specific brain area of male rats. *Brain Res. Bull*. 97, 199-125.

XIN-YI, H. & DUO-LONG, D. (2015) Chiral separation by counter-current chromatography. *Trends Anal. Chem.* 67, 128–133.

YAGI, N., TANIUCHI, T., HAMADA, K., SUDO, J. I. & SEKIKAWA, H. (2002) Pharmacokinetics of ketotifen fumarate after intravenous, intranasal, oral and rectal administration in rabbits. *Biol. Pharm. Bull.* 25**,** 1614–1618.

YAMAMDA, A., MAEDA, K., KAMIYAMA, E., SUGIYAMA, D., KONDO, T, SHIROYANAGI, Y., NAKAZAWA, H., OKANO, T., ADACHI, M., SCHUETZ, J. D., ADACHI, Y., HU, Z., KUSYHARA, H. & SUGIYAMA, Y. (2007) Multiple human isoforms of drug transporters contribute to the hepatic and renal transport of olmesartan, a selective antagonist of the angiotensin II AT1-receptor. *Drug Metab. Dispos.* 35, 2166–2176.

YAMASHITA, M., FUKUI, H., SUGAMA, K., HORIO, I., ITO, S., MIZUGUCHI, H. & WADA, H. (1991). Expression cloning of a cDNA encoding the bovine histamine H_1 receptor. *Proc. Natl. Acad. Sci*. 88, 11515–11520.

YAMAZAKI, M., FUKUOKA, H., NAGATA, O., KATO, H., ITO, Y., TARASAKI, T. &TSUJI, A. (1994a) Transport mechanism if an H_1-antagonist at the blood-brain barrier: Transport mechanism of mepyramine using the carotid injection technique. *Biol. Pharm. Bull*. 17, 676–679.

YAMAZAKI, M., TERASAKI, T., YOSHIOKA, K., NAGATA, O., KATO, H., ITO, Y. & TSUJI, A. (1994b) Carrier-mediated transport of H_1-antagonist at the blood-brain barrier: A common transport system of H_1-antagonists and lipophilic basic drugs. *Pharm. Res*. 11, 1516–1518.

YANAI, K. & TASHIRO, M. (2007) The physiological and pathophysiological roles of neuronal histamine: An insight from human positron emission tomography studies. *Pharmacol. Therapeut*. 113, 1–15.

YANAI, K., YOSHIKAWA, T., YANAI, A., NAKAMURA, T., IIDA, T., LEURS, R. & TASHIRO, M. (2017) The clinical pharmacology of non-sedating antihistamines. *Pharmacol. Ther.* 178, 148–156.

YANAI, K., ZHANG, D., TASHIRO, M., YOSHIKAWA, T., NAGANUMA, F., HARADA, R., NAKAMURA, T., SHIBUYA, K. & OKAMURA, N. (2011) Positron emission tomography evaluation of sedative properties of antihistamines. *Expert Opin. Drug Saf*. 10, 613–622.

YANG, J., MUTKUS, L. A., SUMNER, D., STEVENS, J. T., ELDRIDGE, J. C., STRANDHOY, J. W. & ASCHNER, M. (2001) Transendothelial permeability of chlorpyrifos in RBE4 monolayers is modulated by astrocyte-conditioned medium. *Mol. Brain Res.* 97**,** 43–50.

YANG, L., TUCKER, I. G. & ØSTERGAARD. (2011) Effects of bile salts on propranolol distribution into liposomes studied by capillary electrophoresis. *J. Pharm. Biomed. Anal.* 56, 553–559.

YANG, L., ZHANG, H., MIKOV, M. & TUCKER, I. G. (2009) Physiochemical and biological characterization of monoketocholic acid, a novel permeability enhancer. *Mol. Pharm.* 6, 448–456.

YUAN, H., FENG, B. & YU, Y. (2009) Renal organic anion transporter-mediated drug-drug interaction between gemcabene and quinapril. *J. Pharmacol. Exp. Ther.* 330, 191–197.

ZHANG, D., TASHIRO, M., SHIBUYA, K., OKAMURA, N., FUNAKI, Y., YOSHIKAWA, T., KATO, M. & YANAI, K. (2010) Next-day residual sedative effect after nighttime administration of an over-the-counter antihistamine sleepaid, diphenhydramine, measured by positron emission tomography. *J. Clin. Psychopharmacol*. 30, 694–701.

ZHANG, T., FINN, D. F., BARLOW, J. W. & WALSH, J. J. (2016) Mast cell stabilizers. *Eur. J. Pharmacol*. 778, 158–168.

ZHANG, W., MOJSILOVIC-PETROVIC, J., ANDRADE, M. F., ZHANG, H., BALL, M. & STANIMIROVIC, D. B. (2003) The expression and functional characterization of ABCG2 in brain endothelial cells and vessels. *FASEB. J.* 17, 2085–2087.

ZHAO, R., KALVASS, C. & POLLACK, G. M. (2009) Assessment of blood-brain barrier permeability using the *in situ* mouse brain perfusion technique. *Pharm. Res.* 26, 1657–1664.

ZHOU, W., ZHANG, J., WANG, G., LING, L. & YAN, C. (2016) Permeability and distribution of nerve growth factor in the brain of neonatal rats by periphery venous injection in hypoxic-ischemic state. *SpringerPlus.* 5, 1893–1902.

ZHU, C. J. & ZHANG, J. T. (2008) Stereoselective plasma protein binding and target tissue distribution of clausenamide enantiomers in rats. *Chirality* 21, 402–406.